BEATS_eu
@BEATSeu1

BEATS

BEAmline for Tomography at SESAME

Tomography Beam Line and Instrumentation
The BEATS case

Gianluca Iori

BEATS beamline scientist

Funded by the EU's H2020 framework programme under grant agreement n°822535

ALBA · The Cyprus Institute · DESY. · Elettra Sincrotrone Trieste · ESRF · INFN LNF · PSI · SESAME · SOLARIS

BEAmline for Tomography at SESAME Project

BEATS, the BEAmline for Tomography at SESAME is an H2020 European project to build a beamline for tomography at the SESAME synchrotron in Jordan.

More about the project →

Funded by the EU's H2020 framework programme under grant agreement n°822535

BEATS

BEAmline for Tomography at SESAME

X-ray computed tomography

First Computed Tomography scan
EMI Scanner (1971)

Nobel prize for CT in 1979
Hounsfield & Cormack

https://www.psi.ch/

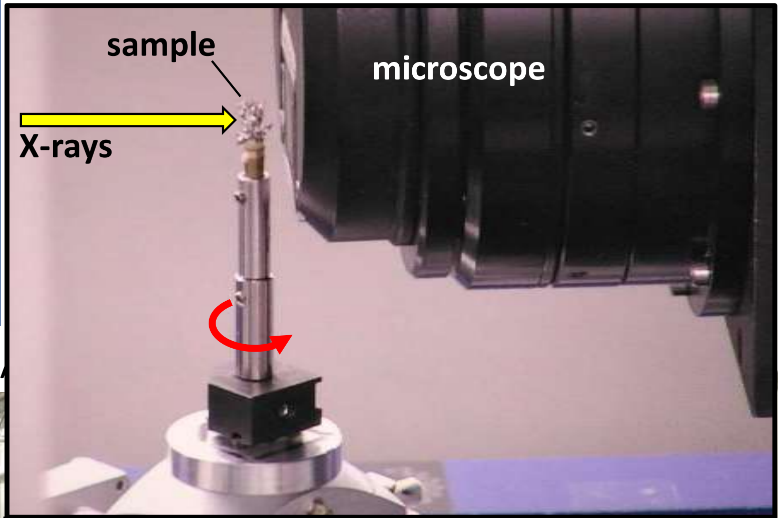

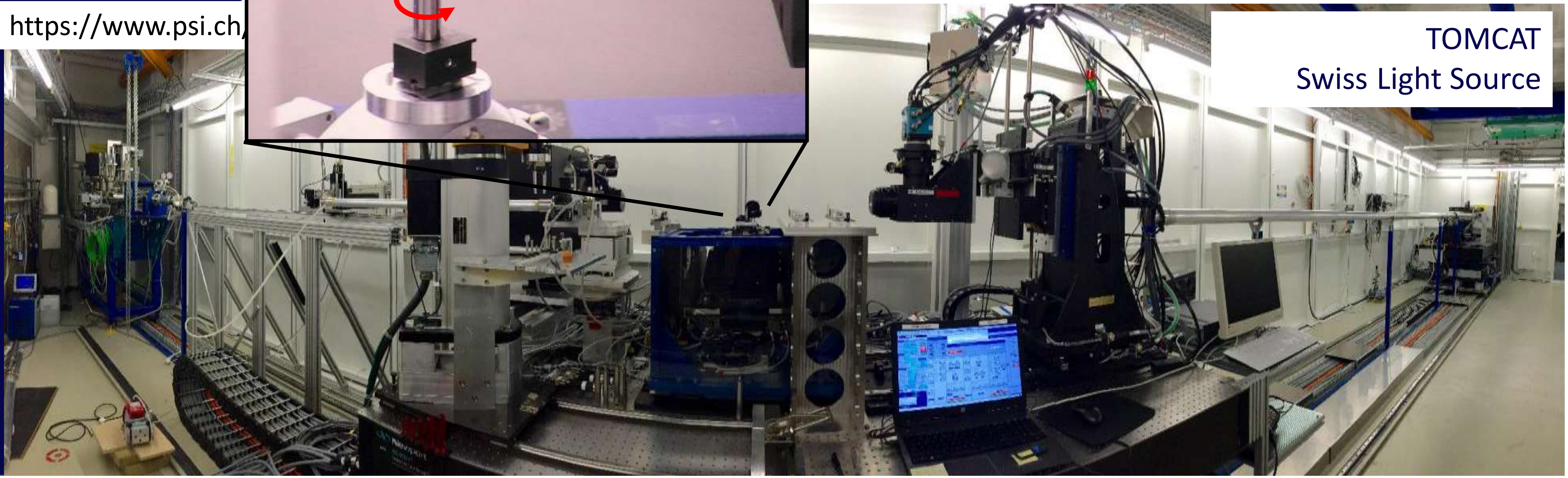

TOMCAT
Swiss Light Source

BEATS

BEAmline for Tomography at SESAME

Outlook

Part 1: Tomography Beam Line Instrumentation (40')

- BEATS Beam Line layout
- X-Ray source
- Front-end
- Optics (Double Multilayer Monochromator)
- Ray-tracing and numerical simulation
- Experimental station
    - Fast shutter design
    - Sample and detectors manipulation
    - Indirect X-ray imaging detectors
    - Sample environments
        - Induction Sample Furnace
        - Mechanical testing stage

BREAK (5')

Part 2: Tomography data acquisition (15')

- Visible light tomography setup and benchmarking @ BEATS: how does a CT scan work?
- Data acquisition architecture @ BEATS

Part 3: Scientific opportunities @ BEATS (20')

- Archaeology and cultural heritage
- Health and biology
- Agriculture and environment
- Material science and engineering

Funded by the EU's H2020 framework programme under grant agreement n°822535

Part 1: Tomography Beam Line Instrumentation

BEATS layout

- **High-flux**; well above 20 keV to see through large, dense samples
- Filtered **white beam** VS **monochromatic beam** (with DMM)
- **High-flux** (primary slits open) VS **high-sensitivity** (primary slits acting as secondary coherent source)

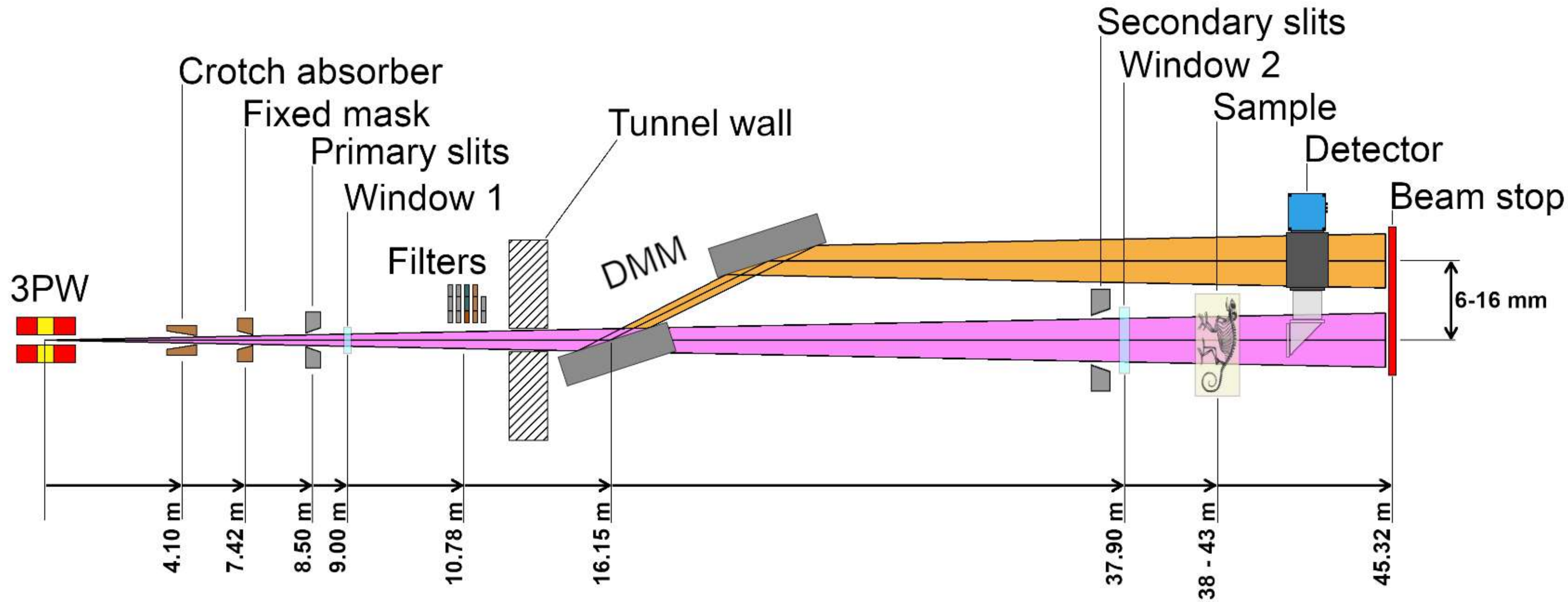

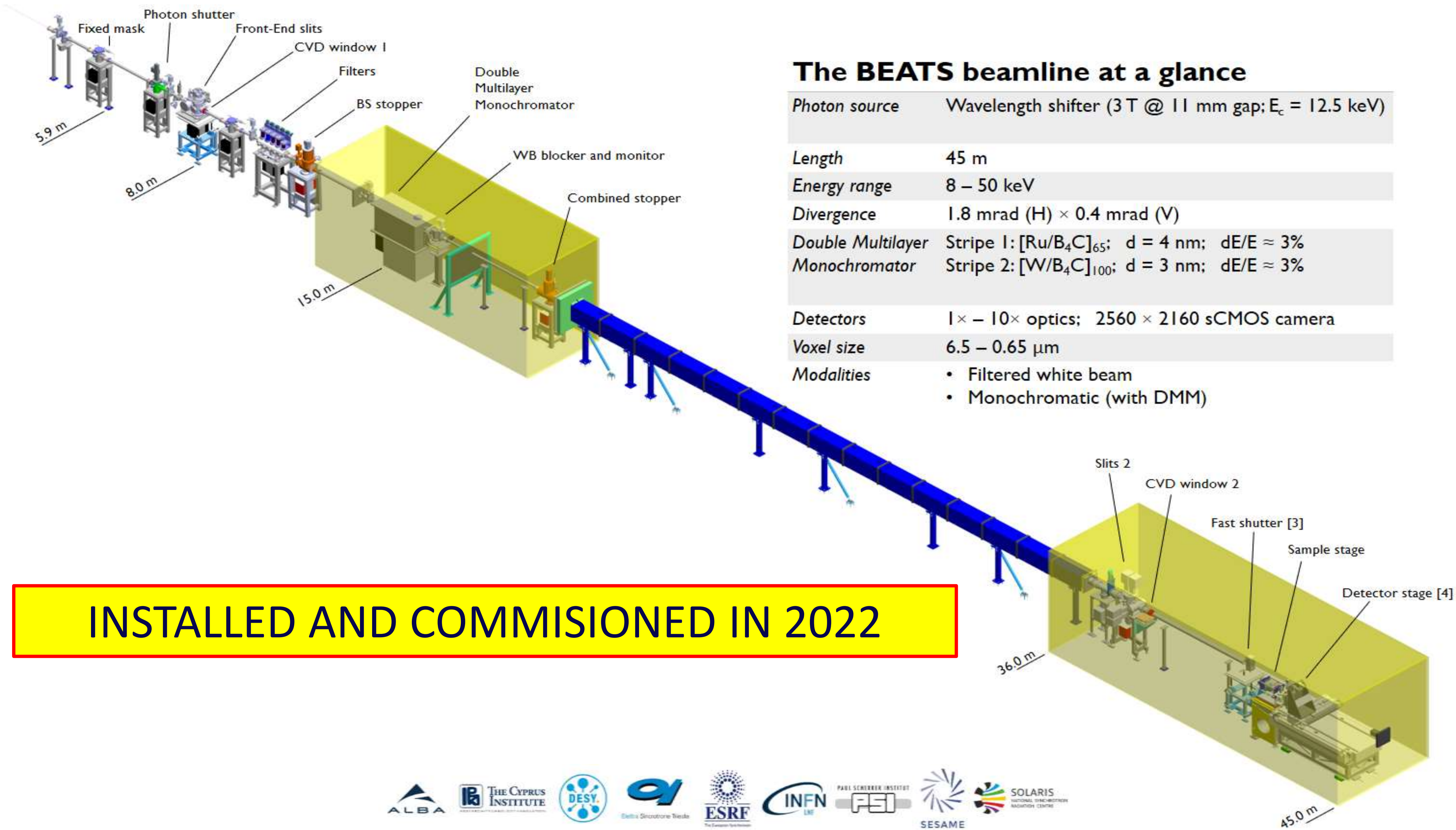

The BEATS beamline at a glance

Photon source	Wavelength shifter (3 T @ 11 mm gap; E_c = 12.5 keV)
Length	45 m
Energy range	8 – 50 keV
Divergence	1.8 mrad (H) × 0.4 mrad (V)
Double Multilayer Monochromator	Stripe 1: $[Ru/B_4C]_{65}$; d = 4 nm; dE/E ≈ 3% Stripe 2: $[W/B_4C]_{100}$; d = 3 nm; dE/E ≈ 3%
Detectors	1× – 10× optics; 2560 × 2160 sCMOS camera
Voxel size	6.5 – 0.65 μm
Modalities	• Filtered white beam • Monochromatic (with DMM)

INSTALLED AND COMMISIONED IN 2022

BEATS X-Ray source

Concept

3 T 3-pole wiggler

- A 3-pole wiggler of 3 T magnetic field, operating in a SESAME short straight section.
- Very low multipolar effects on the SESAME storage ring optics.
- Reduce attractive forces between the magnetic structures -> minor mechanical constraints.

3 T superbend

- Replace an existing dipole of the SESAME storage ring
- 2 new quadrupoles; completely new vacuum chamber for the chosen section of the storage ring; modification (or new design) of the affected girder

2.9 T superbend (TOMCAT, SLS)

BEATS X-Ray source

3-pole wiggler

- Minimum gap: 11 mm
- Maximum field: ~3 T
- Magnetic length: < 1 m
- 20-50 keV spectral range

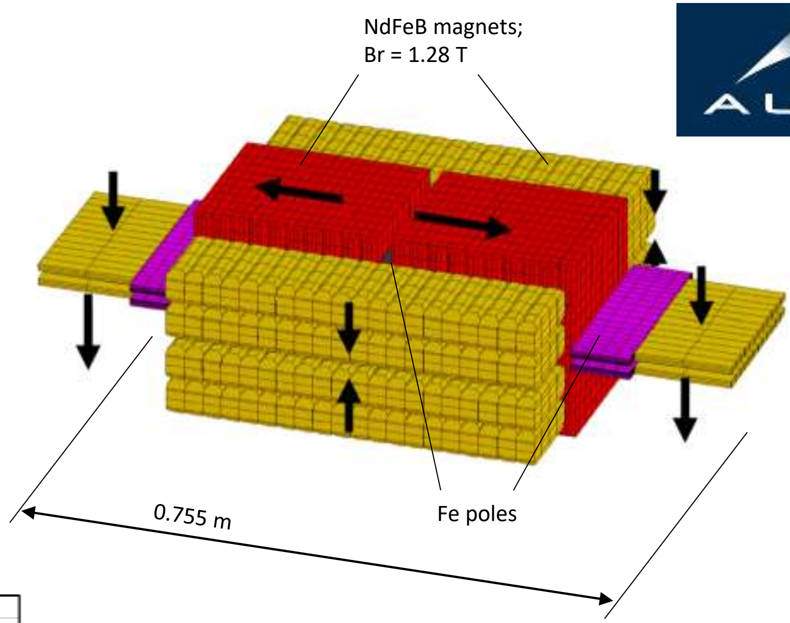

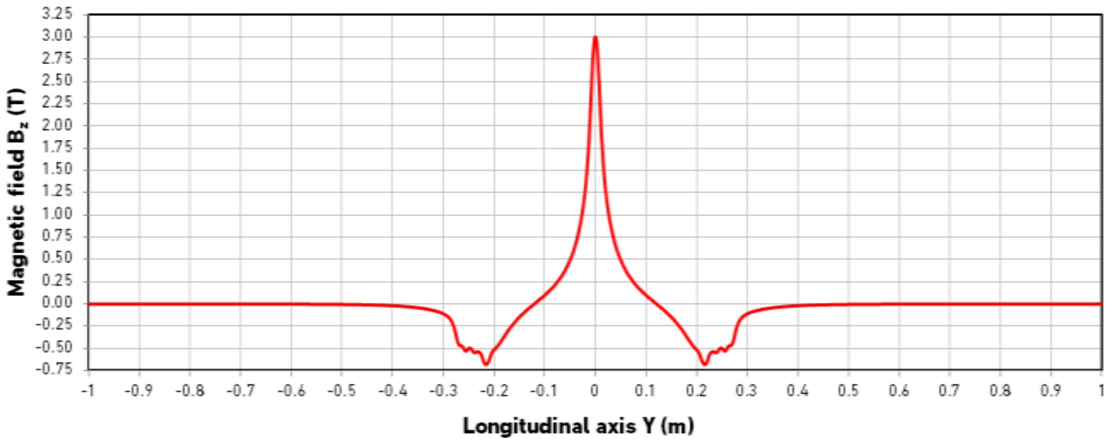

BEATS X-Ray source

3-pole wiggler

- Minimum gap: 11 mm
- Maximum field: 2.94 T
- Magnetic length: 0.41 m
- 20-50 keV spectral range

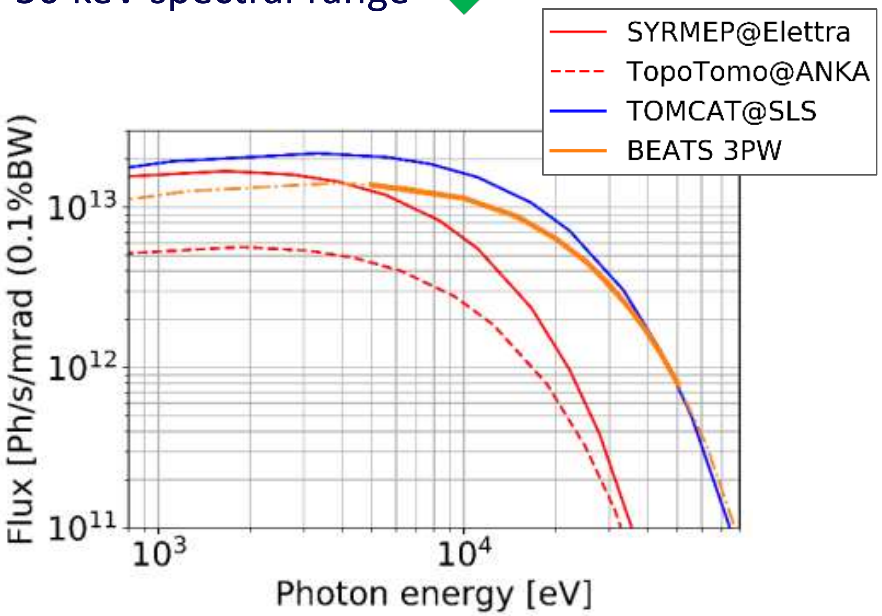

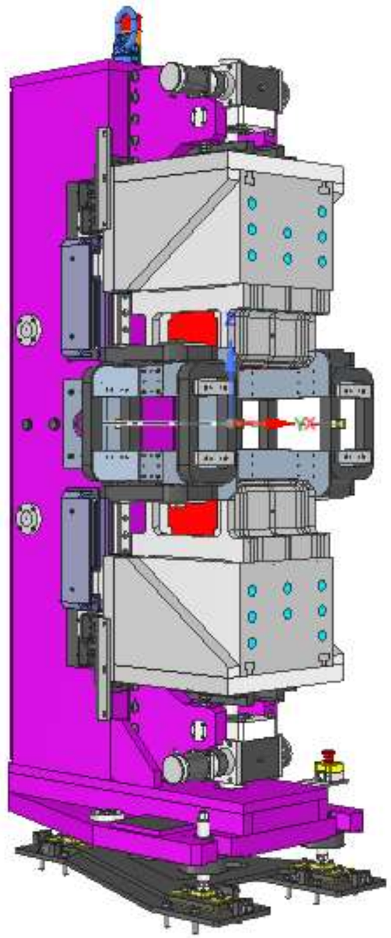

BEATS front-end

- Collimate and shape the X-Ray beam

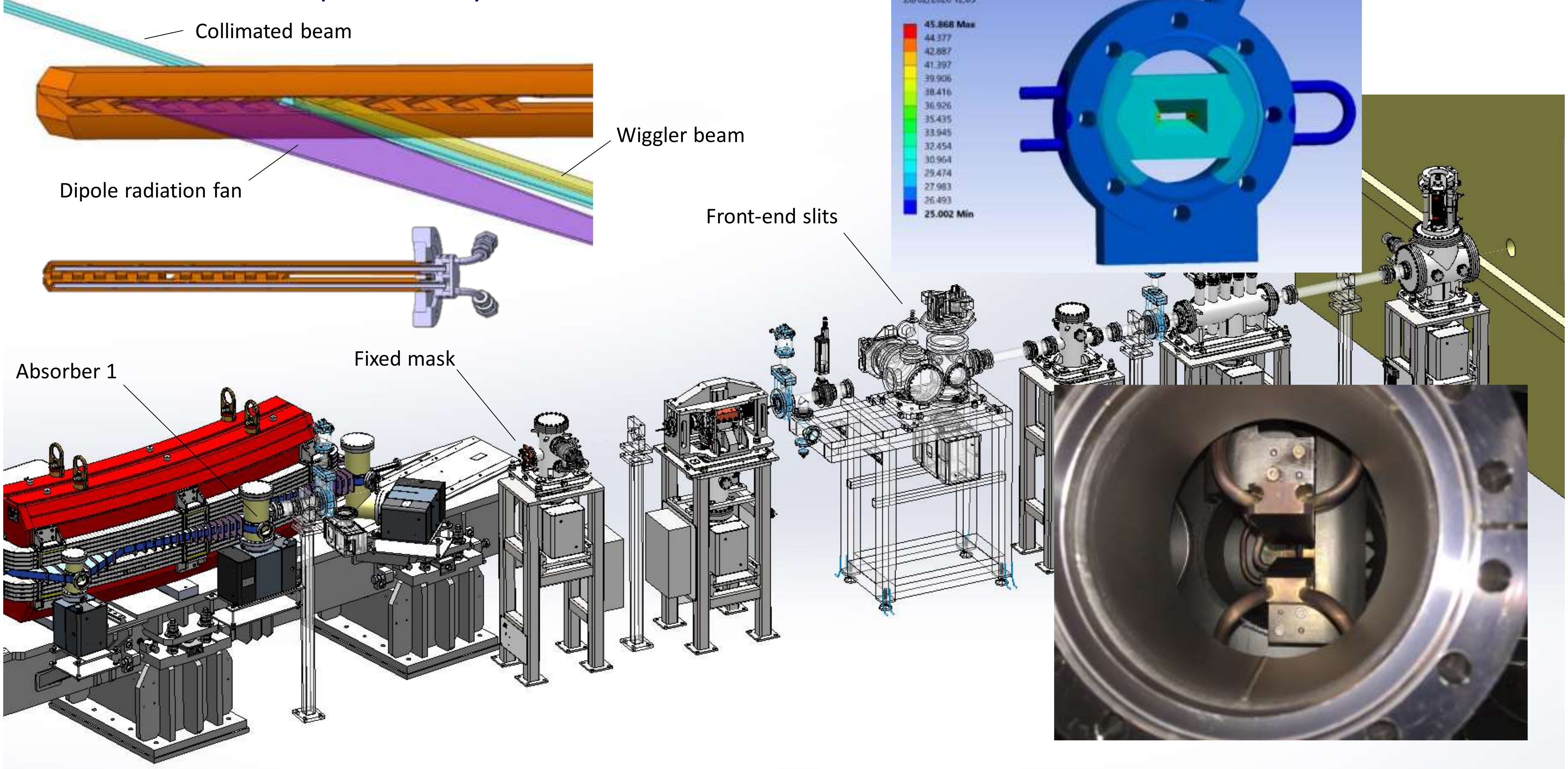

BEATS front-end

- Stop the beam: allow access to the downstream beamline components in full safety

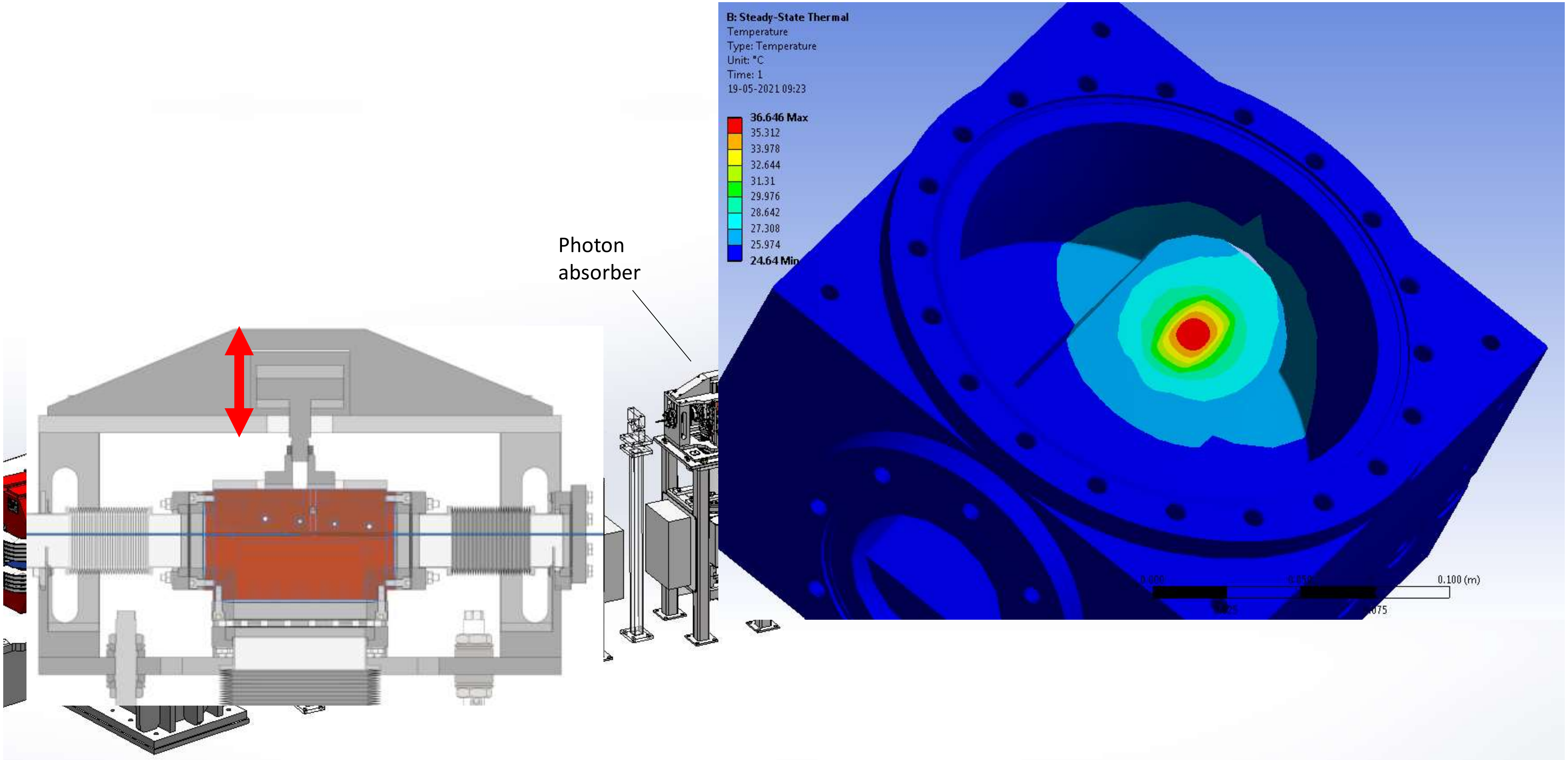

BEATS front-end

- Stop the beam: allow access to the downstream beamline components in full safety

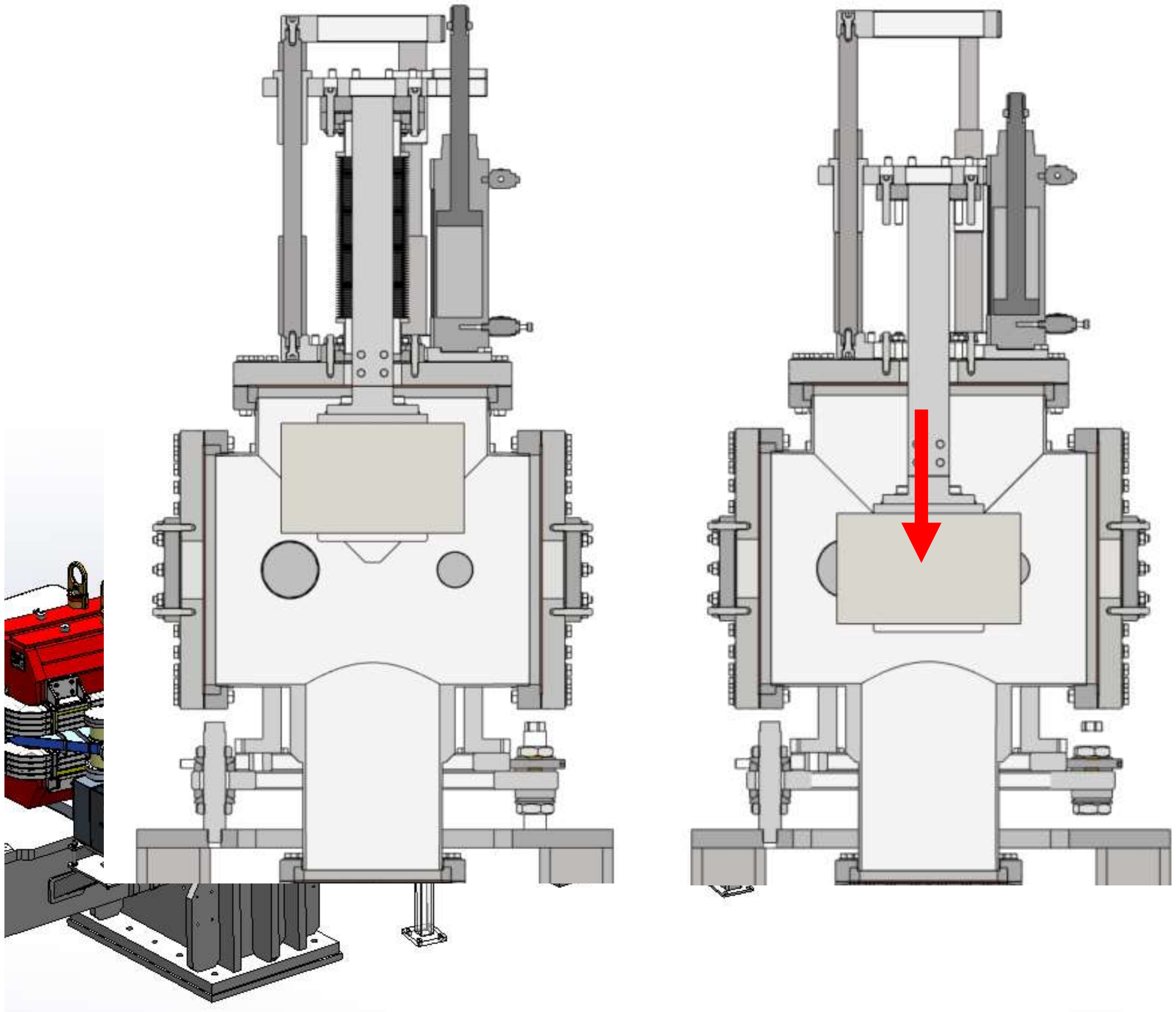

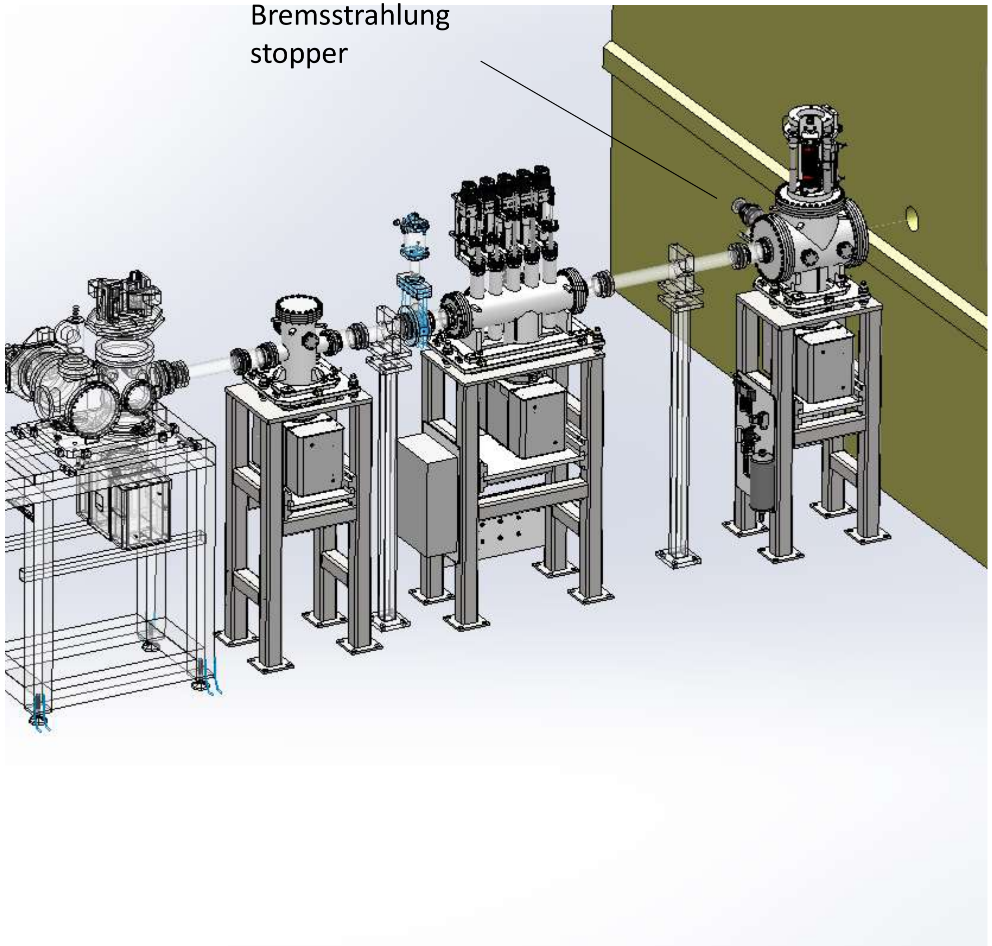

BEATS front-end

- Tune the energy spectrum of the extracted beam through the use of filters

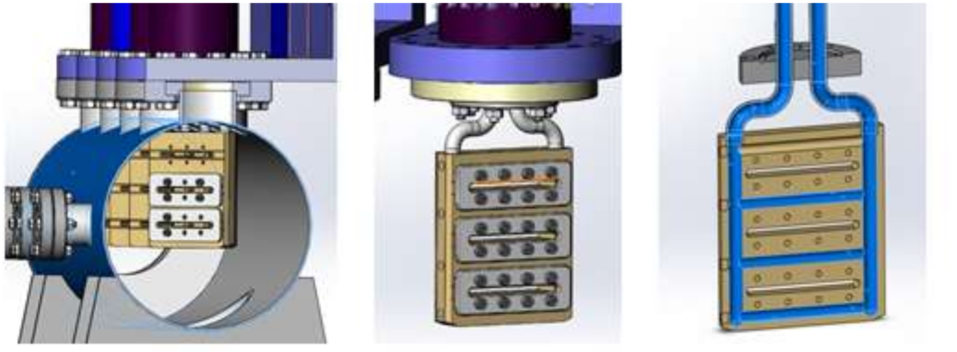

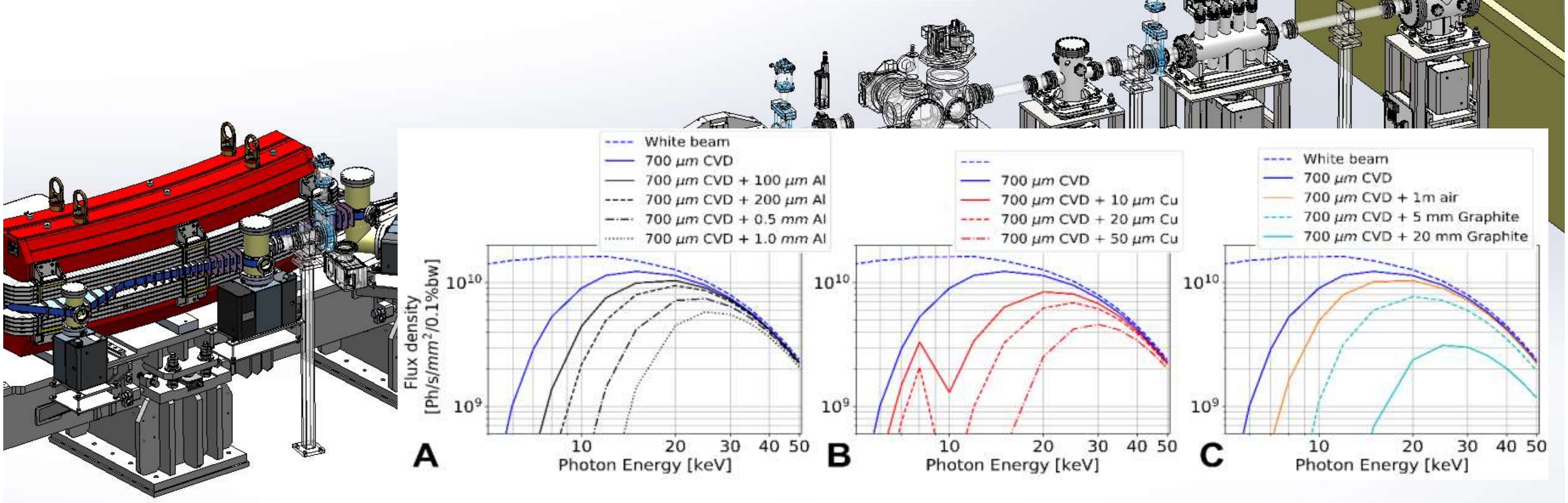

BEATS front-end

- Assures the integrity of the storage ring vacuum

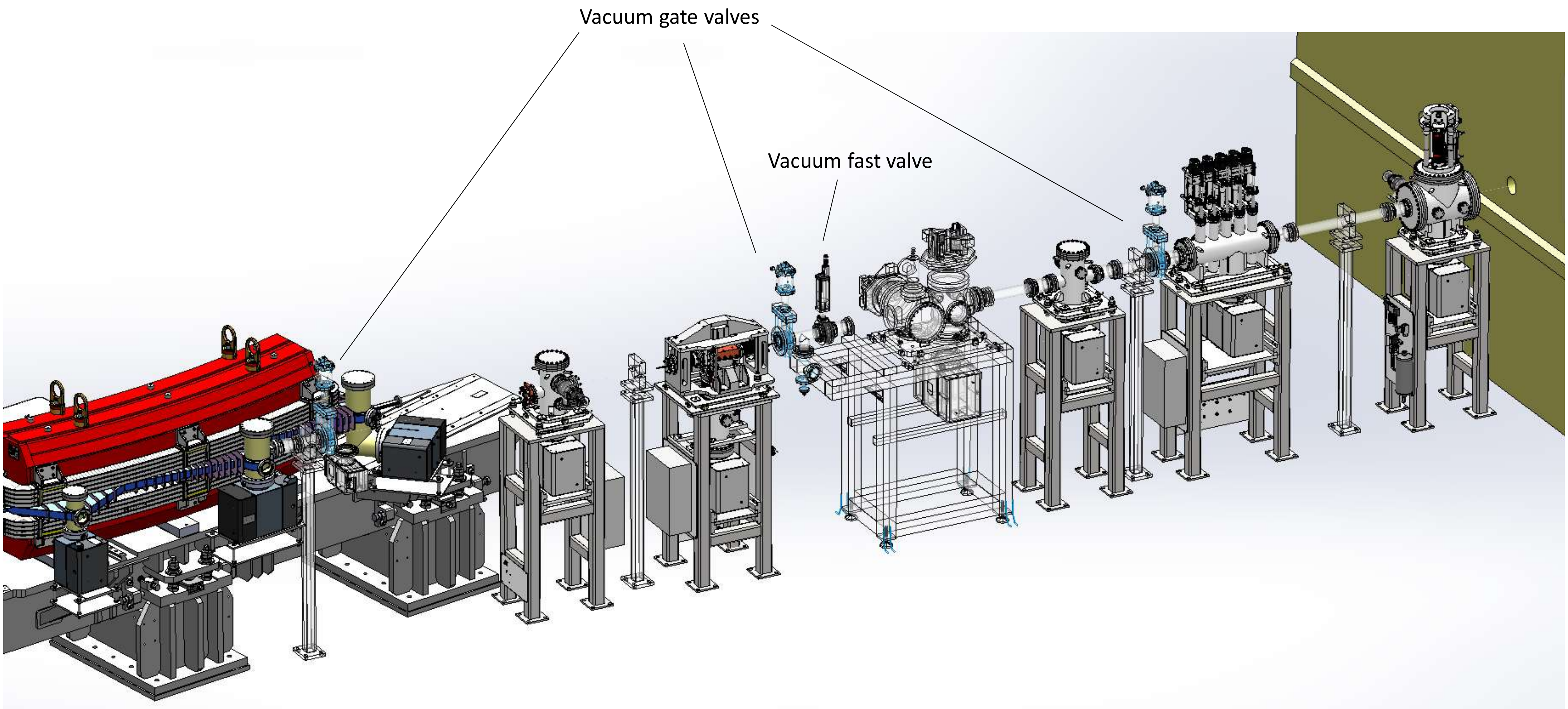

BEATS front-end

- Provide diagnostic on the X-Ray beam position

X-Ray Beam Position Monitor

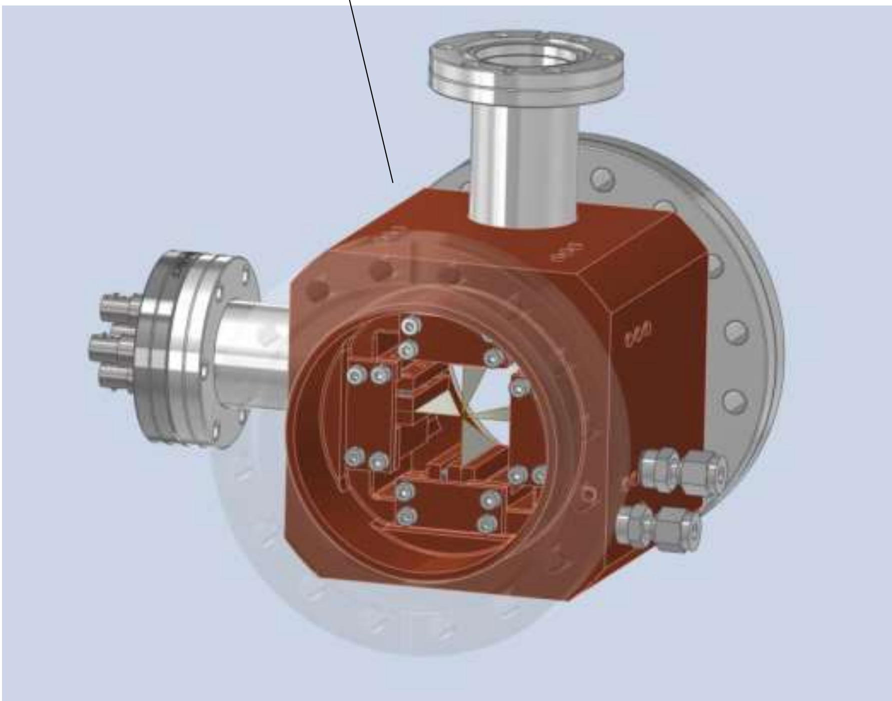

BEATS front-end

- Collimate and shape the X-Ray beam
- Stop the beam: allow access to the downstream beamline components in full safety
- Tune the energy spectrum of the extracted beam through the use of filters
- Assure the integrity of the storage ring vacuum
- Provide diagnostic on the X-Ray beam position

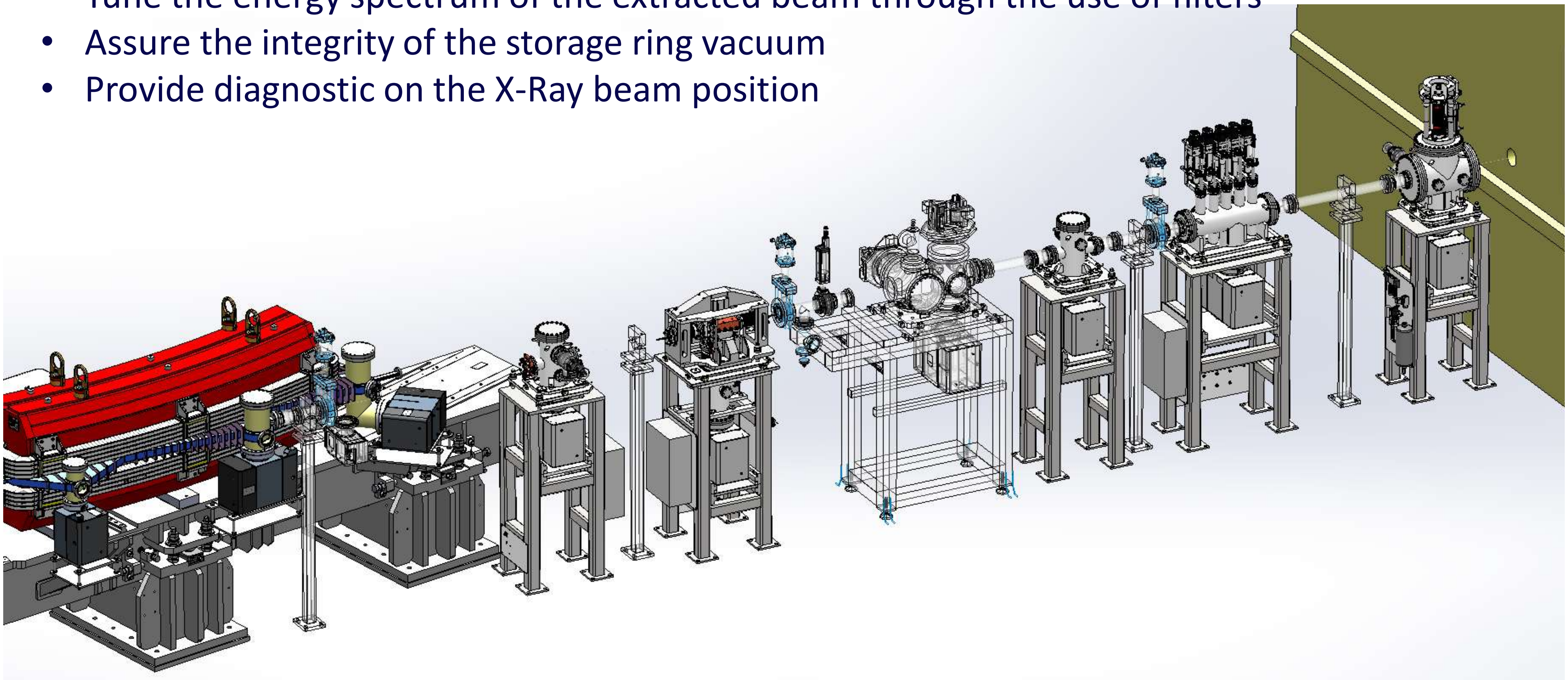

Beamline Optics:
Double Multilayer Monochromator (DMM)

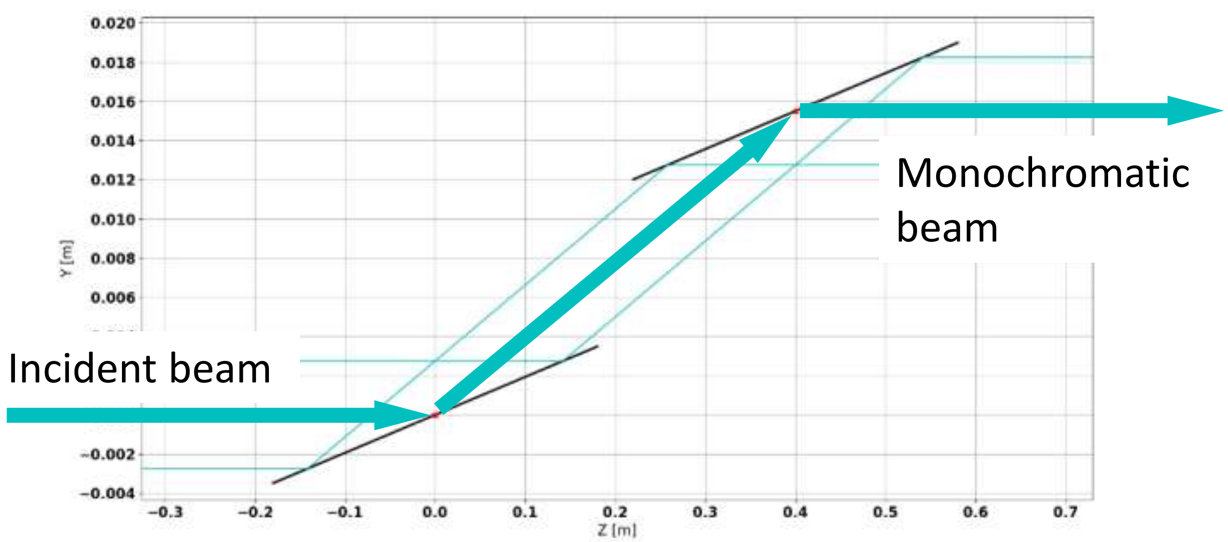

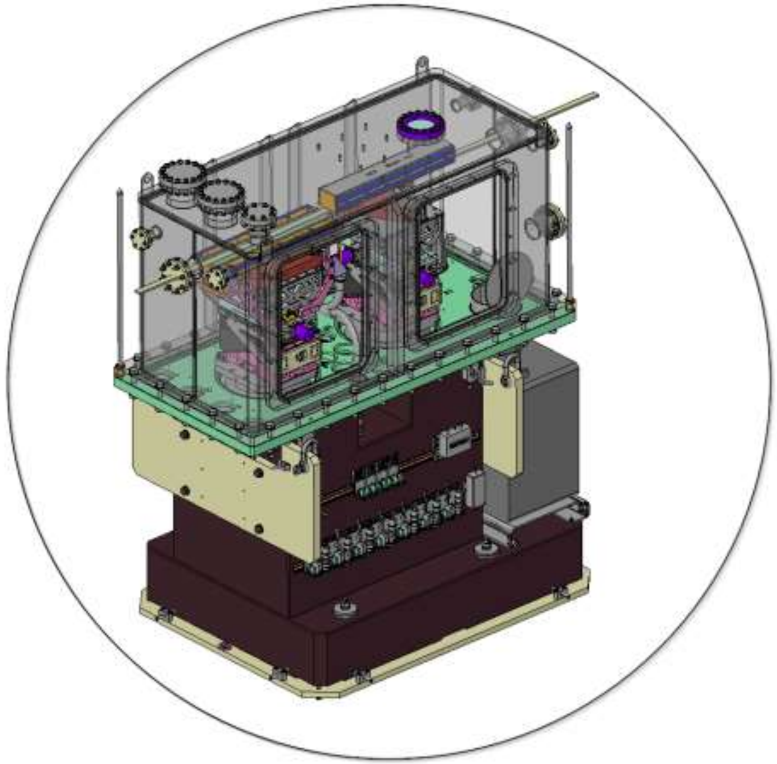

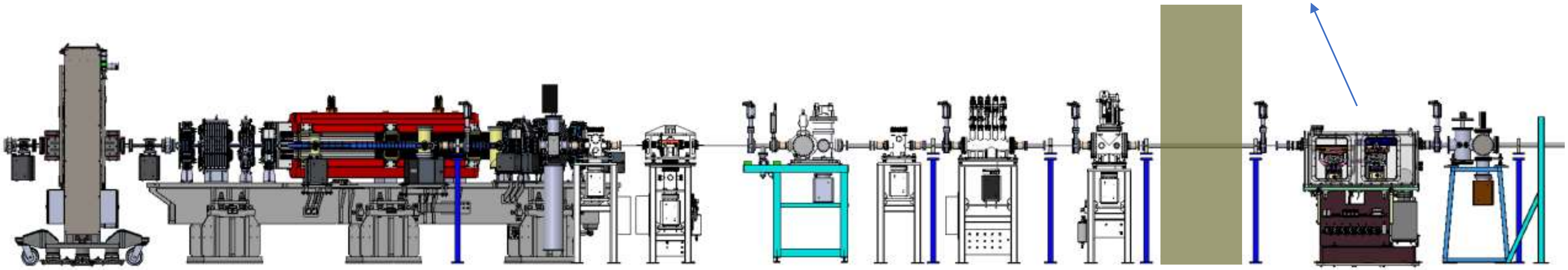

Double Multilayer Monochromator (DMM)

Multilayers

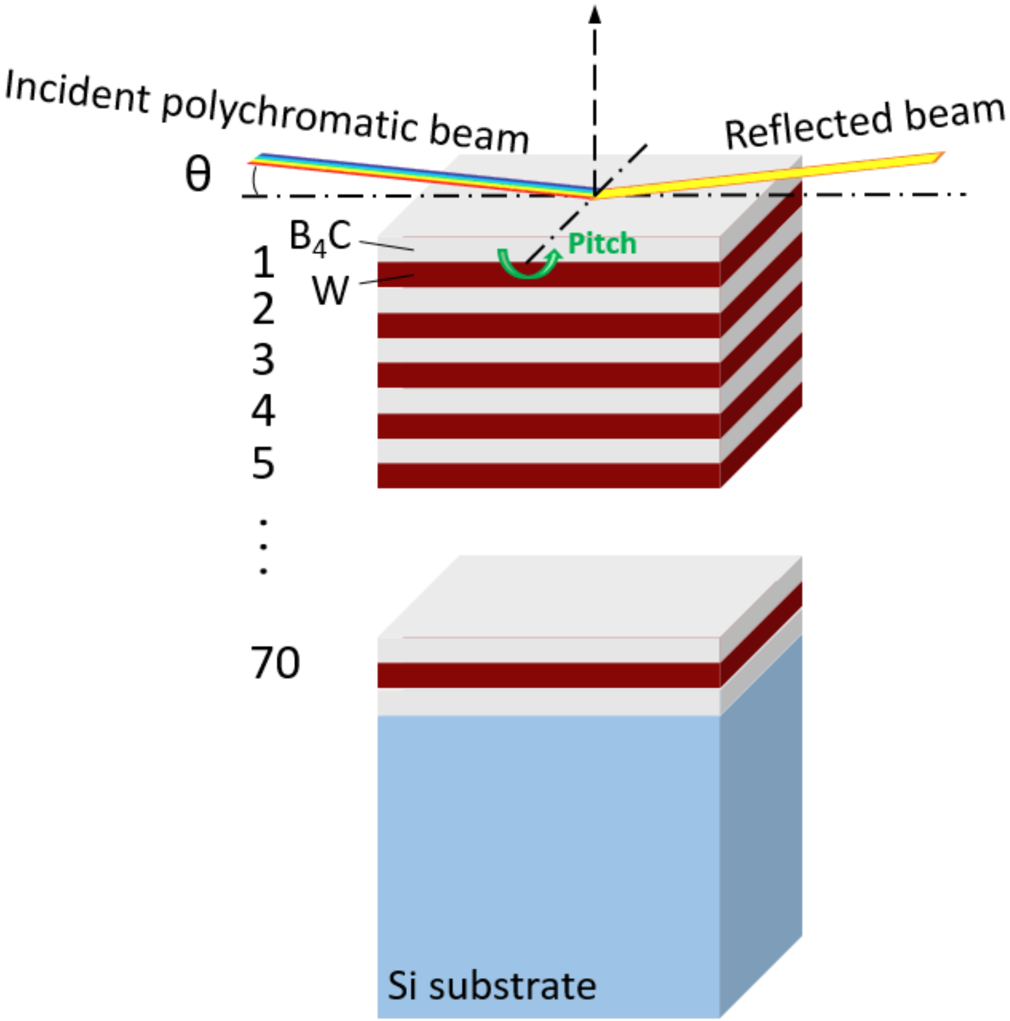

- Multilayers are produced by coating a Si substrate with periodic bi-layers of a high-Z and a low-Z material.
- The deposition process is called magnetron sputtering.
- Bragg's law for a multilayer:

$$\lambda = 2\, d \sin(\vartheta)$$

Bi-layer thickness

Double Multilayer Monochromator (DMM)

Multilayers

- Limited number of scattering planes: less degree of monochromaticity and larger bandwidth than DCMs

ΔE/E	
DCM:	$10^{-4} \div 10^{-5}$
DMM:	10^{-2}

- Ru- and B_4C sublayers are equally thick: even harmonics suppressed

- Reflectivity as a function of photon energy for a Ru/B_4C multilayer for $\theta = 1.15°$ (BM5, ESRF)

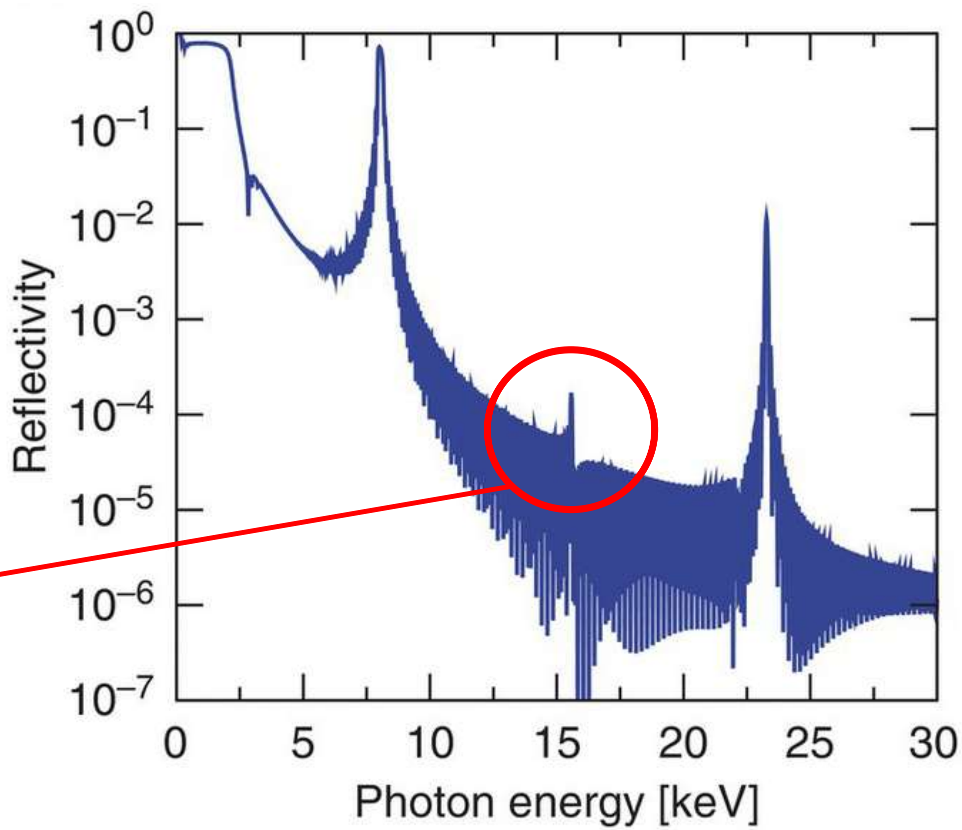

[An Introduction to Synchrotron Radiation: Techniques and Applications 2nd edition - Philip Willmott, 2018]

Double Multilayer Monochromator (DMM)

Substrates (BEATS)

Dimensions	500 mm × 65 mm × 60 mm
Coatings area	480 mm × 25 mm (2 stripes)
Surface roughness (RMS)	< 0.10 nm
Meridional slope error (RMS)	< 0.2 μrad

Bi-layer thickness

$$\lambda = 2\, d \sin(\vartheta)$$

- Larger d implies smaller grazing angle and longer Si substrates than those of DCMs

Multilayers (BEATS)

	Stripe 1	Stripe 2
	$[W/B_4C]_{100}$	$[Ru/B_4C]_{65}$
Energies [keV]	20 – 50	8(10) – 22
d-spacing [nm]	3.0	4.0
Duty cycle γ	0.5	0.5
N. bilayers	100	65
dE/E [%]	~ 3.0	~ 3.1 %
Theta (Bragg angle) [deg]	0.22 – 0.75	0.40 – 1.10

ESRF The European Synchrotron
Multilayer laboratory

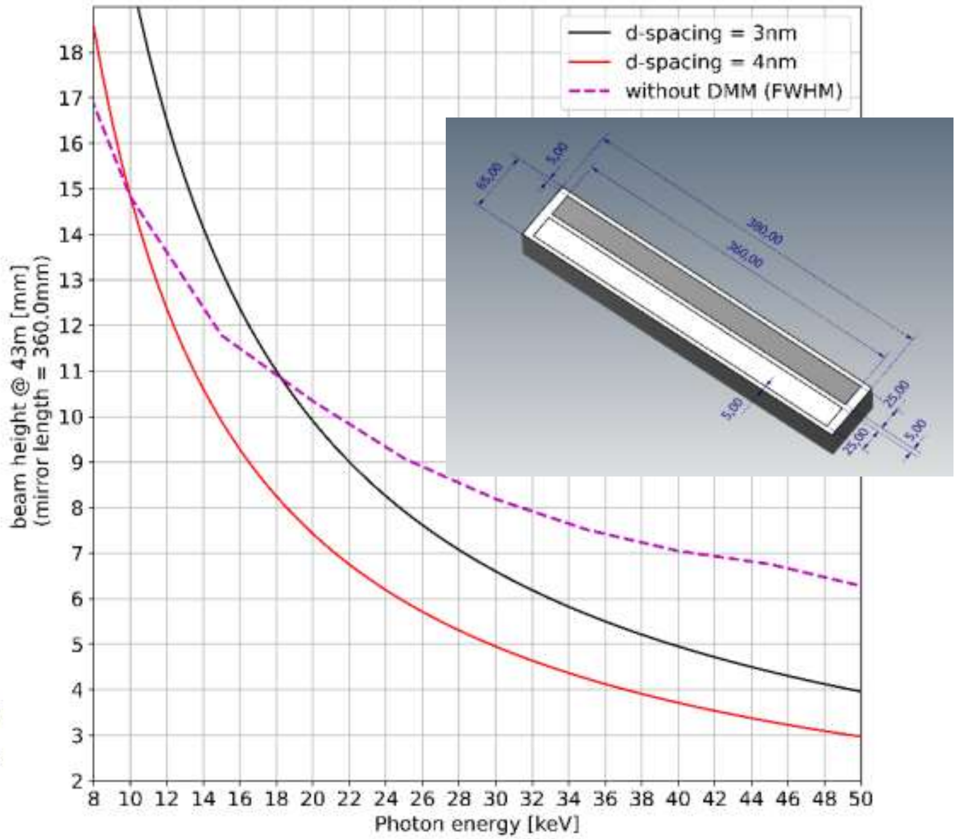

Double Multilayer Monochromator (DMM)

Substrates (BEATS)

Dimensions	500 mm × 65 mm × 60 mm
Coatings area	480 mm × 25 mm (2 stripes)
Surface roughness (RMS)	< 0.10 nm
Meridional slope error (RMS)	< 0.2 *μrad*

- $[W/B_4C]100$ DMM stripe @ 45 keV
- Meridional slope error: 0.1 – 0.5 µrad..

..The quality of the flat field deteriorates for mirror slope errors > 0.2 µrad!

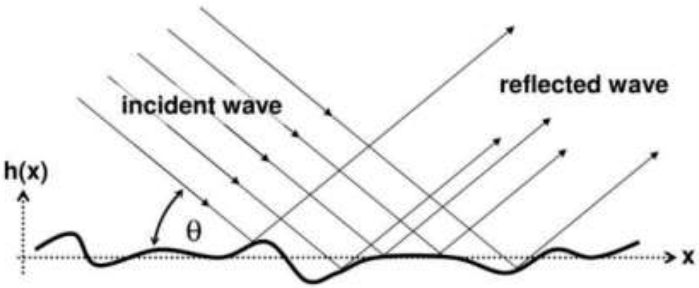

[A. Rack et al., "Comparative study of multilayers used in monochromators for synchrotron-based coherent hard X-ray imaging," J Synchrotron Rad. 2010]

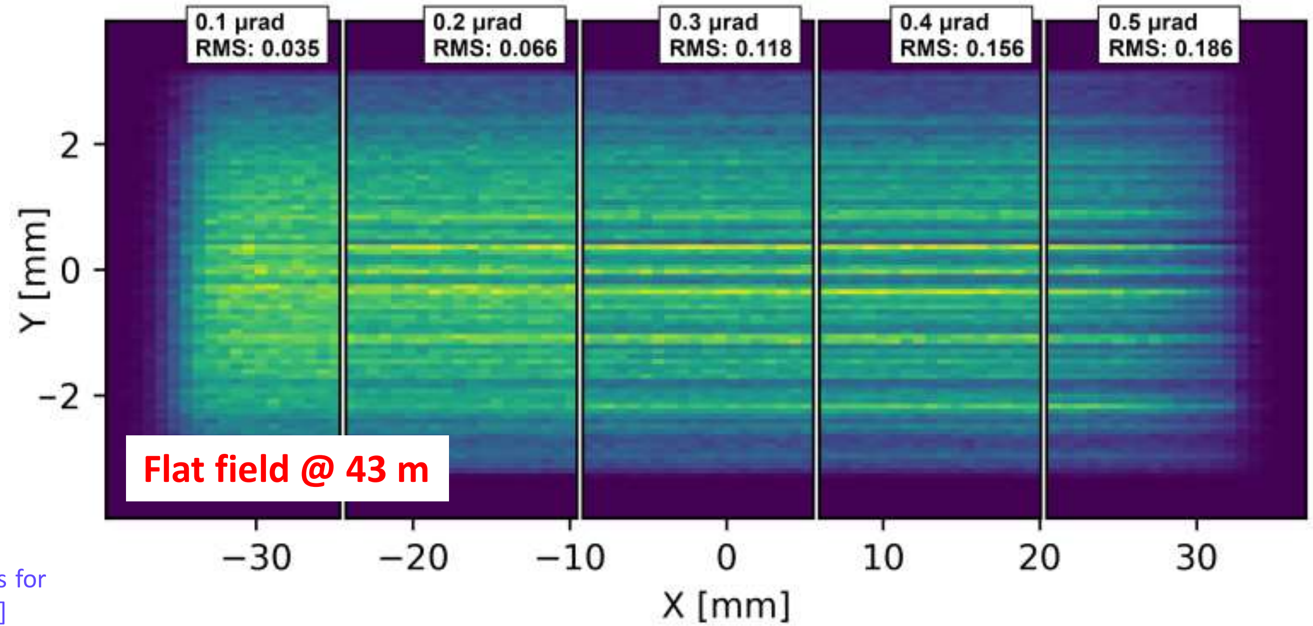

Double Multilayer Monochromator (DMM)

Mechanics

- **Independent ML towers**
  - Variable offset: 6.2 – 15.5 mm
  - Stroke 2nd multilayer: 400 – 750 mm

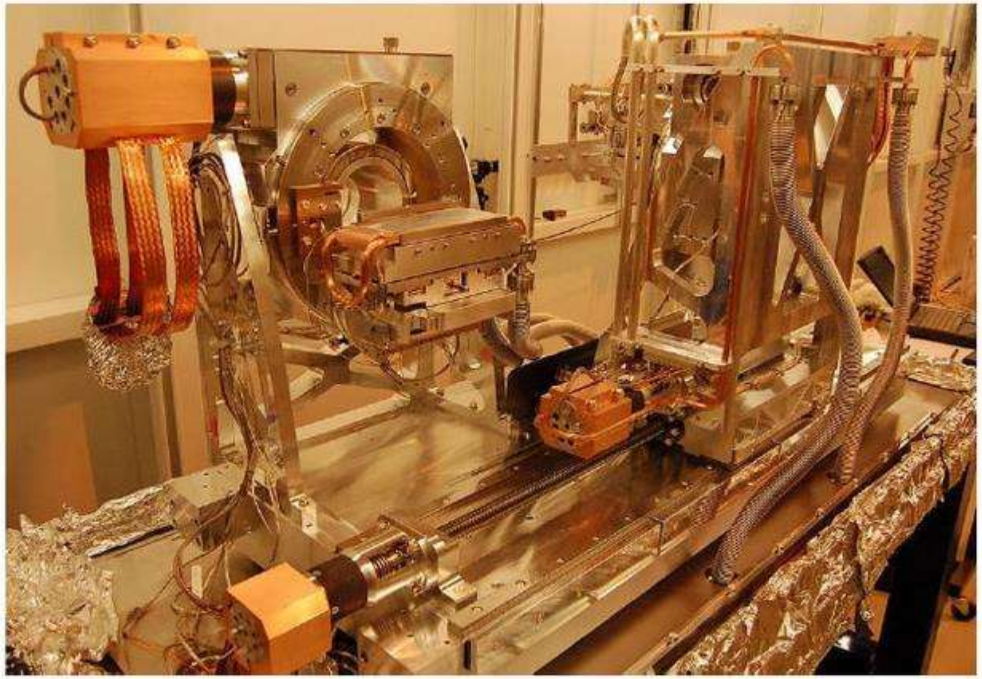

DMM @ TOMCAT, PSI; Cinel Scientific Instruments

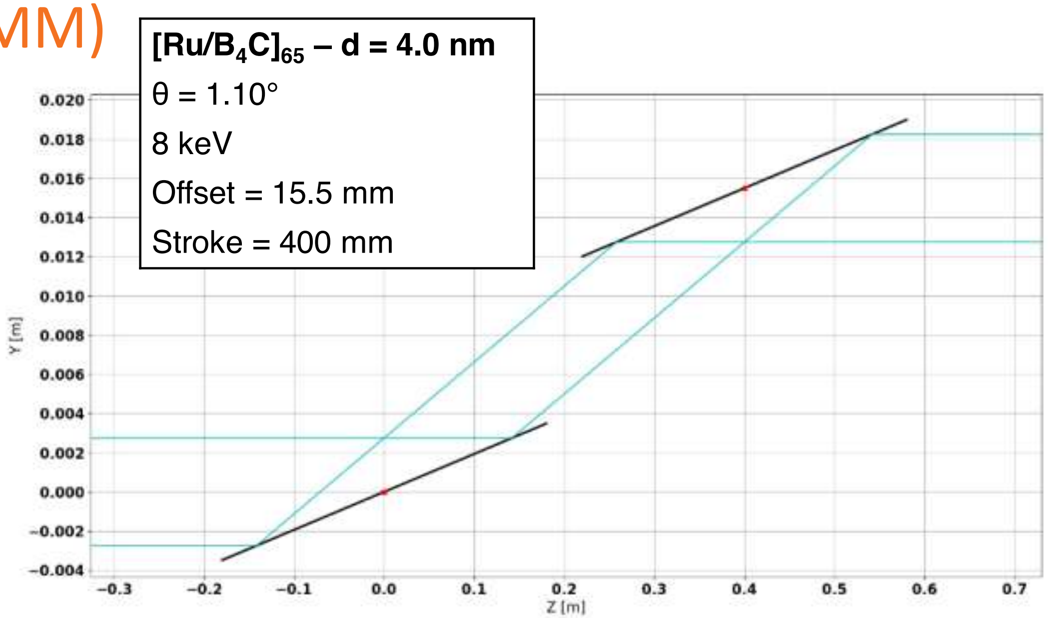

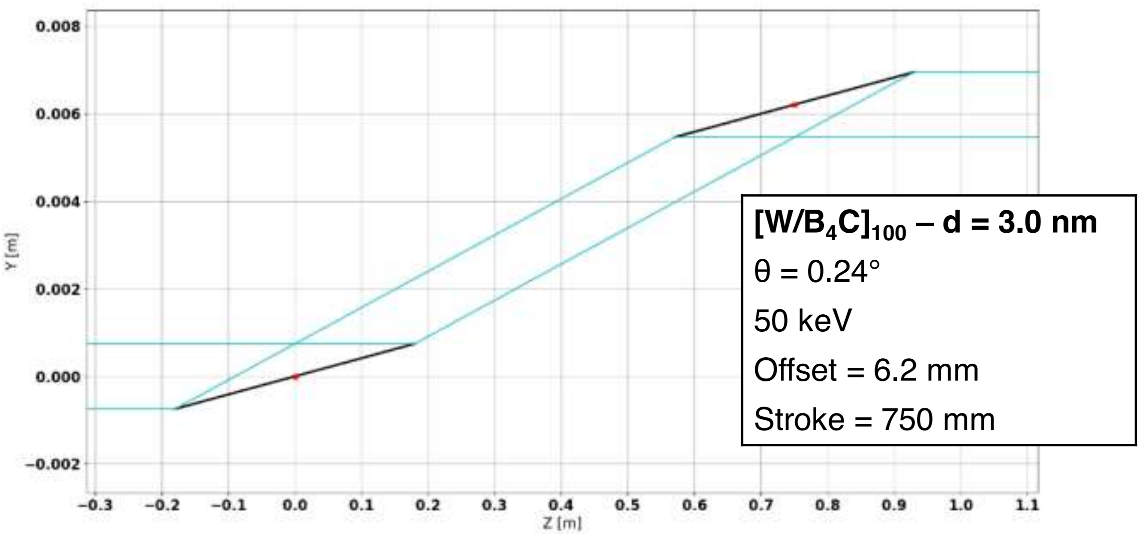

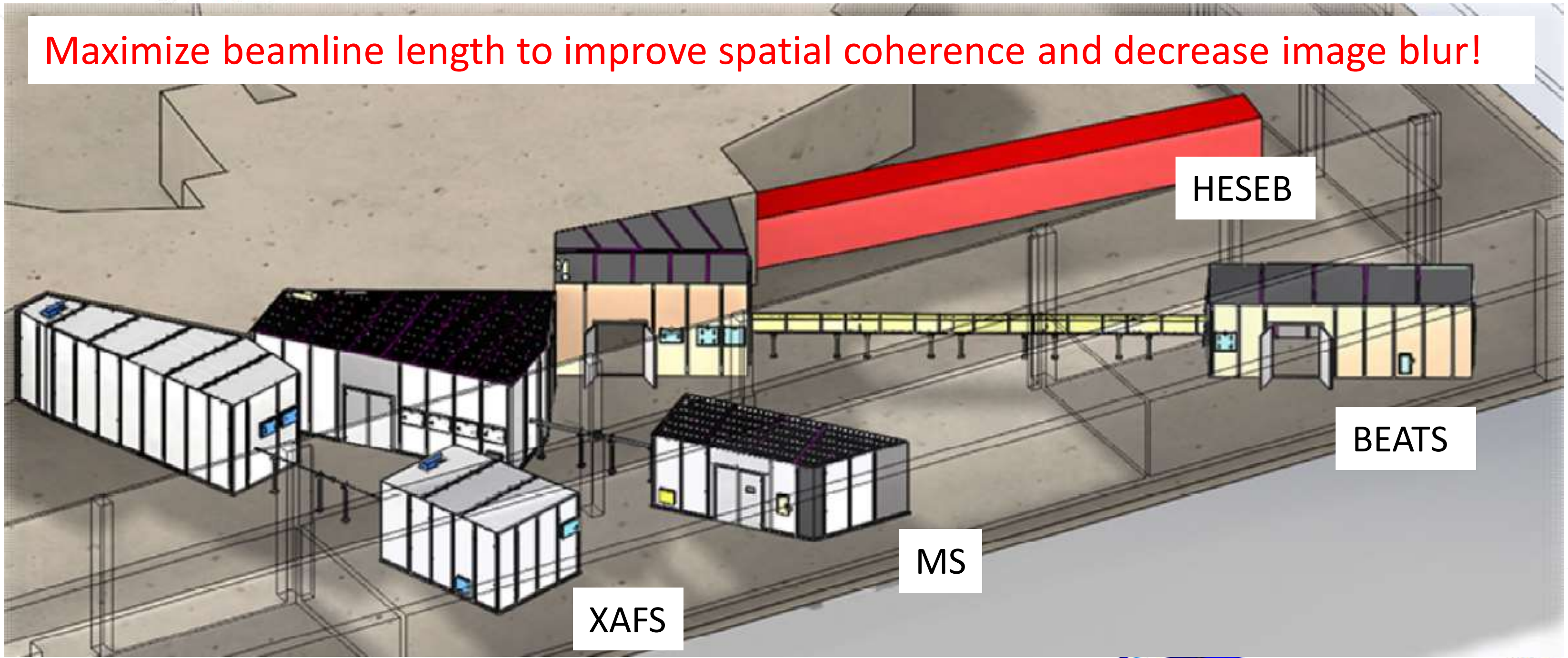

$$blur = \frac{SDD\ \sigma_x}{d}$$

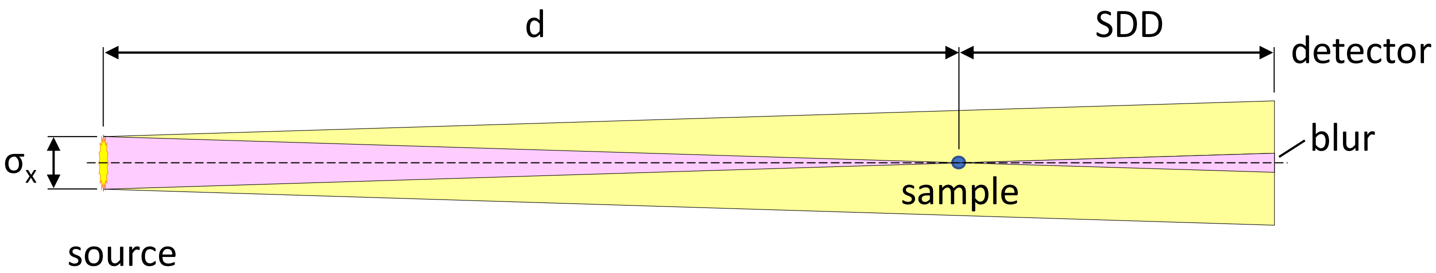

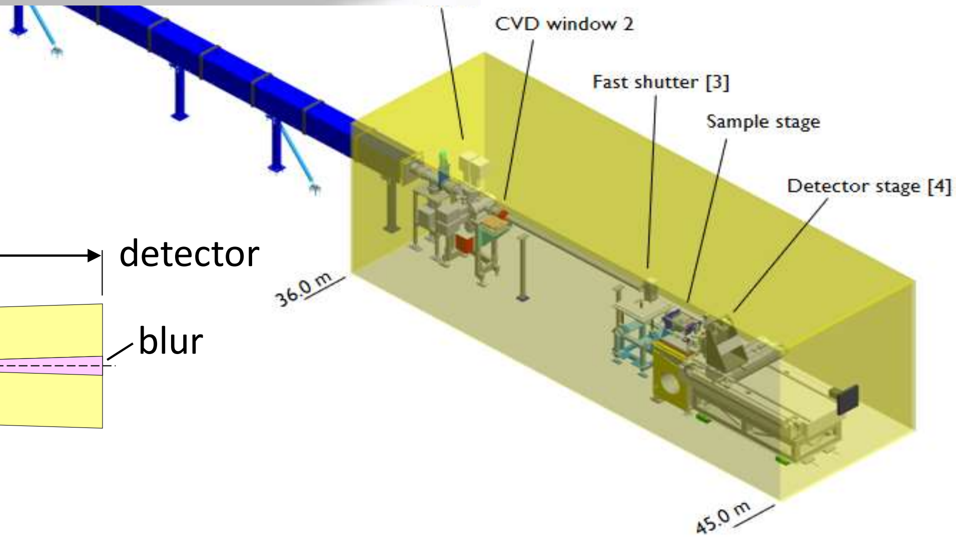

Raytracing and numerical simulation

- Design and verification of beamline optics
- Heat load on critical components
- Beamline performance
- Multilayers design
- DMM operation

Raytracing and numerical simulation

- Coherence length and blur

$$l_{coh} = \frac{2\lambda d}{\sigma_x}$$

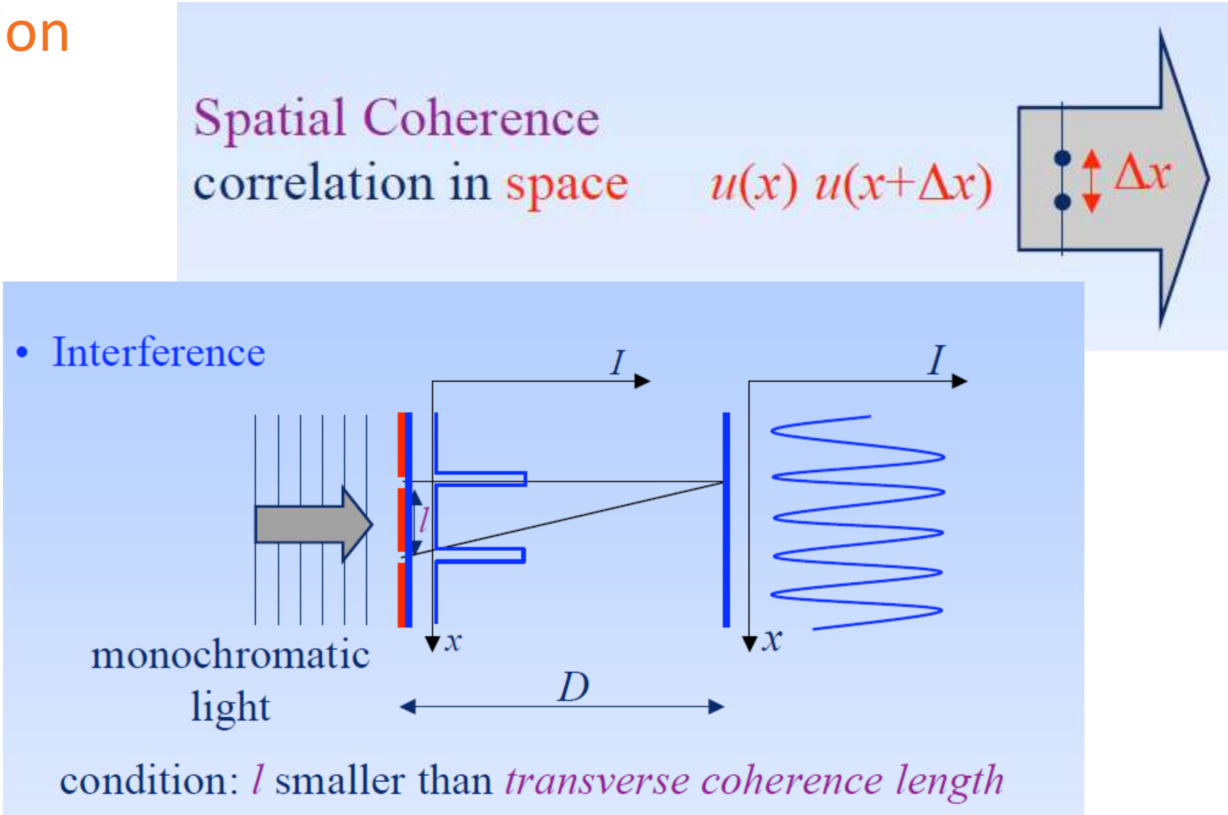

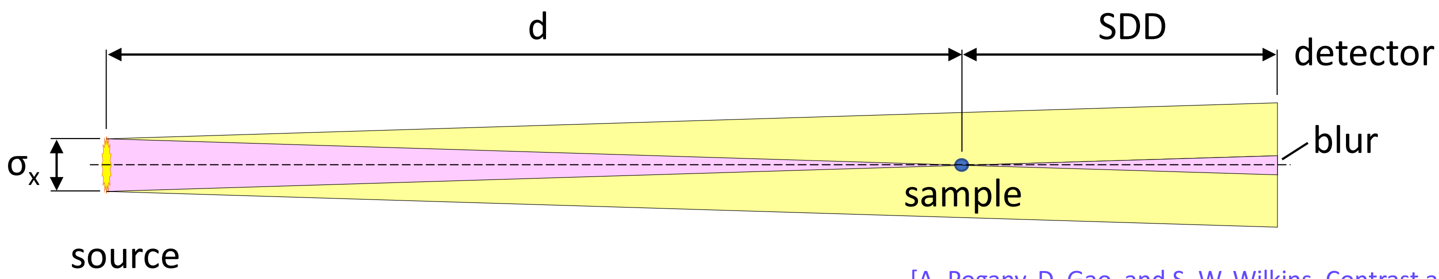

[A. Pogany, D. Gao, and S. W. Wilkins, Contrast and resolution in imaging with a microfocus x-ray source, 1997]
[P. Cloetens, Phase Contrast Imaging - Coherent Beams, School on X-ray Imaging Techniques at the ESRF, 2007]

Raytracing and numerical simulation

- Close Front-End slits (secondary source) for improved coherence

  ↓

  <u>phase contrast</u>

- This reduces available flux and beam size!

Beamline	d [m]	σ_x [µm]	Transverse coherence length [µm]
ID19@ESRF	145	25	720.1
TOMCAT@SLS	34	140	30.2
SYRMEP@Elettra	23	197	14.5
TopoTomo@ANKA	33	500	8.2
BEATS - Primary slits OPEN	43	1978	2.7
BEATS - Primary slits: 1 mm (H)	34.6	1000	4.3
BEATS - Primary slits: 0.5 mm (H)	34.6	500	8.6

Table 9: transverse coherence length at 20 keV. Comparison of BEATS with other tomography beamlines.

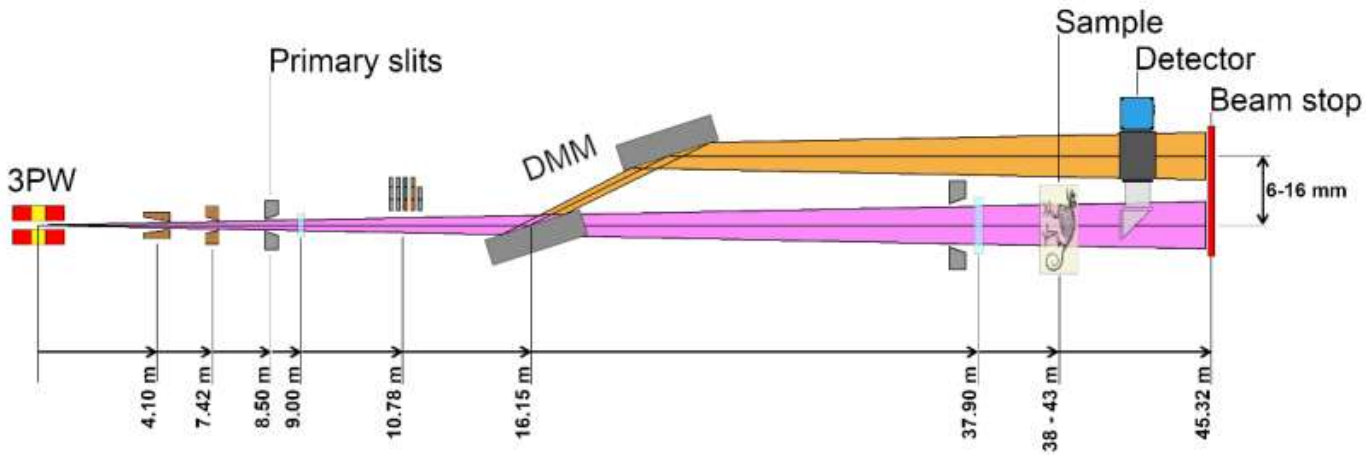

Raytracing and numerical simulation

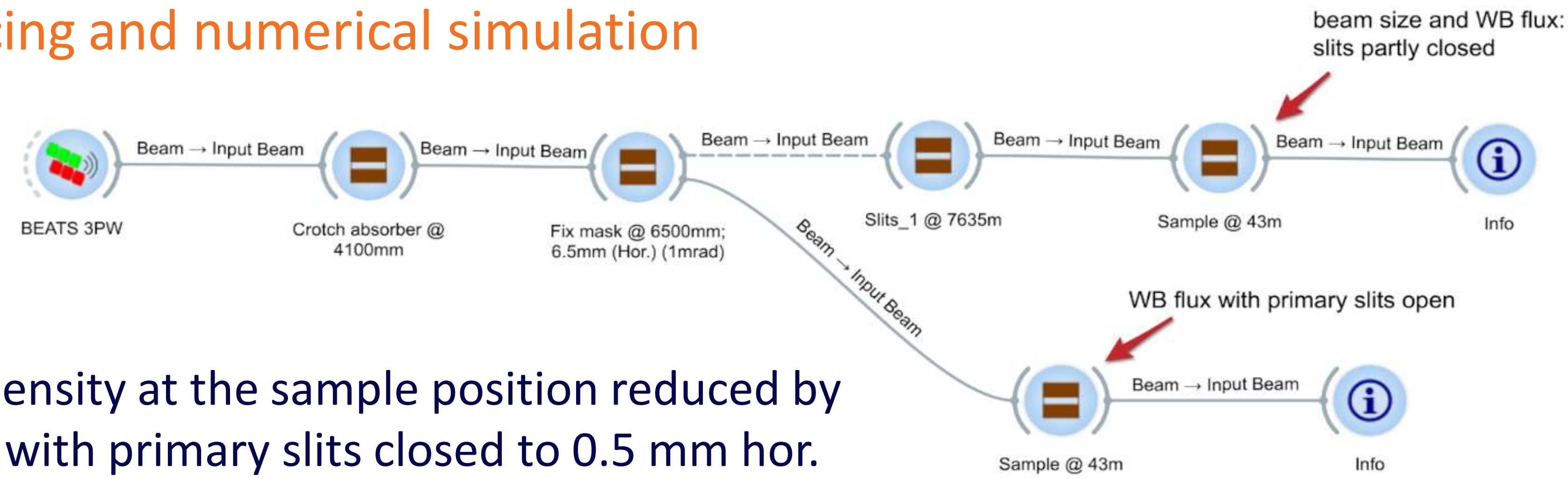

- Flux density at the sample position reduced by ~70% with primary slits closed to 0.5 mm hor.

- The beam size is OK

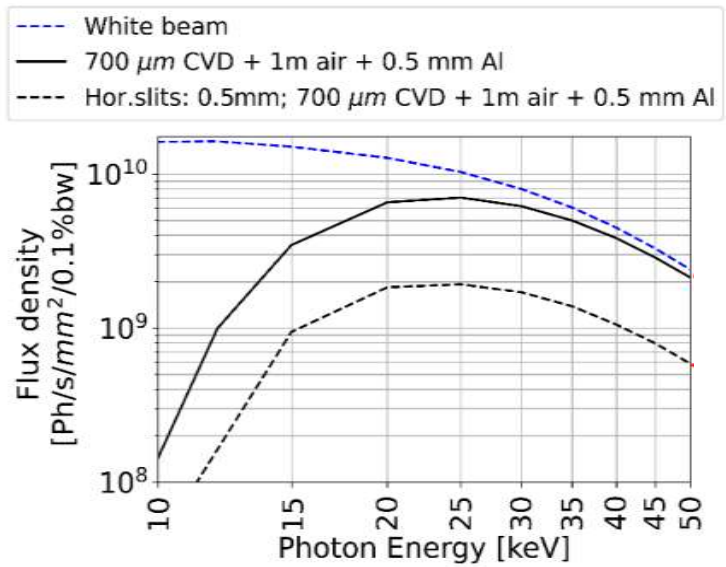

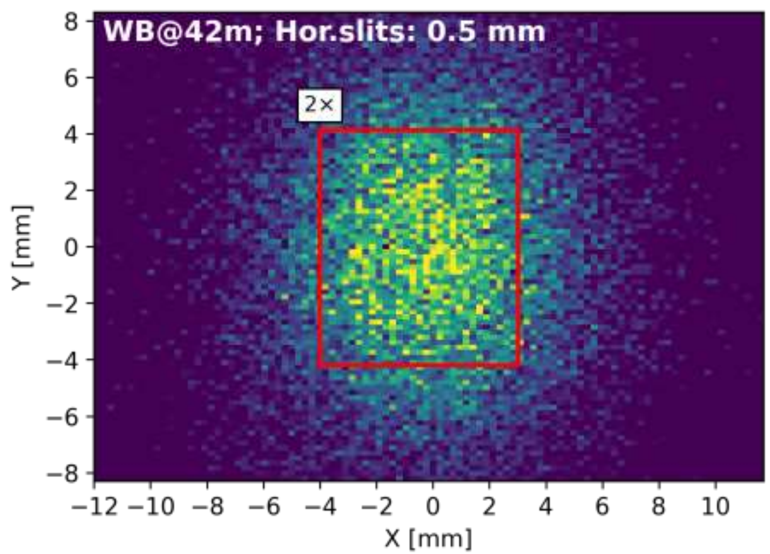

Thermal and mechanical verification

Chemical Vapor Deposition (CVD) diamond window

- Power density distribution simulated with XOP is used as input for ANSYS non-linear thermal-structural analysis
- The window must sustain the white beam heat load and Δp = 1 bar

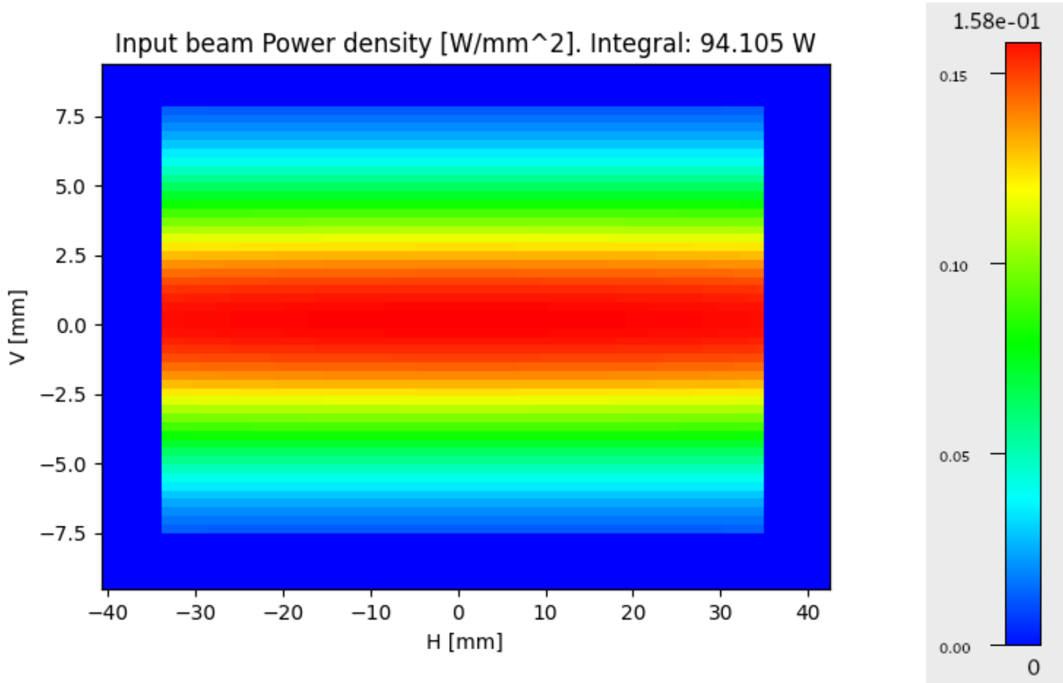

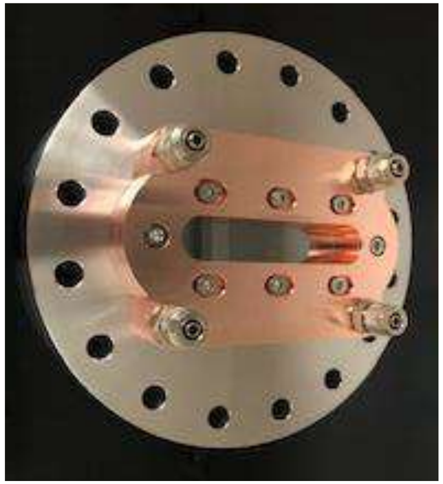

Diamond Materials GmbH

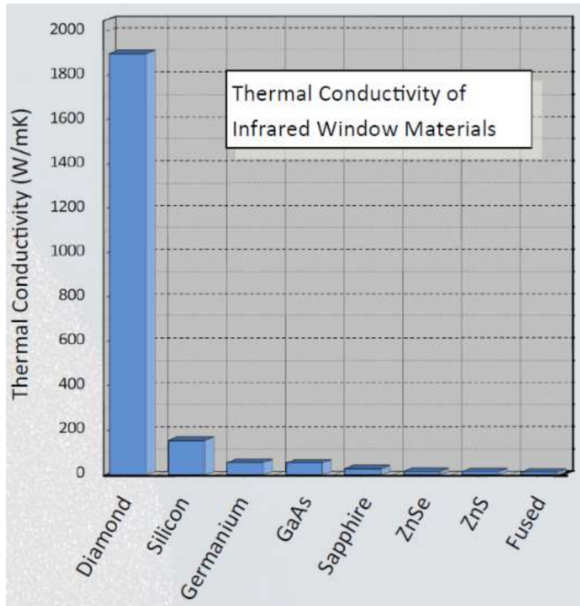

Thermal and mechanical verification

Chemical Vapor Deposition (CVD) diamond window

- Power density distribution simulated with XOP is used as input for ANSYS non-linear thermal-structural analysis
- The window must sustain the white beam heat load and Δp = 1 bar

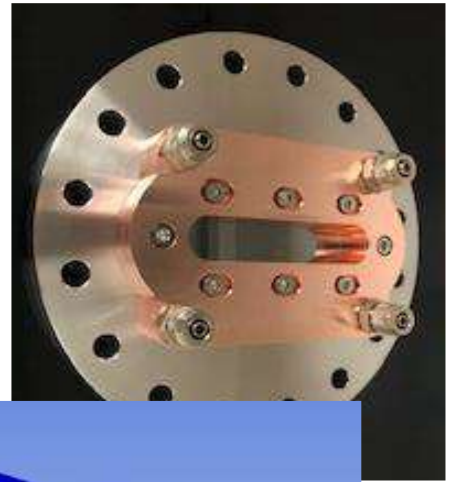

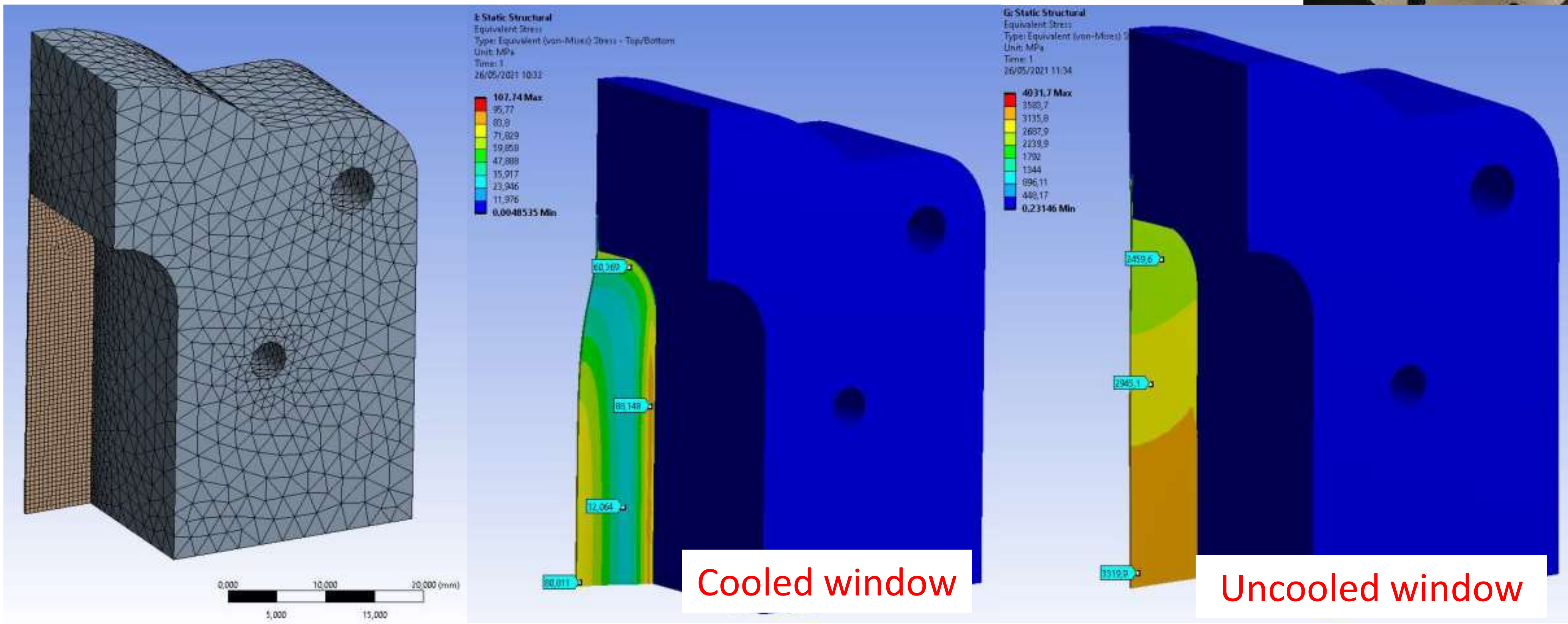

BEATS experimental station

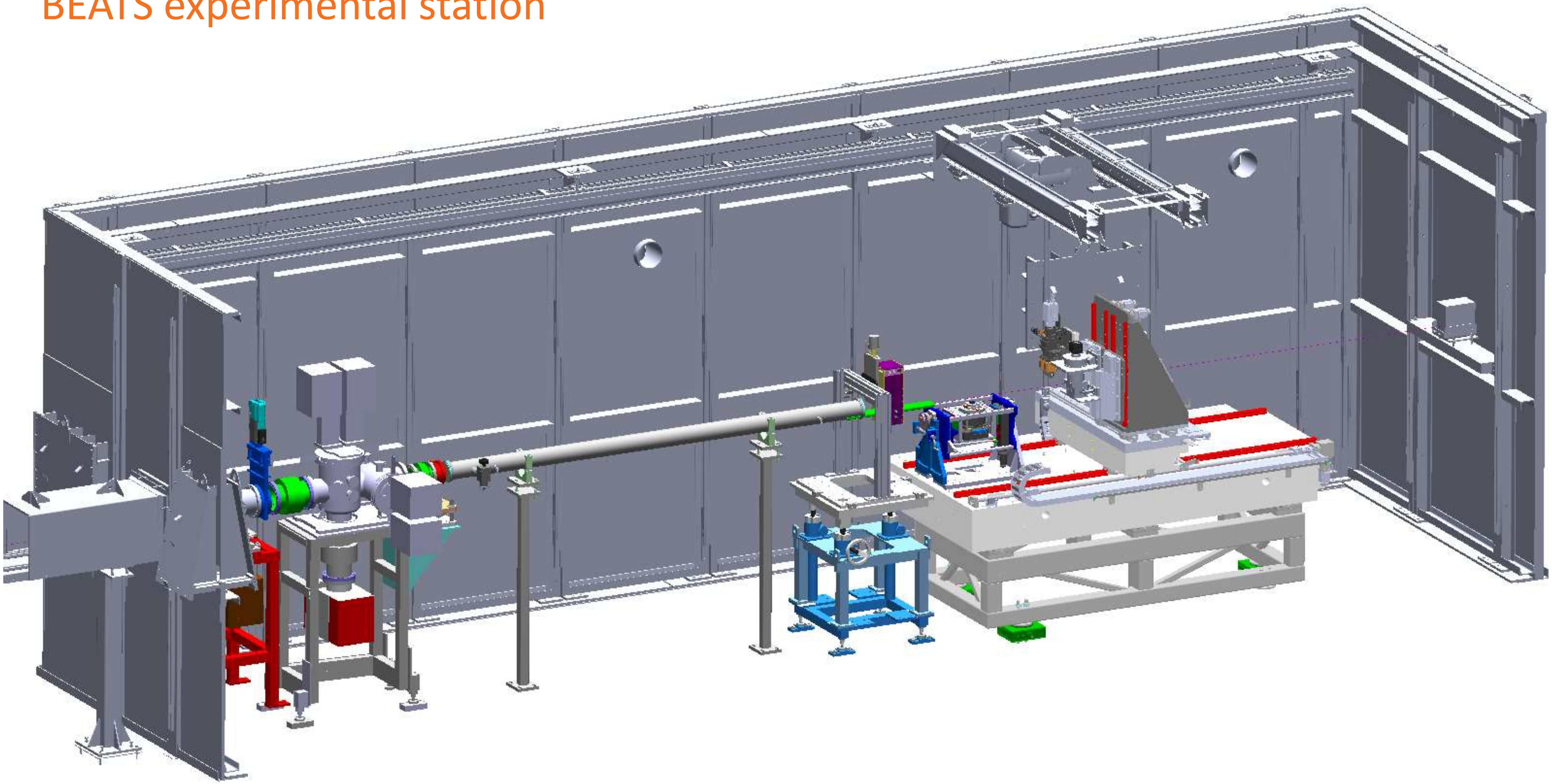

BEATS experimental station

Fast shutter: protect samples and limit X-Ray exposure time

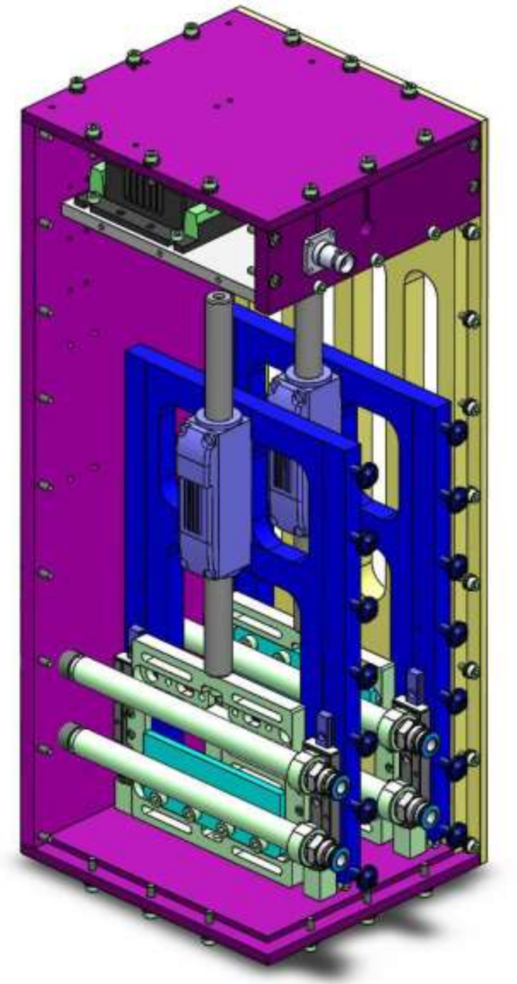

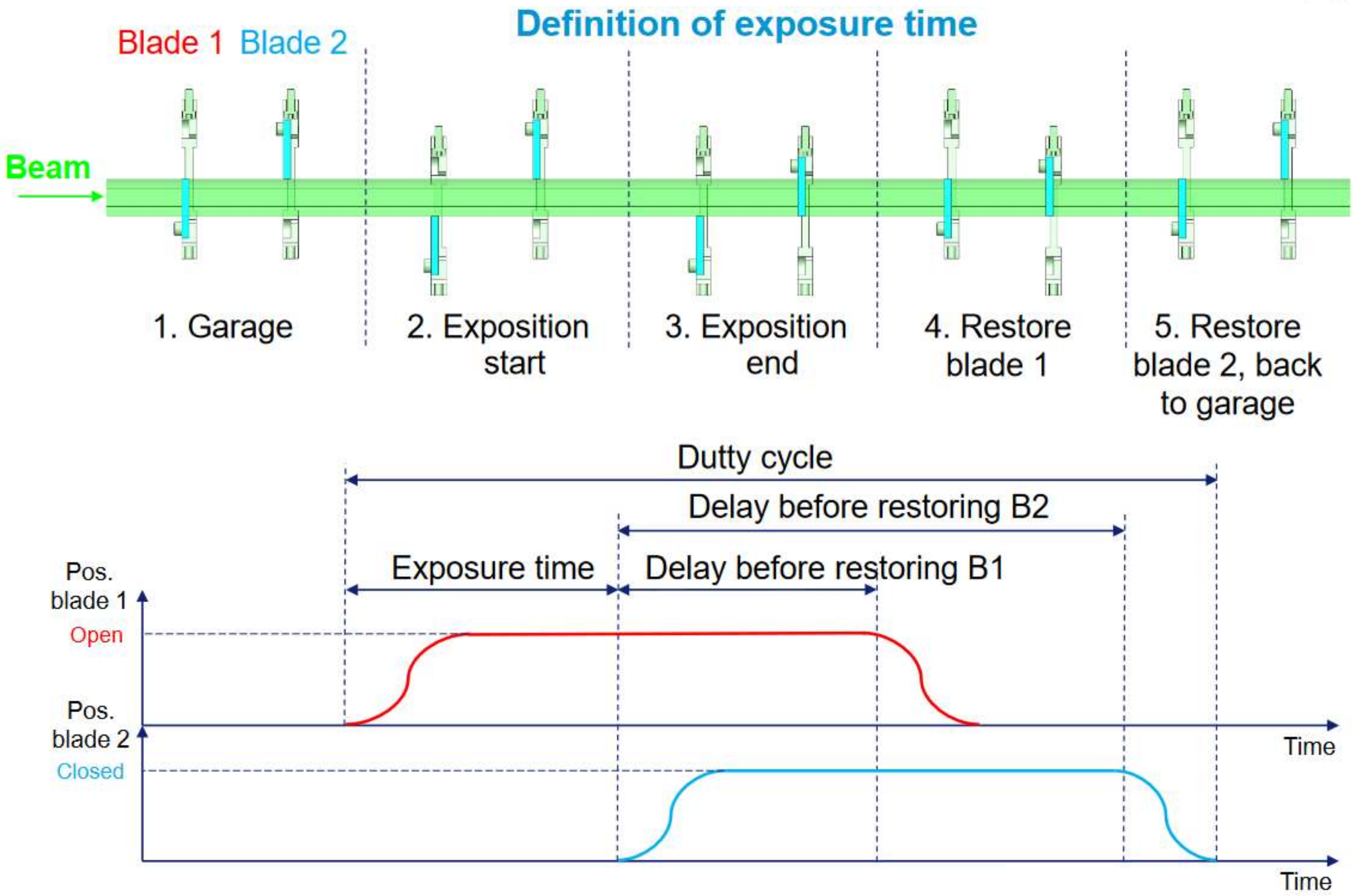

[C. Muñoz Pequeño et al., "Development of a Linear Fast Shutter for BM05 at ESRF and BEATS at SESAME", MEDSI'20]

BEATS experimental station

Sample and detectors stage

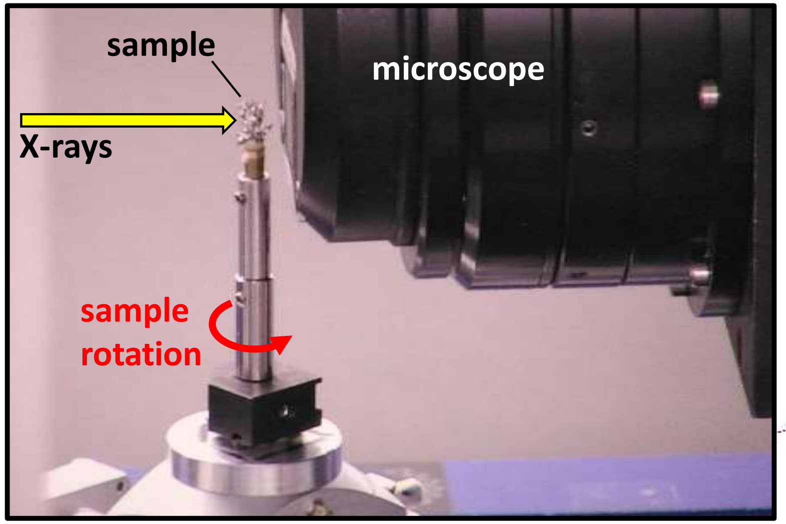

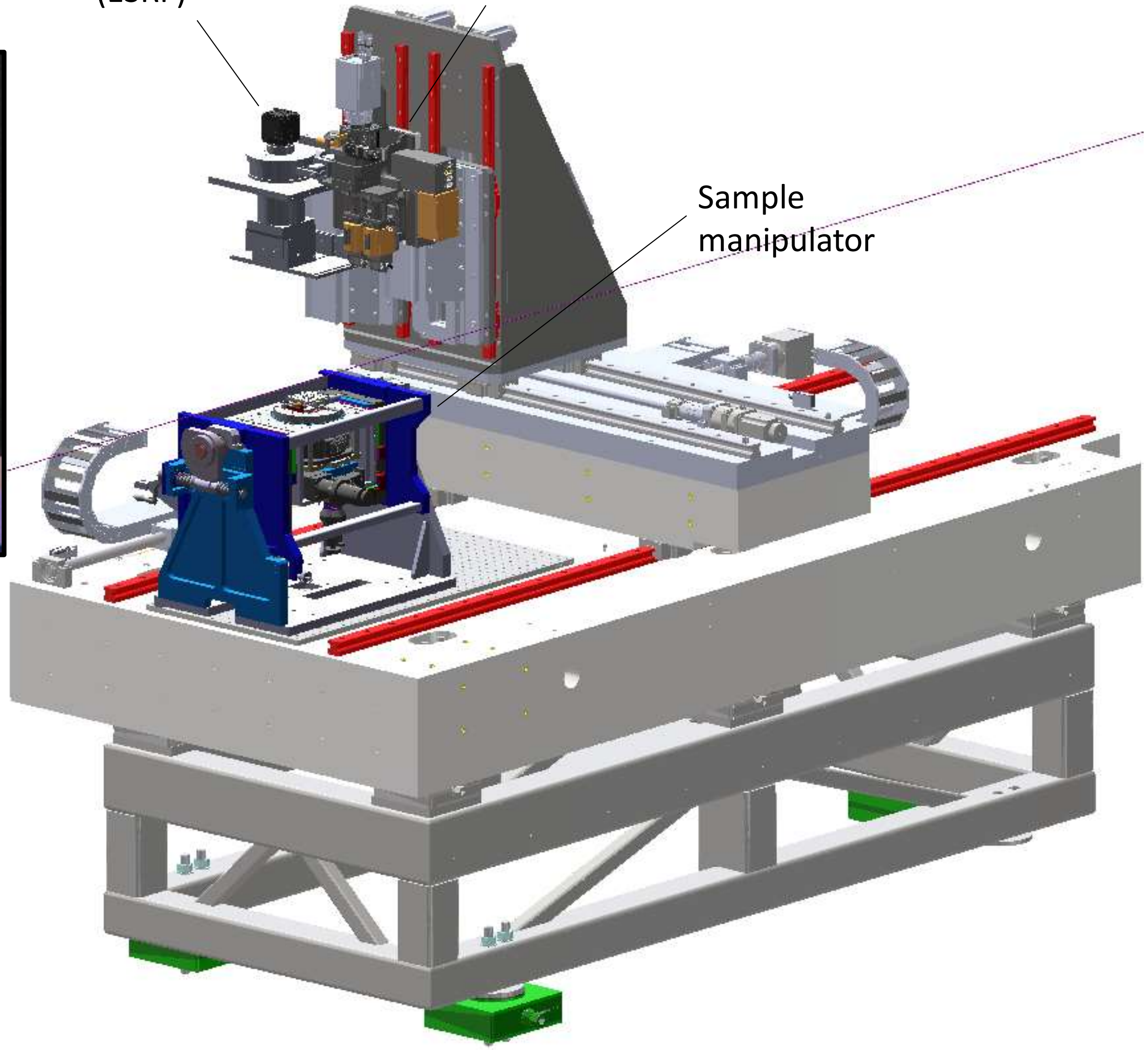

- Sample rotation
- Sample pitch
- X-Y rot. axis positioning
- Remove sample from Field Of View
  (for flat fields)
- Sample-detector propagation distance
- Scan Region Of Interest

BEATS

BEAmline for Tomography at SESAME

BEATS experimental station

Detector stage

Fortune Mokoena (University of Johannesburg)
Pierre Van Vaerenbergh (ESRF)

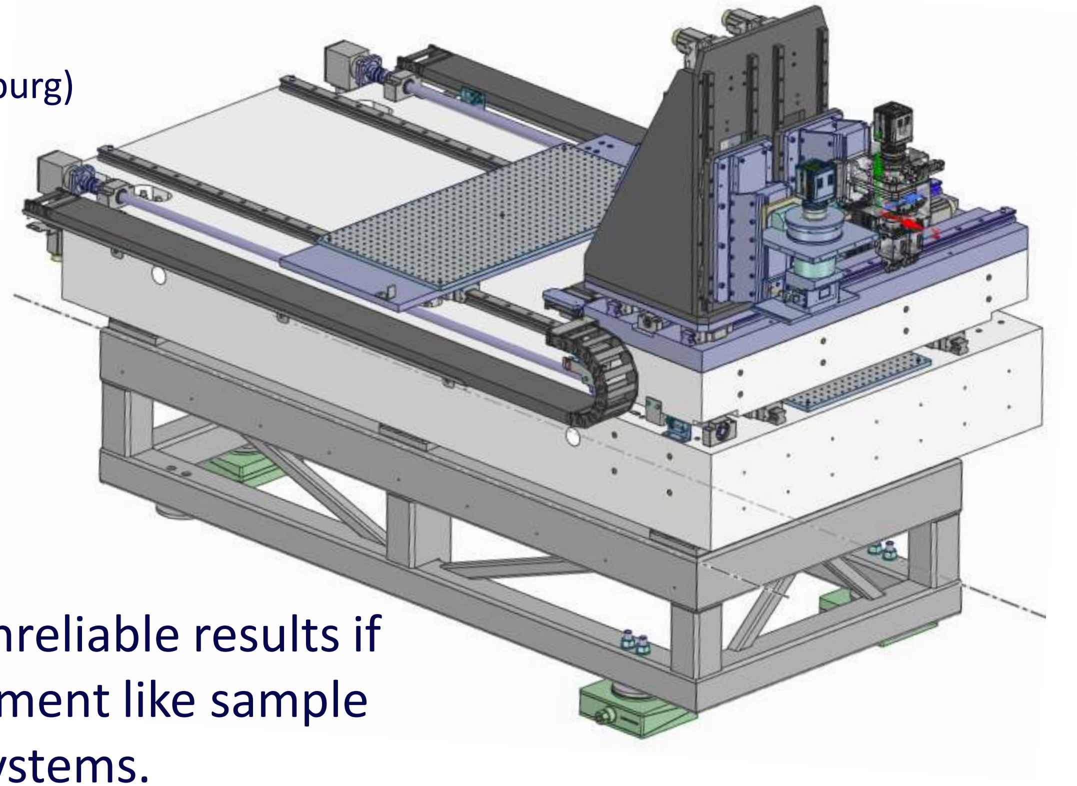

- Synergy with ESRF BM5
- Support for 2 detectors

- Floor vibrations can lead to unreliable results if transmitted to sensible equipment like sample environment and detection systems.

- Characterize vibrational stability to minimize the effect of vibrations on the detectors.

ALBA · The Cyprus Institute · DESY. · Elettra Sincrotrone Trieste · ESRF · INFN · PSI · SESAME · SOLARIS · UNIVERSITY OF JOHANNESBURG

BEATS experimental station

BEATS Detector stage Random Vibration Analysis

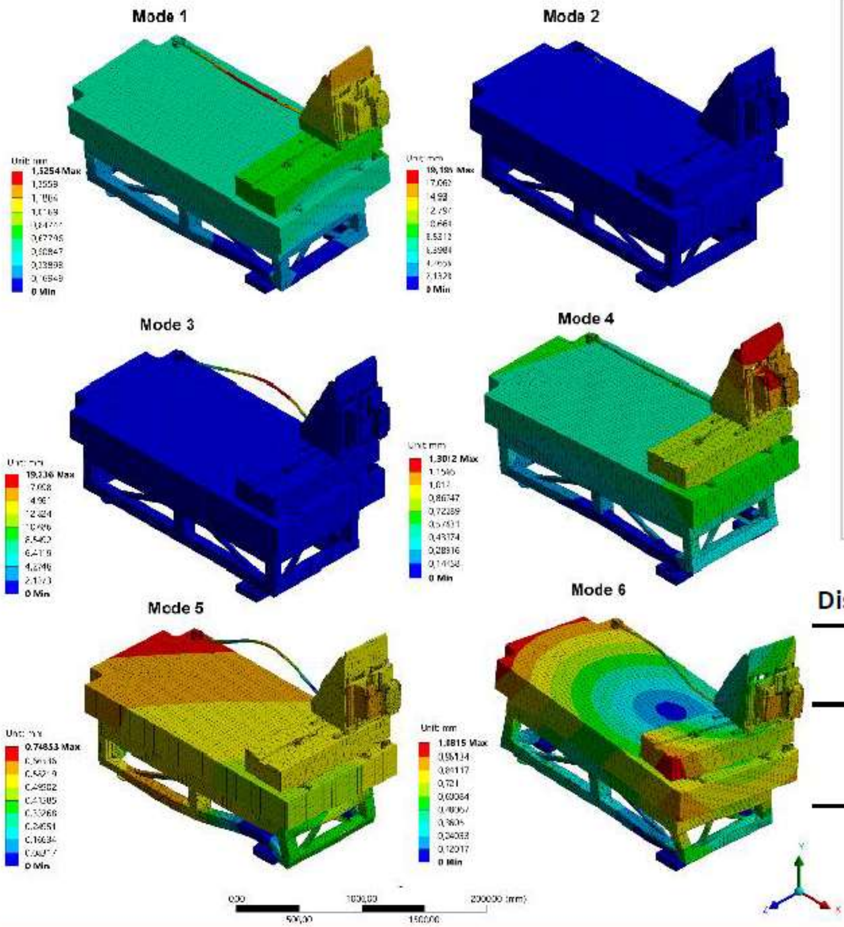

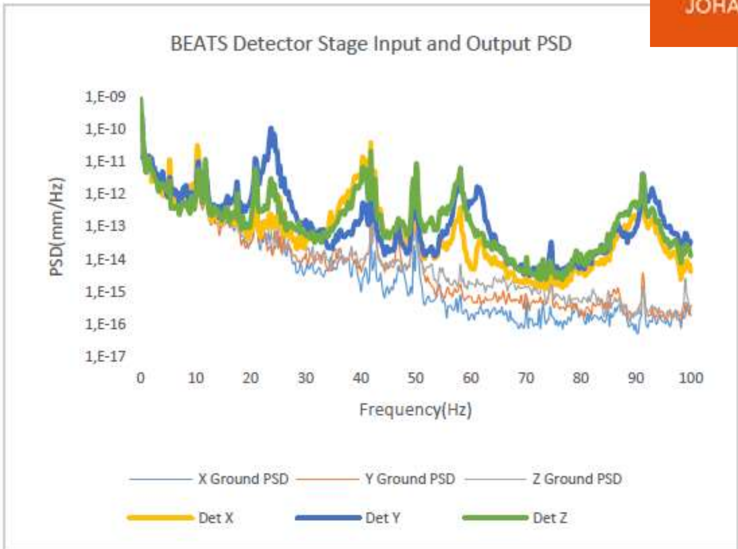

Displacement RMS values

Direction	Ground [nm]	Detector [nm]
X(H)	8	10
Y(H)	12	17
Z(V)	14	15

Modal Frequencies

Mode	Frequency [Hz]
1	24
2	35
3	35
4	41
5	62

[F. Mokoena et al., "An FEA Investigation of the Vibration Response of the BEATS Detector Stage", MEDSI'20]

BEATS experimental station

X-Ray microscope

- Absorption efficiency of different scintillator screens of 350 µm thickness

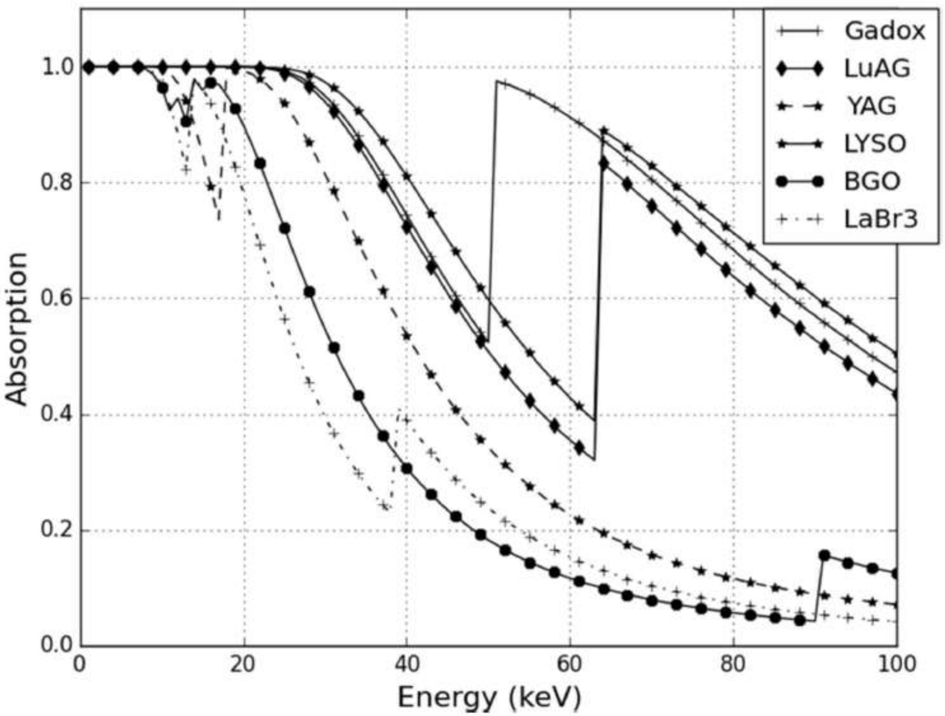

[A. Mittone et al. Journal of Synchrotron Radiation, 2017]

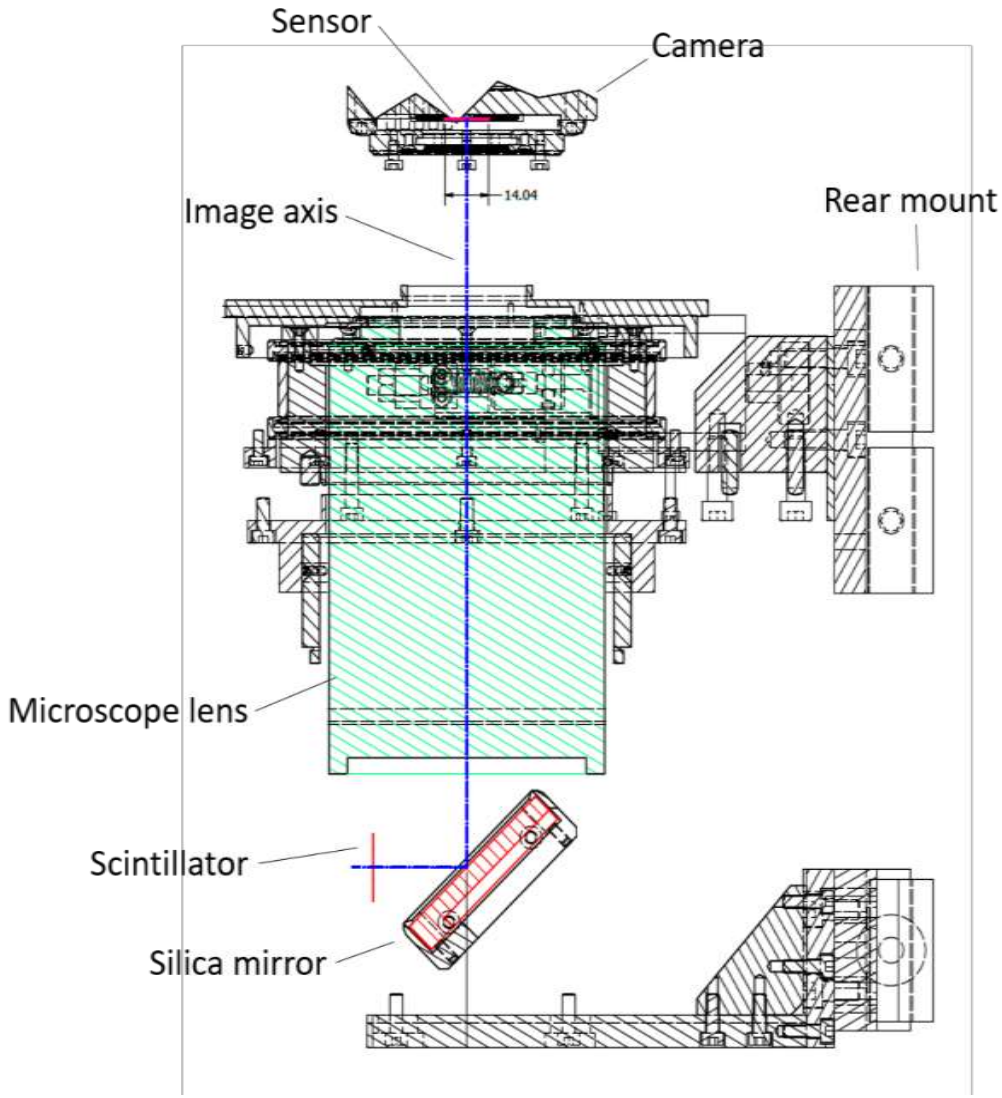

White beam @42m

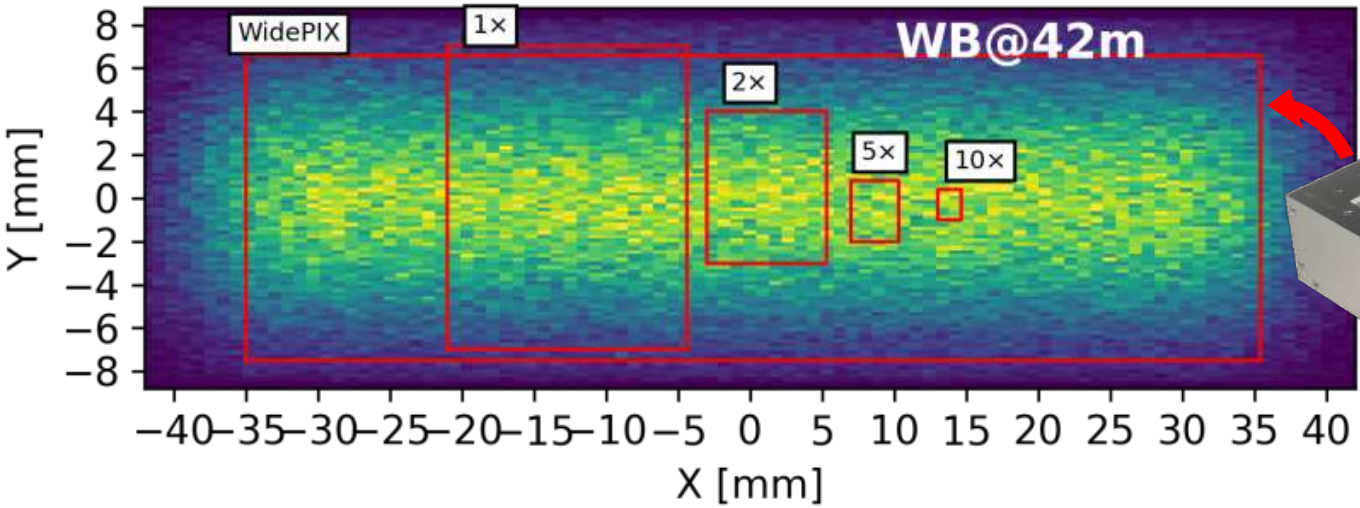

Magnif.	Field of view	Pixel size
1×	16.6 × 14.0 mm^2	6.5 µm
2×	8.3 × 7.0 mm^2	3.25 µm
5×	3.4 × 2.8 mm^2	1.3 µm
10×	1.7 × 1.4 mm^2	0.65 µm

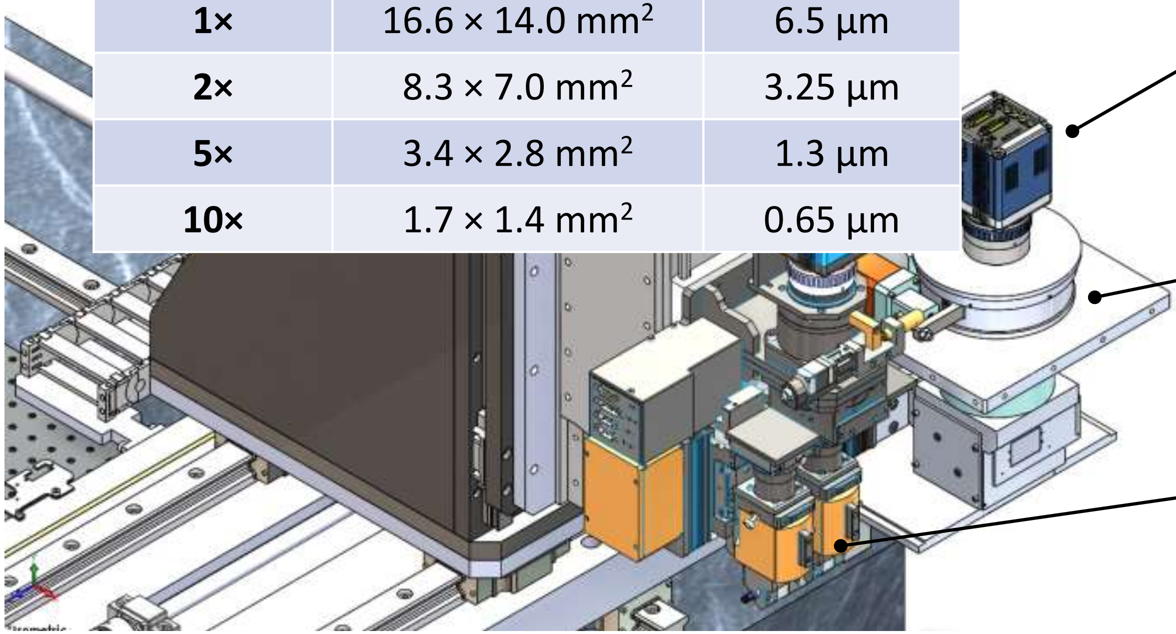

Sample environments for in-situ studies

Sample furnace

- Review of sample furnace implementations
- Resistive vs inductive heating

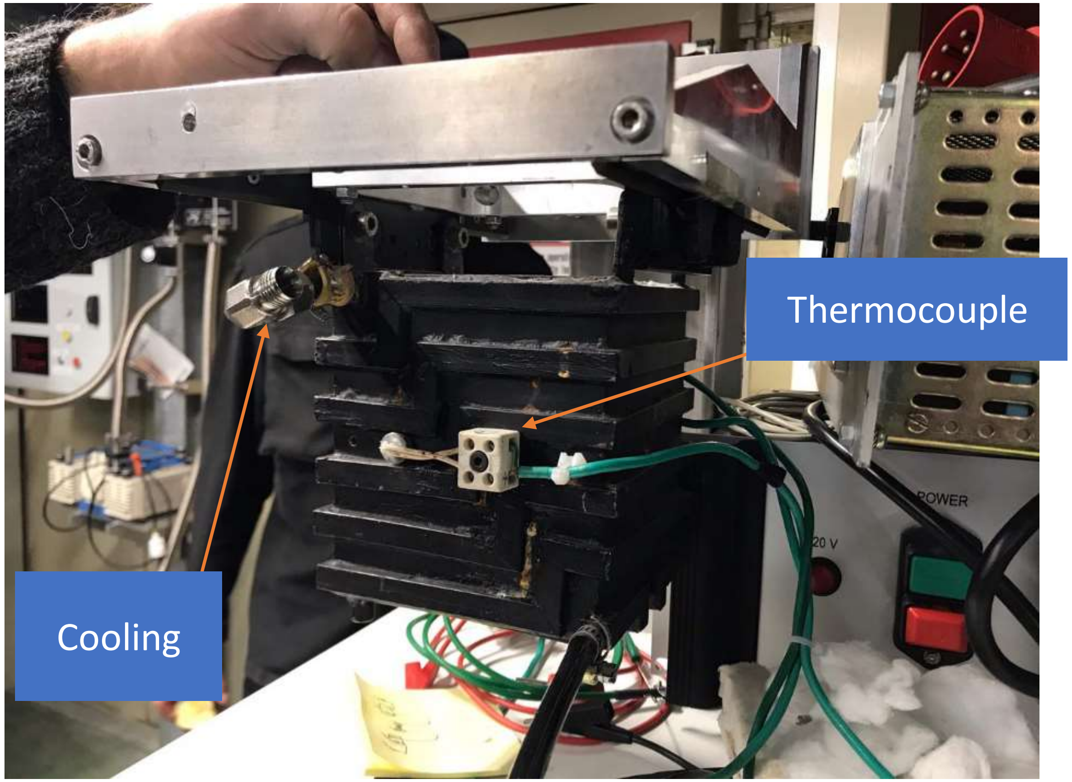

Sample environments for in-situ studies

Sample furnace – Induction heating

UNIVERSITY OF JOHANNESBURG

- Enables control of sample environment during heating
- Superior control of heating gradient up to 1800 C
- Requires slip ring for coolant and flushing with inert gas

[F. Mokoena, M.Sc. thesis]

Sample environments for in-situ studies

Sample furnace – Induction heating

- Design optimization:
  - Crucible architecture
  - Temperature control and convection regime around sample
  - Isolation of slip ring and sensitive equipment
  - Simulate different sample materials and sizes
  - Predict cooling flow rate for experiments at the beamline

Fortune Mokoena

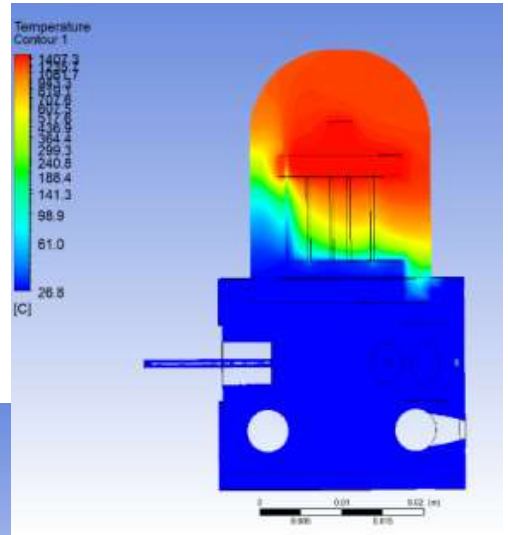

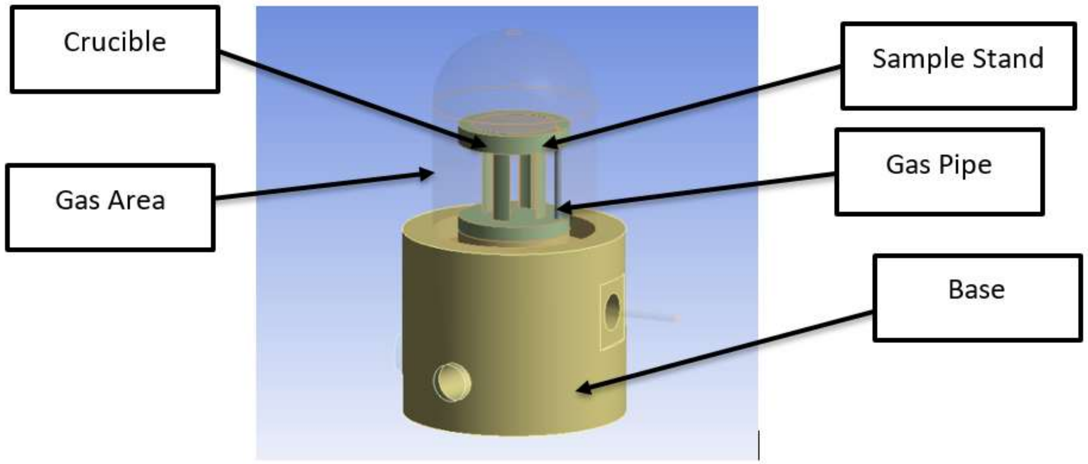

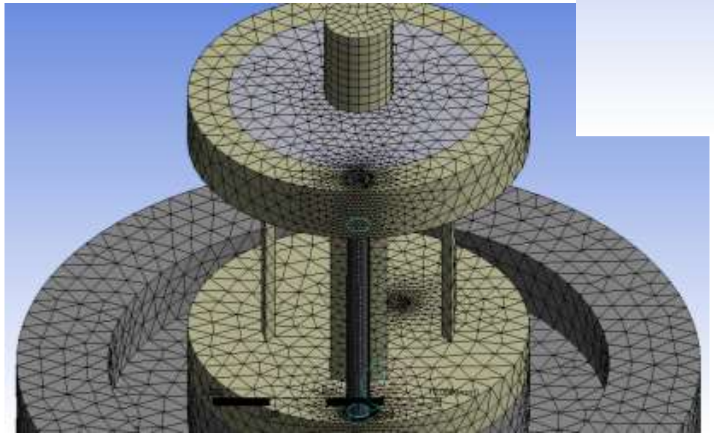

[F. Mokoena, M.Sc. thesis]

Sample environments for in-situ studies

Mechanical testing stage

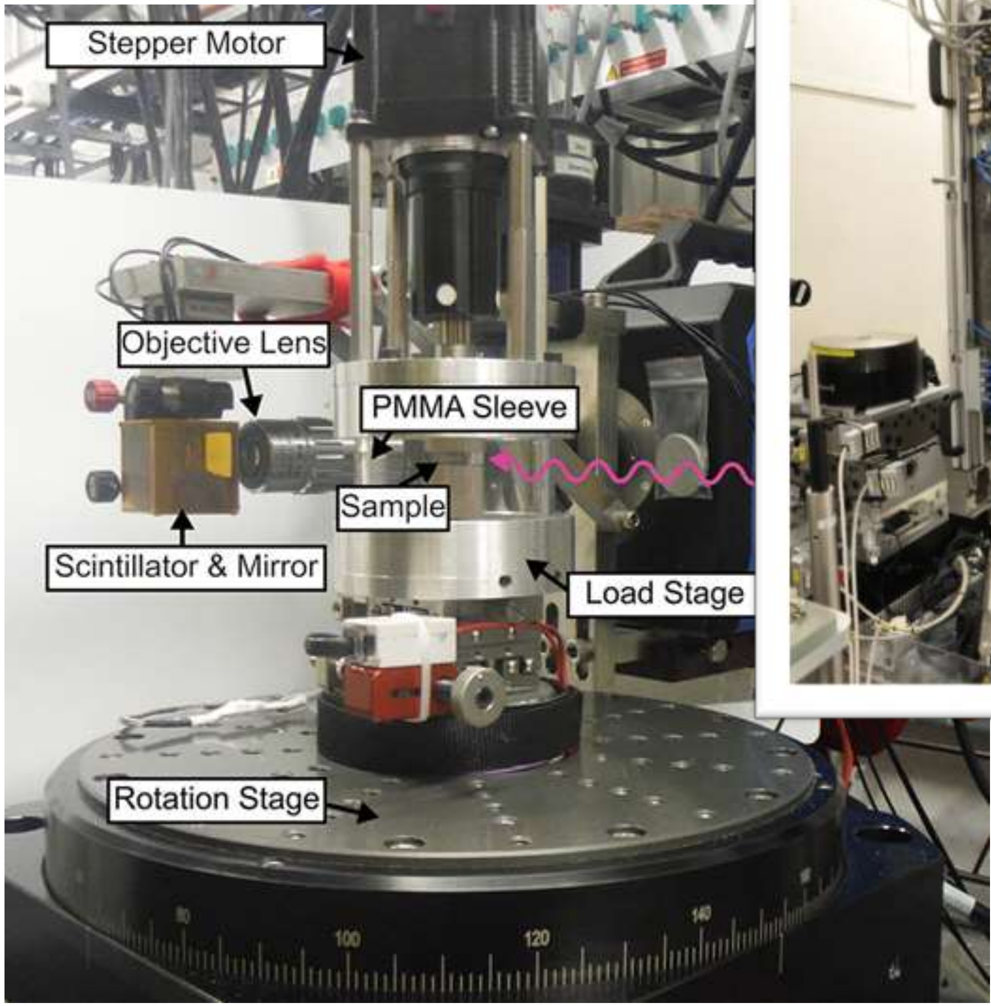

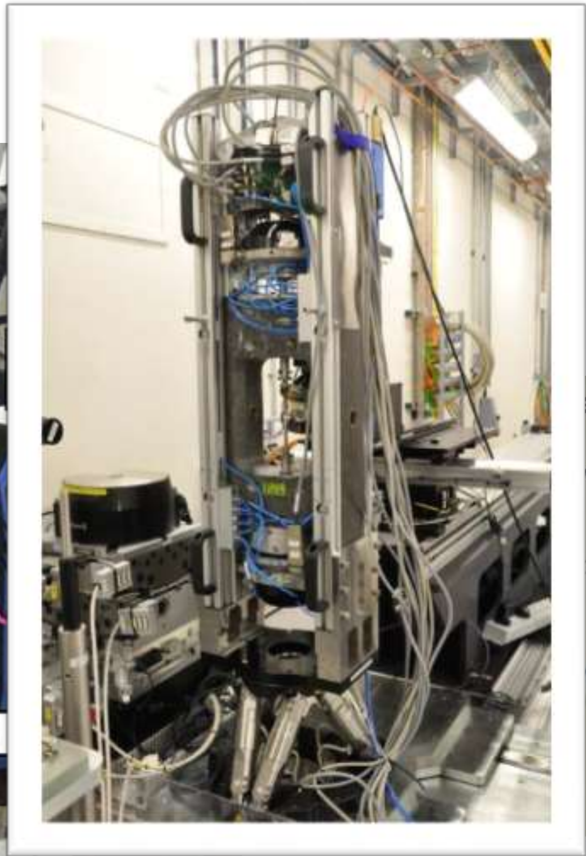

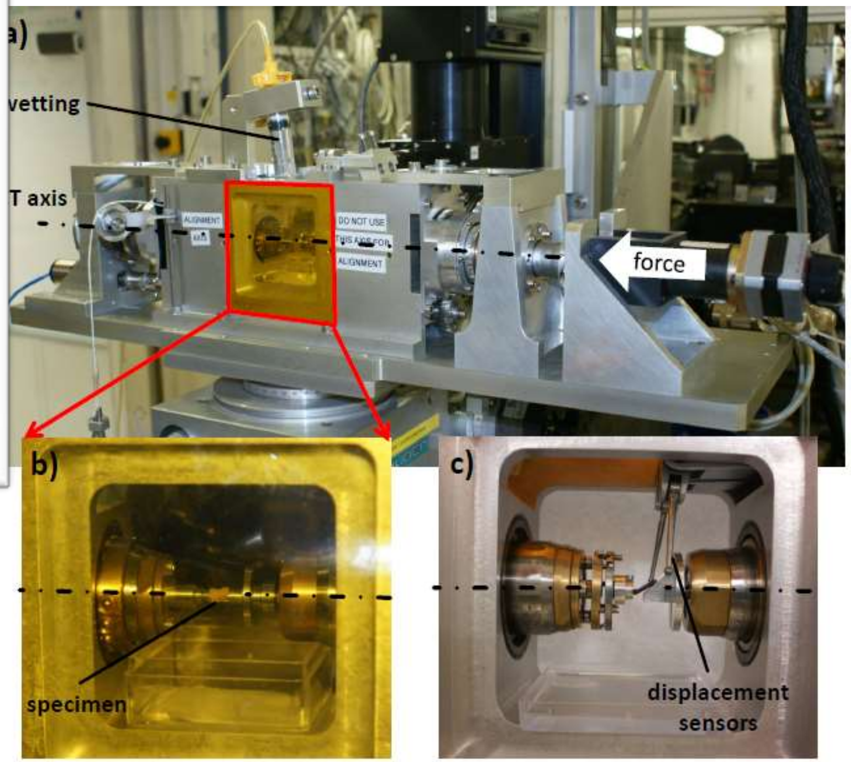

Part 2: Tomography Data Acquisition

Visible light benchmarking

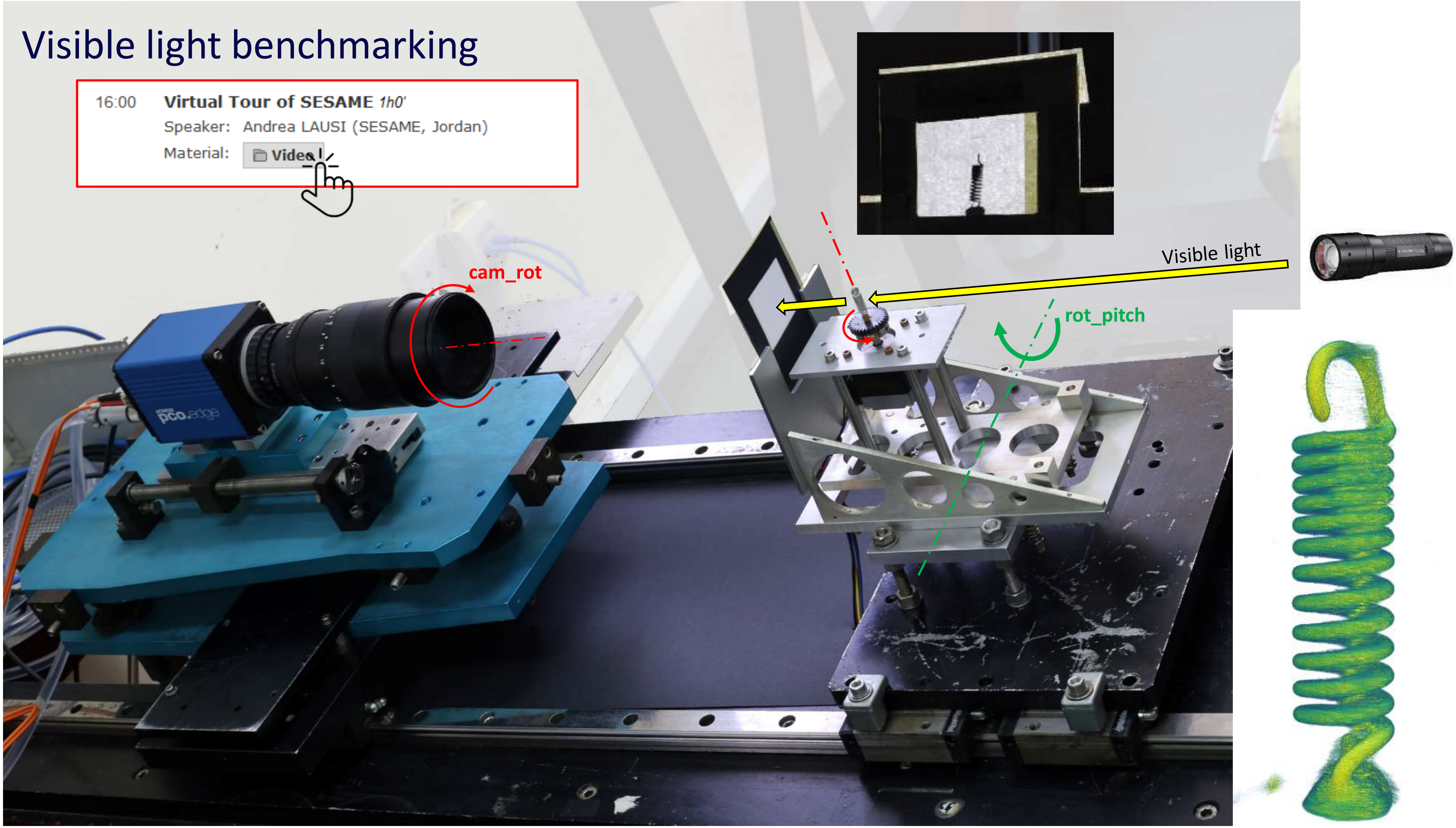

Tomographic data acquisition

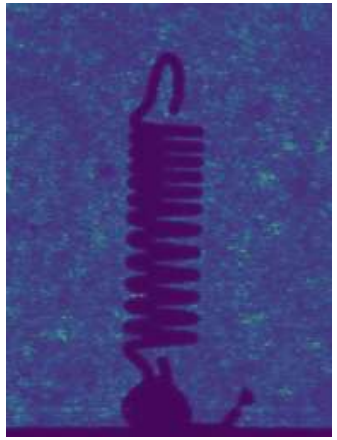

1. set rot motor to constant speed; start rot
2. wait until rot speed is stable
3. start record of n projections
4. stop record; stop rotation

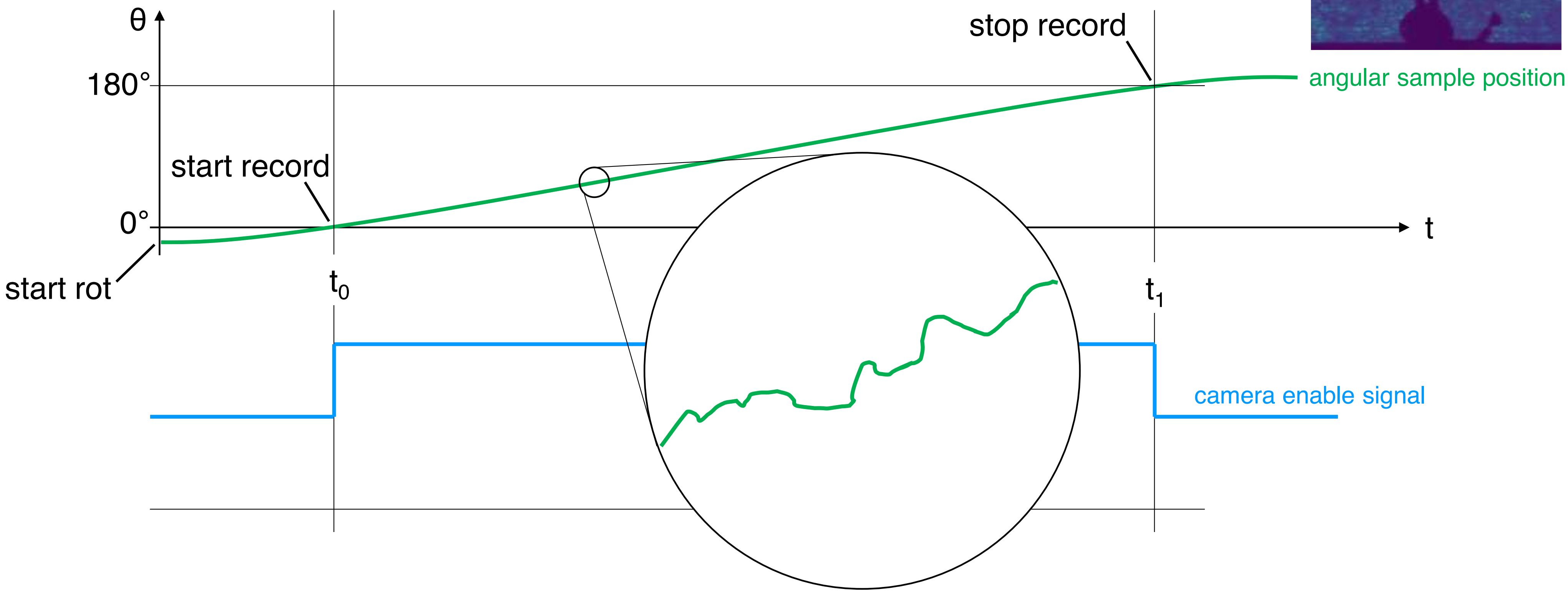

Tomographic data acquisition

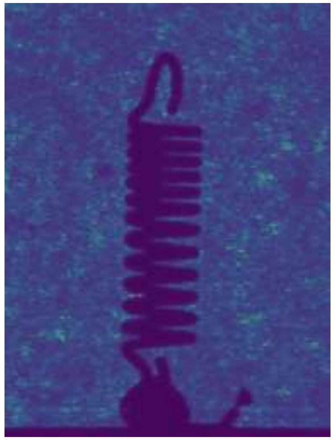

1. set rot motor to constant speed; start rot
2. wait until rot speed is stable
3. start record of n projections; **read angle position**
4. stop record; stop rotation

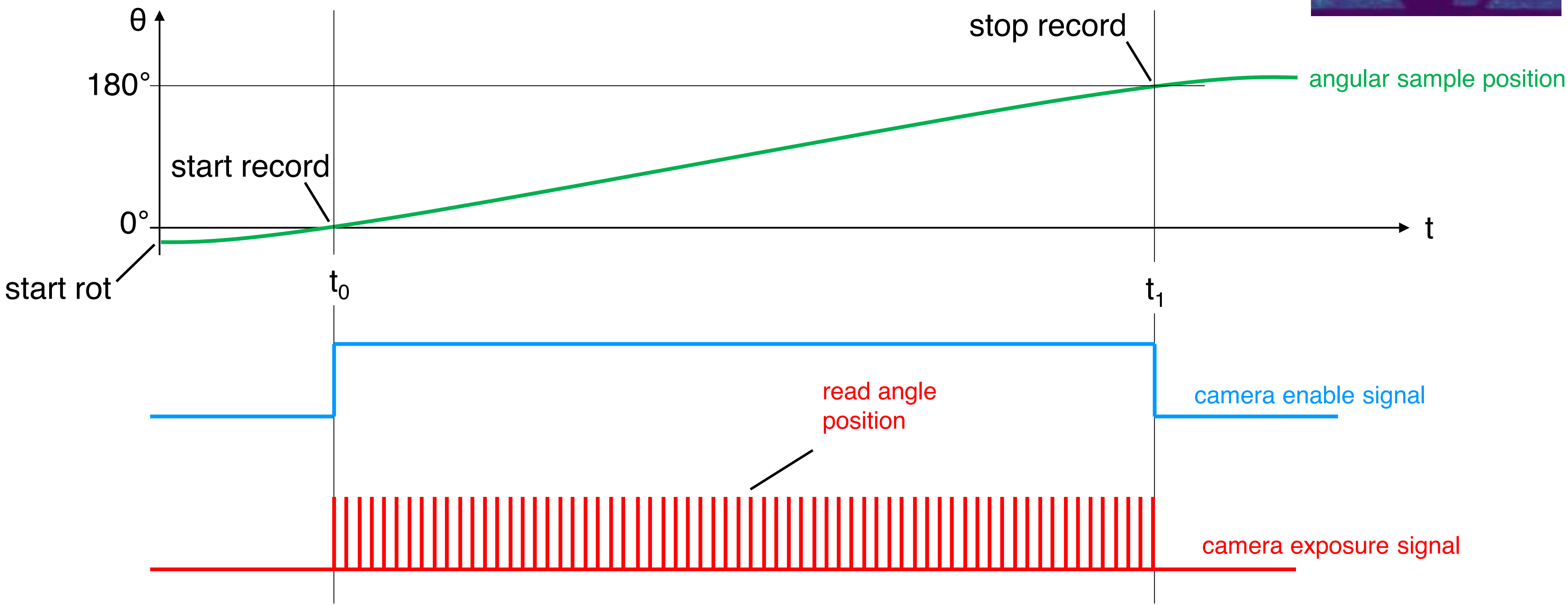

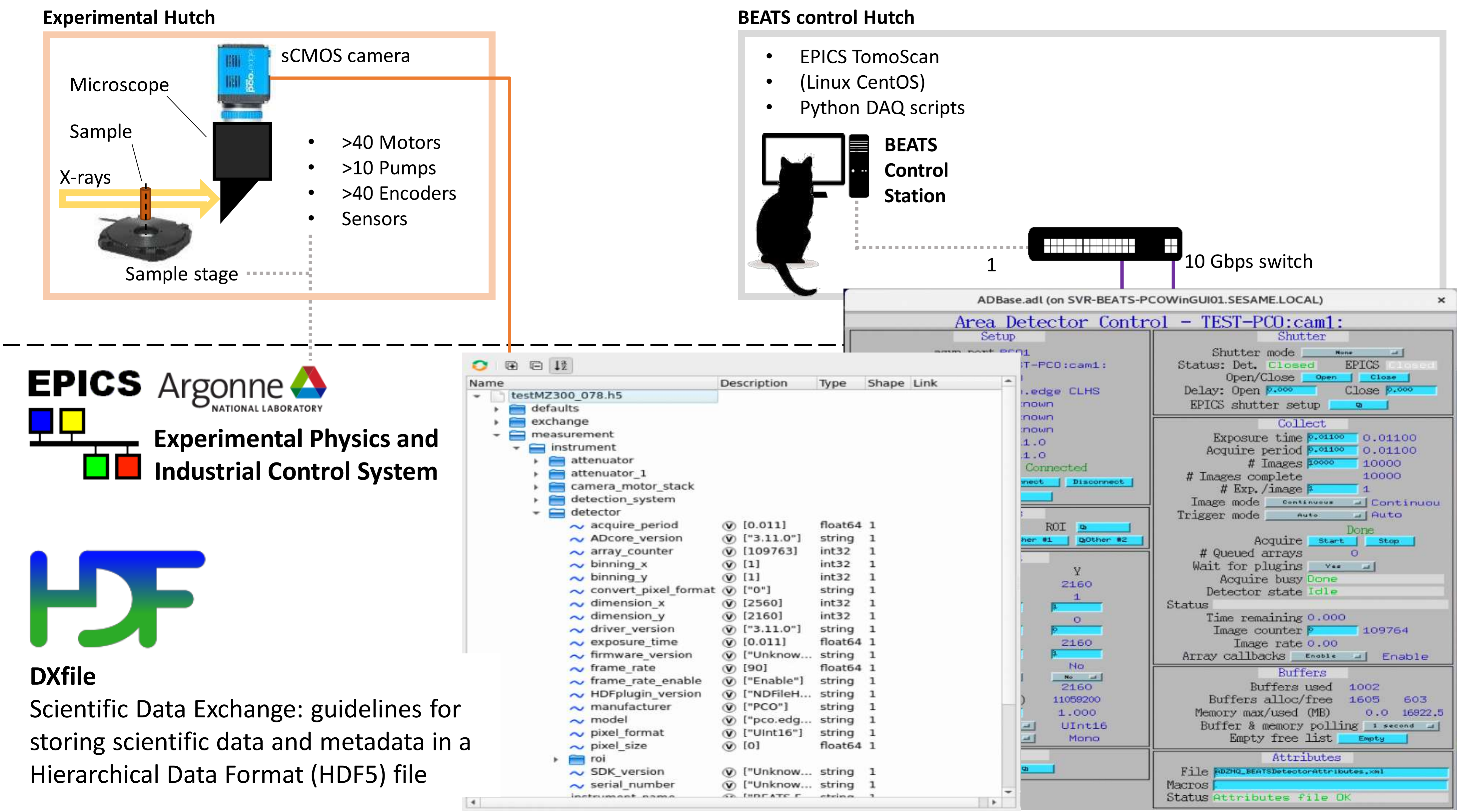

Experimental Hutch
sCMOS camera
Microscope
Sample
X-rays
Sample stage
>40 Motors
>10 Pumps
>40 Encoders
Sensors
BEATS control Hutch
EPICS TomoScan
(Linux CentOS)
Python DAQ scripts
BEATS Control Station
1
10 Gbps switch
EPICS
Argonne NATIONAL LABORATORY
Experimental Physics and Industrial Control System
DXfile
Scientific Data Exchange: guidelines for storing scientific data and metadata in a Hierarchical Data Format (HDF5) file
ADBase.adl (on SVR-BEATS-PCOWinGUI01.SESAME.LOCAL)
Area Detector Control - TEST-PCO:cam1:
Setup
Shutter
Collect
Buffers
Attributes
testMZ300_078.h5
defaults
exchange
measurement
instrument
attenuator
attenuator_1
camera_motor_stack
detection_system
detector
roi

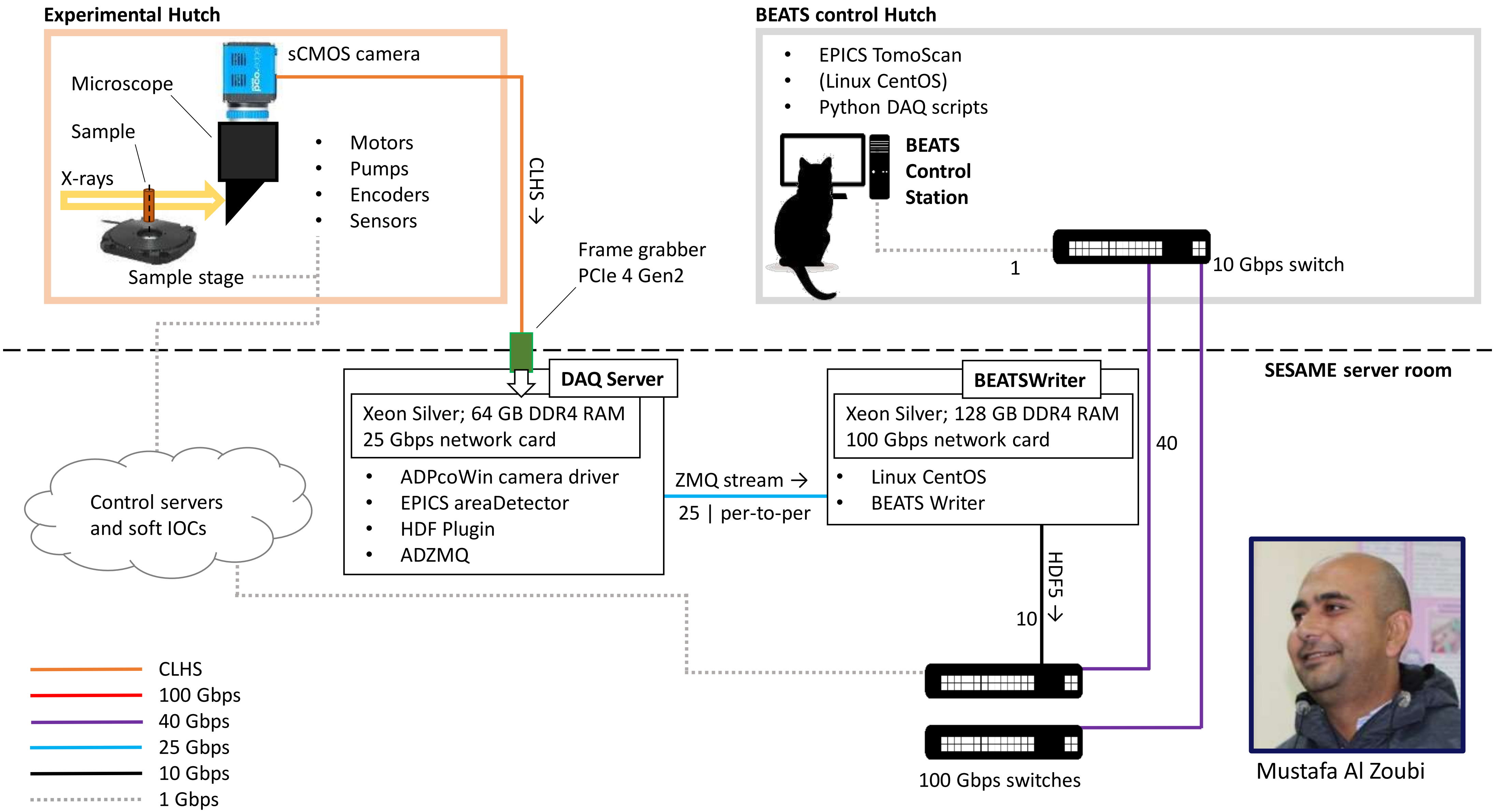

Experimental Hutch
sCMOS camera
Microscope
Sample
X-rays
Motors
Pumps
Encoders
Sensors
Sample stage
CLHS →
Frame grabber
PCIe 4 Gen2
BEATS control Hutch
EPICS TomoScan
(Linux CentOS)
Python DAQ scripts
BEATS
Control
Station
1
10 Gbps switch
SESAME server room
DAQ Server
Xeon Silver; 64 GB DDR4 RAM
25 Gbps network card
ADPcoWin camera driver
EPICS areaDetector
HDF Plugin
ADZMQ
ZMQ stream →
25 | per-to-per
BEATSWriter
Xeon Silver; 128 GB DDR4 RAM
100 Gbps network card
Linux CentOS
BEATS Writer
40
HDF5 →
10
Control servers
and soft IOCs
CLHS
100 Gbps
40 Gbps
25 Gbps
10 Gbps
1 Gbps
100 Gbps switches
Mustafa Al Zoubi

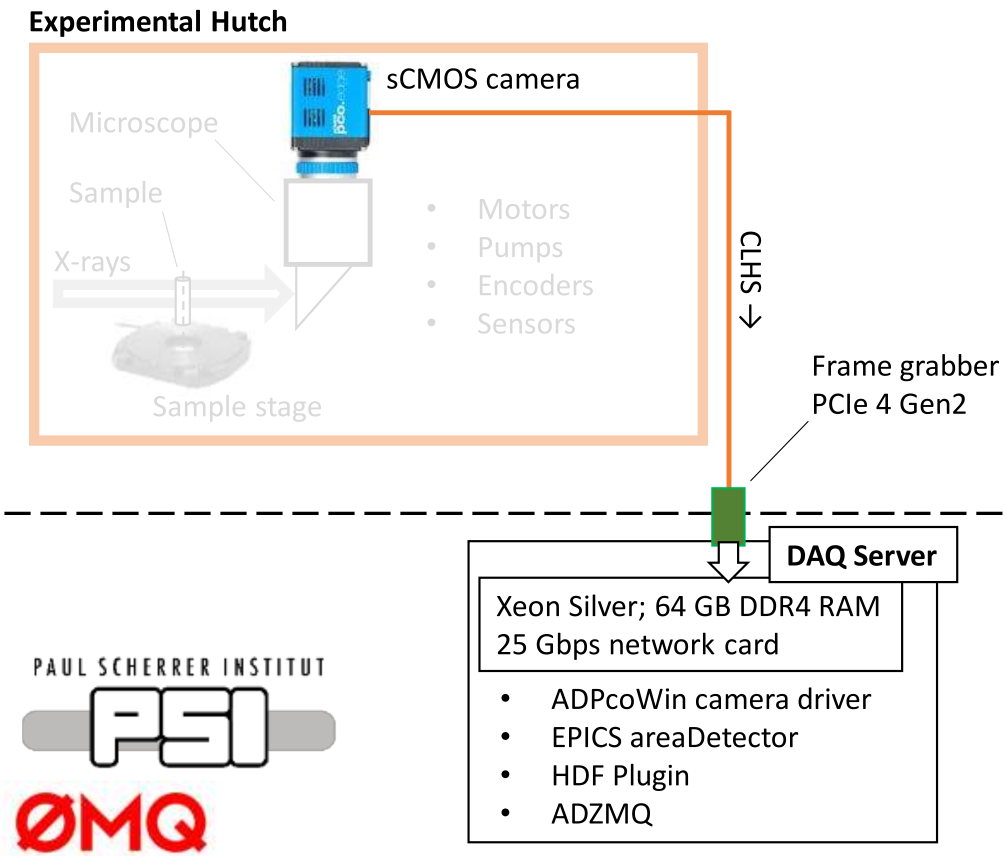

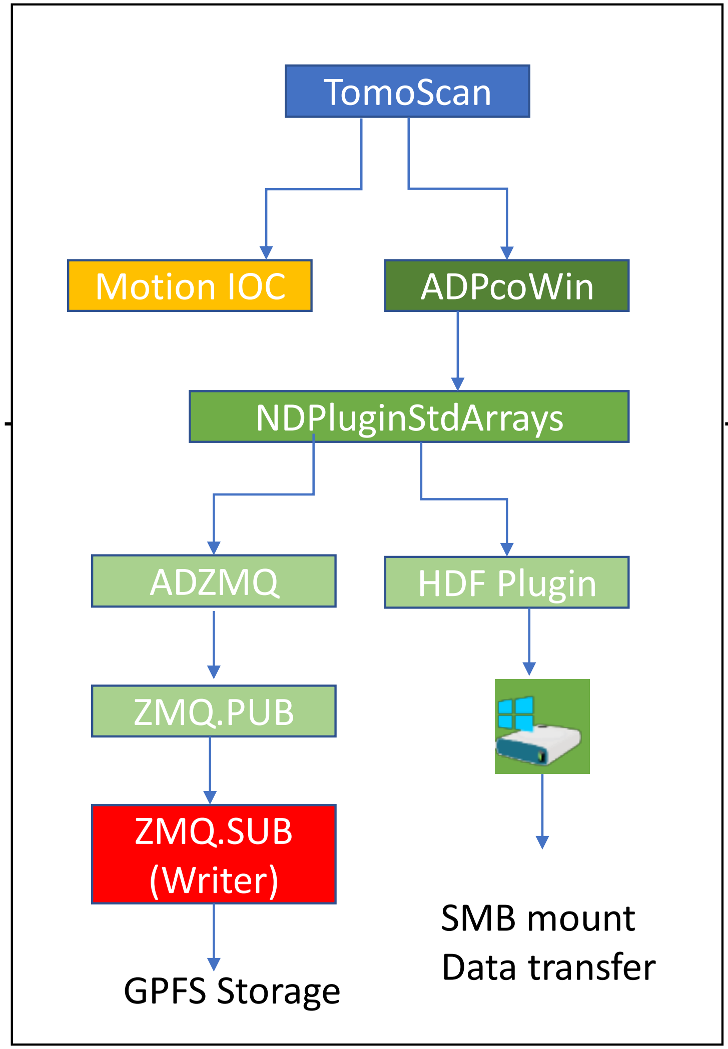

PAUL SCHERRER INSTITUT

ZeroMQ

An open-source universal messaging library

- a driver pulls data from a ZeroMQ server and generates NDArray
- a plugin publishes NDArray as ZeroMQ server.

Mustafa Al Zoubi

BEATSWriter

- **BEATSWriter** parallel processes: receiving ZMQ stream and writing of HDF5 files


Mustafa Al Zoubi

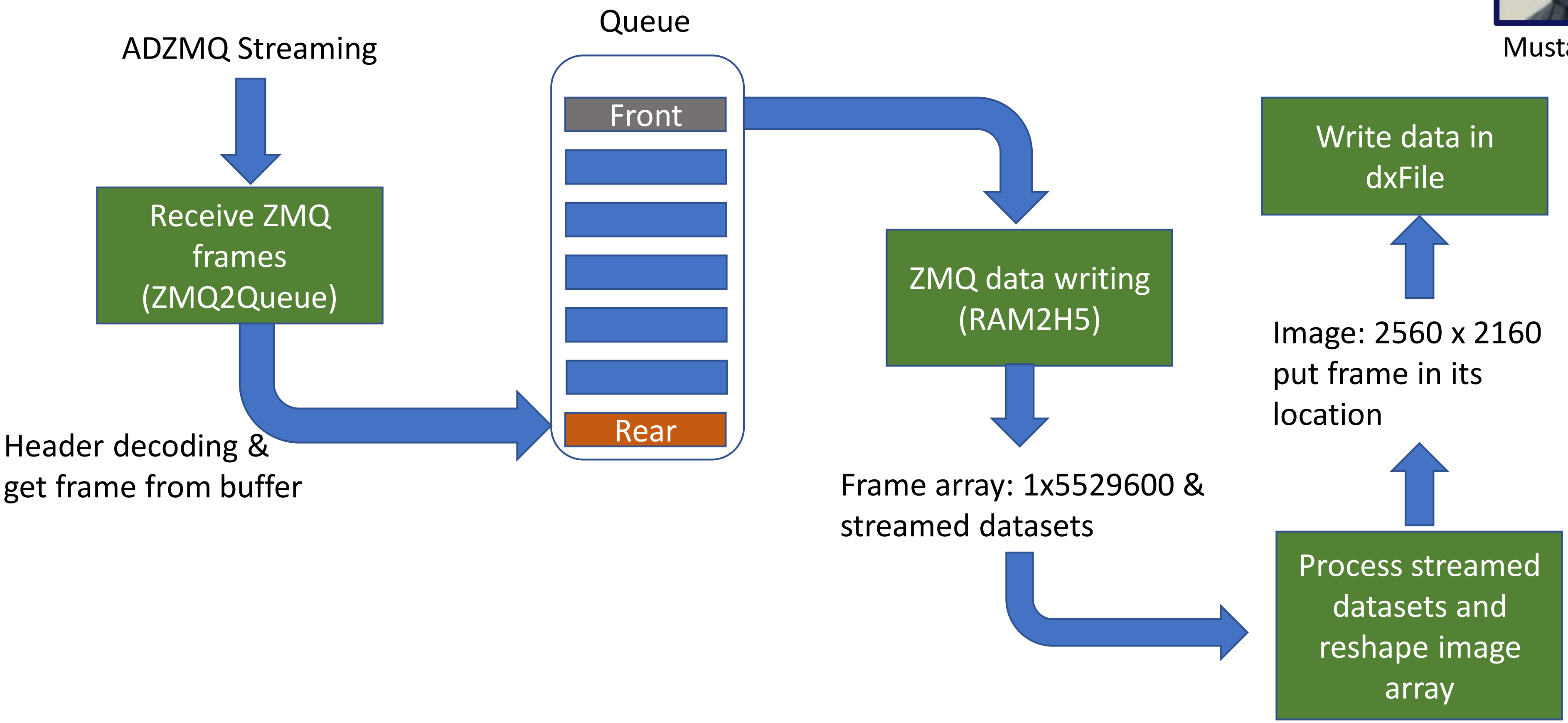

BEATS | Data Acquisition Performance Test

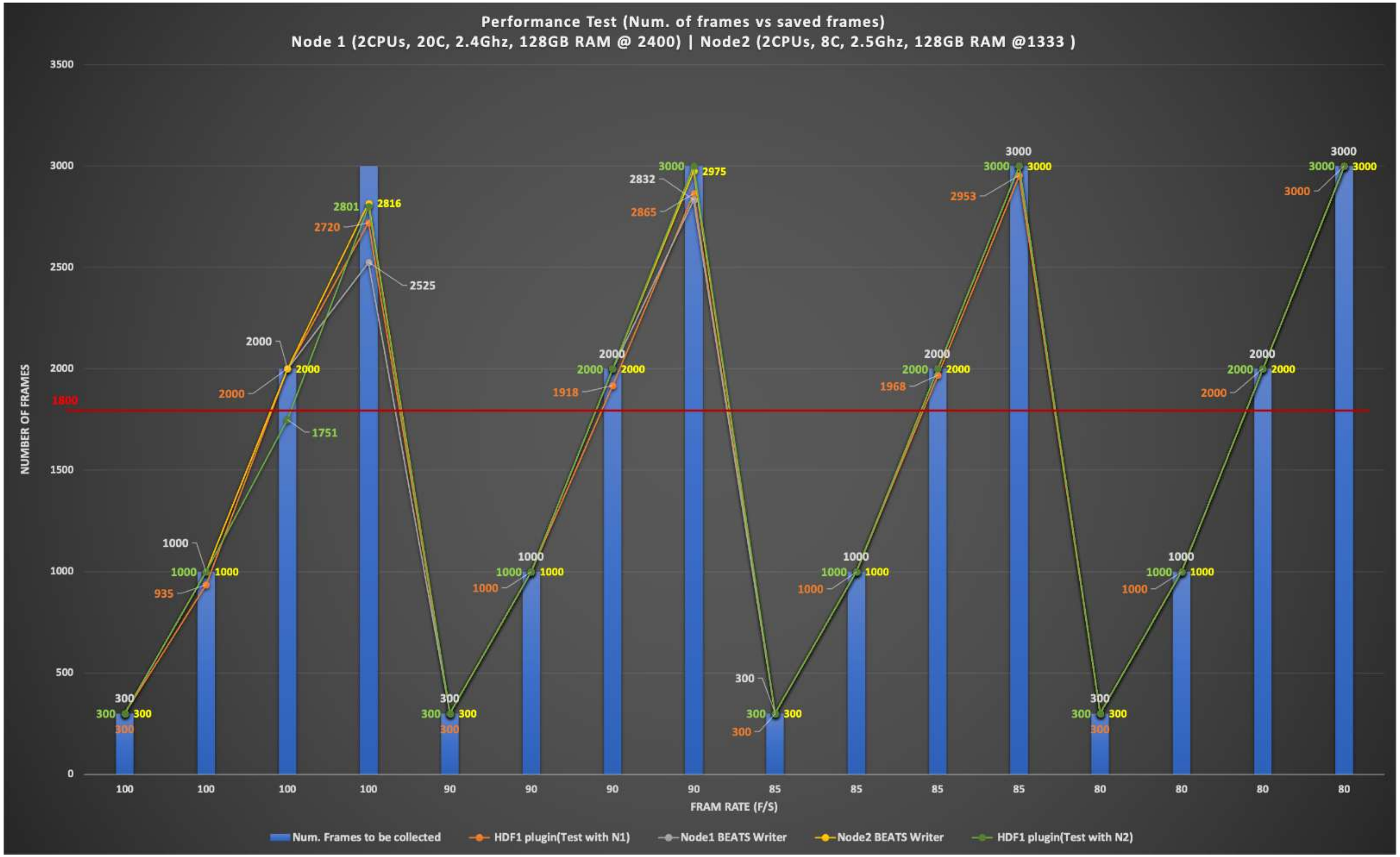

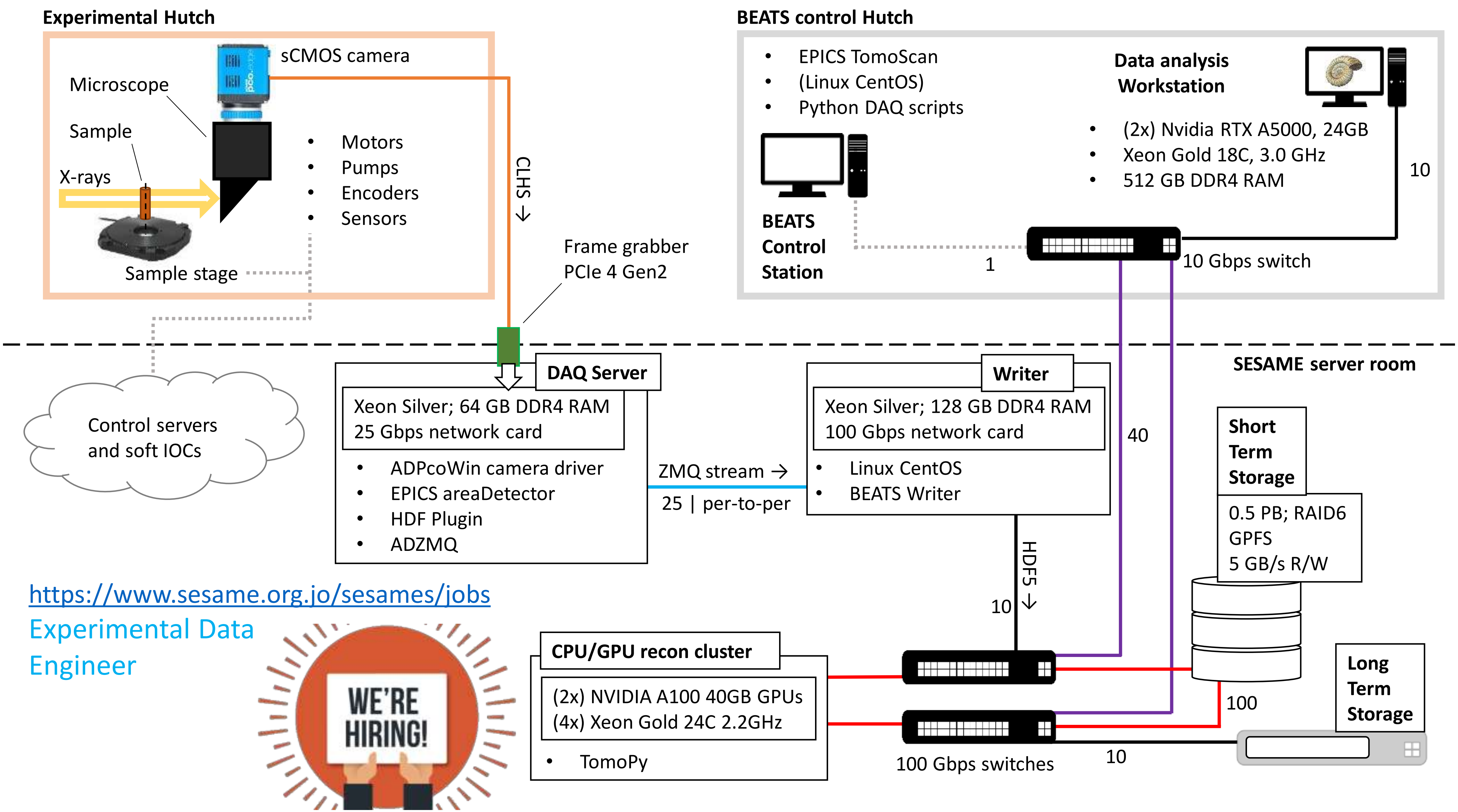

https://www.sesame.org.jo/sesames/jobs

Experimental Data Engineer

Part 3: Scientific Opportunities at BEATS

BEAmline for Tomography at SESAME

Scientific Opportunities at BEATS

Synchrotron Tomography @ BEATS

Archaeology and Cultural Heritage
- Archaeological Materials
- Human bioarchaeology
- Plant remains
- Animal remains and artefacts

Health, Biology and Food
- Musculoskeletal research
- Bone and dental implants
- Soft tissue imaging
- Animal and plant characterization
- Food science

Agriculture and Environment
- Simulation of rock properties
- Soil characterization
- Sustainable agriculture

Material science and Engineering
- Light materials and alloys
- Materials under mechanical stress
- Energy materials research

Services to Industry and Private sector

Funded by the EU's H2020 framework programme under grant agreement n°822535

BEAmline for Tomography at SESAME

Scientific Opportunities at BEATS

Archaeology and Cultural Heritage:

- Archaeological Materials
  - Pottery and Ceramics
  - Glass
  - Textile
  - Wood
  - Manuscripts

- Plant remains
- Animal remains
  - Bone
  - Antler
  - Teeth




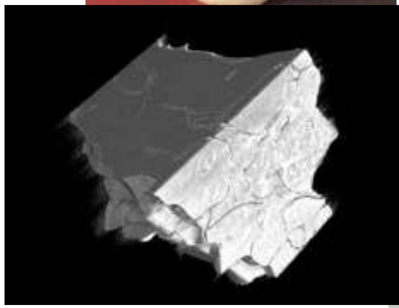


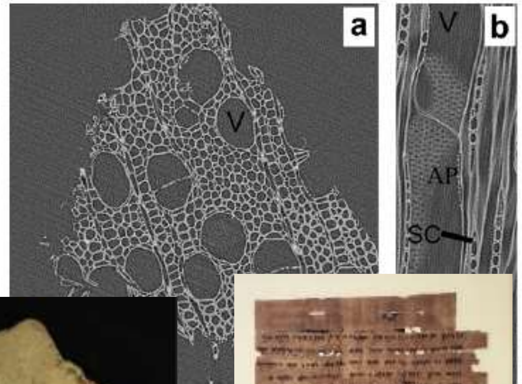

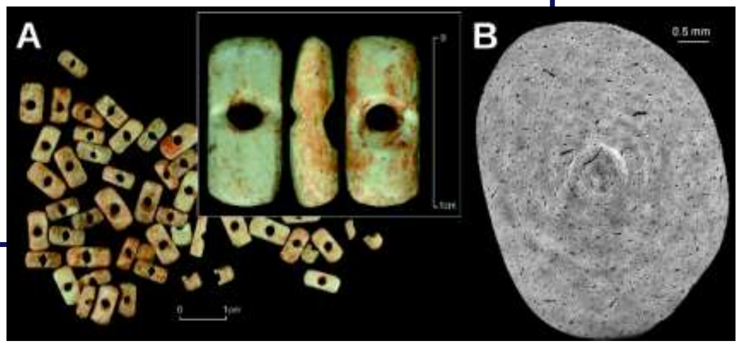


Funded by the EU's H2020 framework programme under grant agreement n°822535

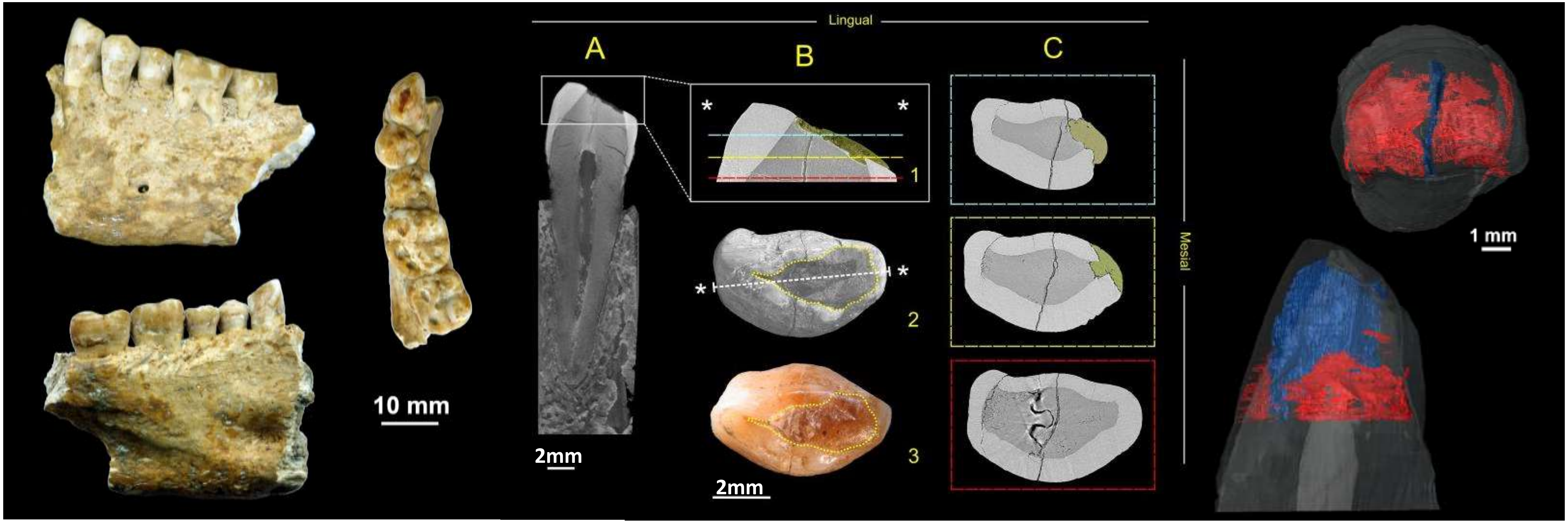

Beeswax as Dental Filling on a Neolithic Human Tooth. Bernardini et al. 2012. PLoS ONE 7 (9).
https://doi.org/10.1371/journal.pone.0044904

- The Lonche canine: lab XCT (resolution 18 µm) and phase-contrast SXCT (resolution 9 µm)
- Non-destructive 3D characterization of wear pattern and therapeutic-palliative dental filling

Over the rainbow? Micro-CT scanning to non-destructively study Roman and early medieval glass bead manufacture. Ngan-Tillard et al. 2018. Journal of Archaeological Science; 98:7–21. https://doi.org/10.1016/j.jas.2018.07.007

- Glass beads from Roman and Early Medieval burials (500 – 800 AD)
- XCT reveals manufacturing processes and tools used
- Technological level of glass bead production as social-anthropological hint

Lentseveld cemetery, the Netherlands

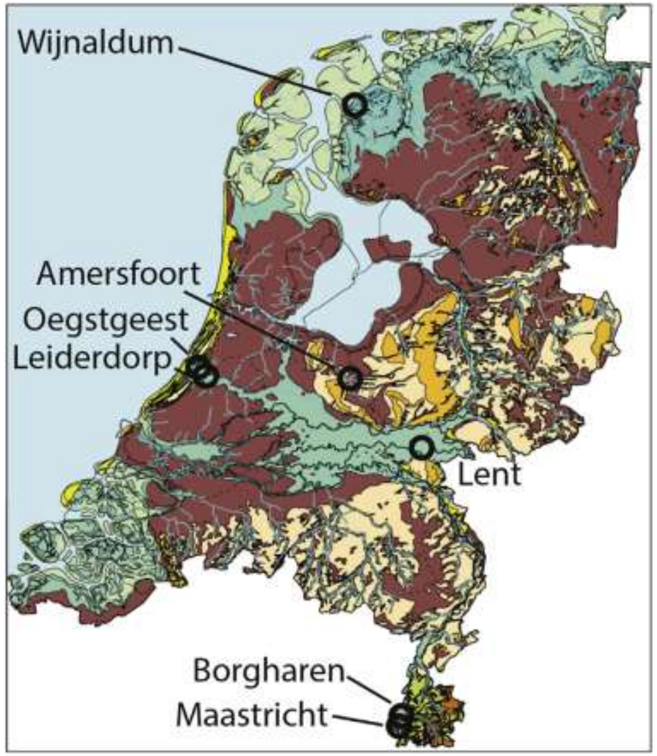

Over the rainbow? Micro-CT scanning to non-destructively study Roman and early medieval glass bead manufacture. Ngan-Tillard et al. 2018. Journal of Archaeological Science; 98:7–21.
https://doi.org/10.1016/j.jas.2018.07.007

- Different colours give different X-ray attenuation: yellow and white opaque glass contains many small highly attenuating inclusions.
- Heterogeneous glass composition, defects, voids and imperfections.
- White rounded inclusions are globules of metallic lead.

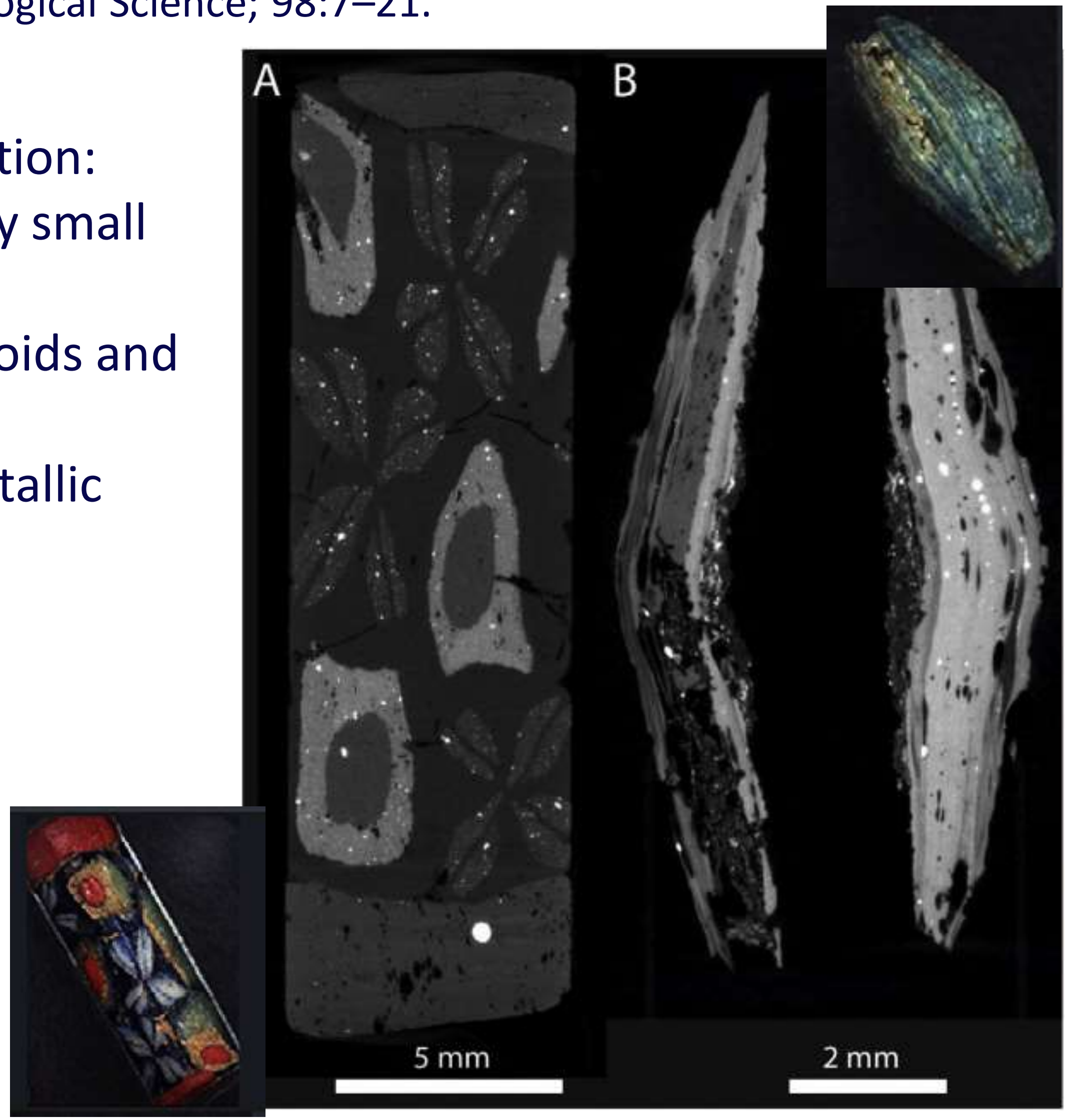

Over the rainbow? Micro-CT scanning to non-destructively study Roman and early medieval glass bead manufacture. Ngan-Tillard et al. 2018. Journal of Archaeological Science; 98:7–21.
https://doi.org/10.1016/j.jas.2018.07.007

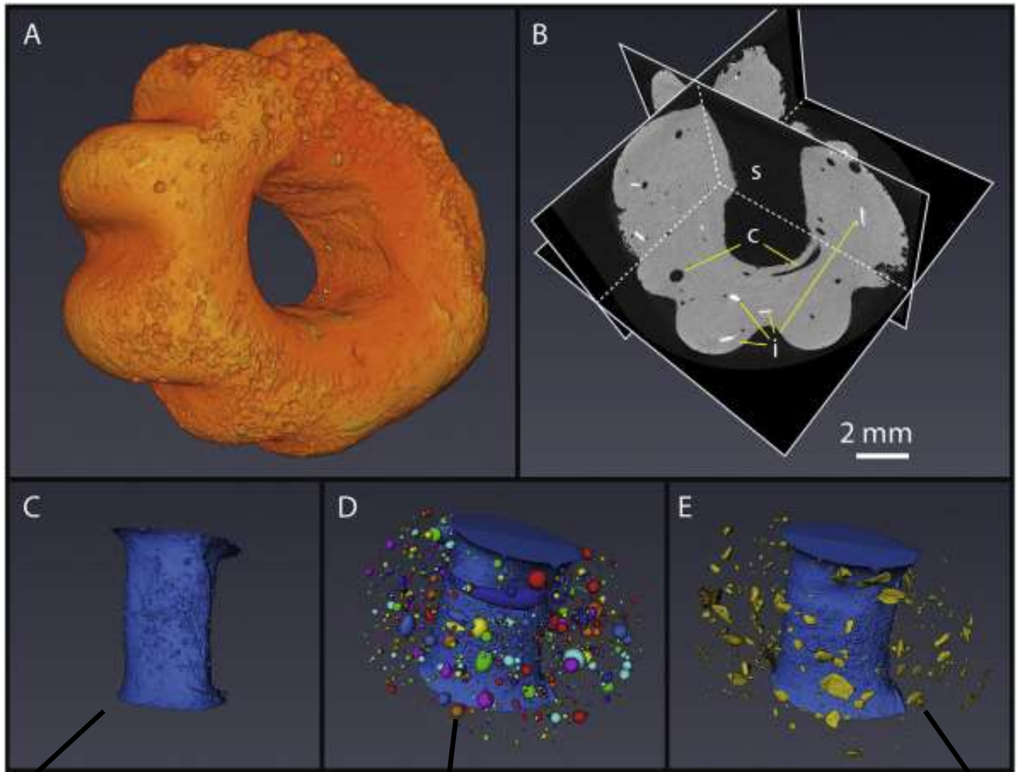

Taper size indicates shape of tool used

Voids (air bubbles) formed during winding and shaping

Mineral precipitations of opacifier

Over the rainbow? Micro-CT scanning to non-destructively study Roman and early medieval glass bead manufacture. Ngan-Tillard et al. 2018. Journal of Archaeological Science; 98:7–21.
https://doi.org/10.1016/j.jas.2018.07.007

- “Millefiori” beads: stacked patterned of polychrome glass blocks
- Polychrome blocks were compressed or drawn

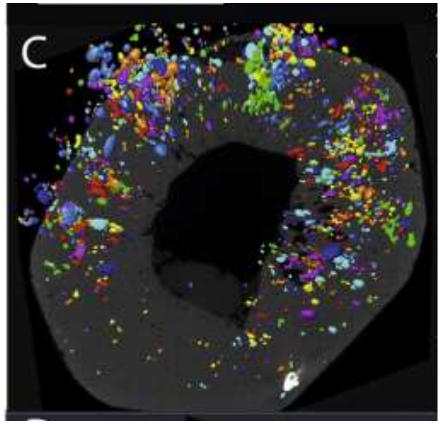

Shape distribution of Gas bubbles in millefiori bead: bubbles are flattened close to the shaft, but spherical near the surface.

Beads were assembled from blocks of polychrome glass.

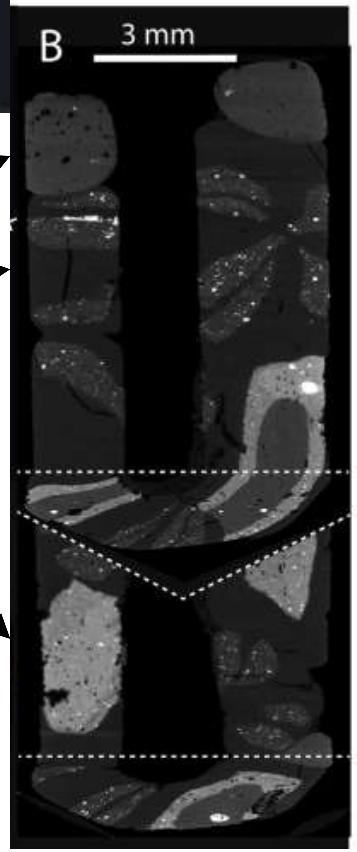

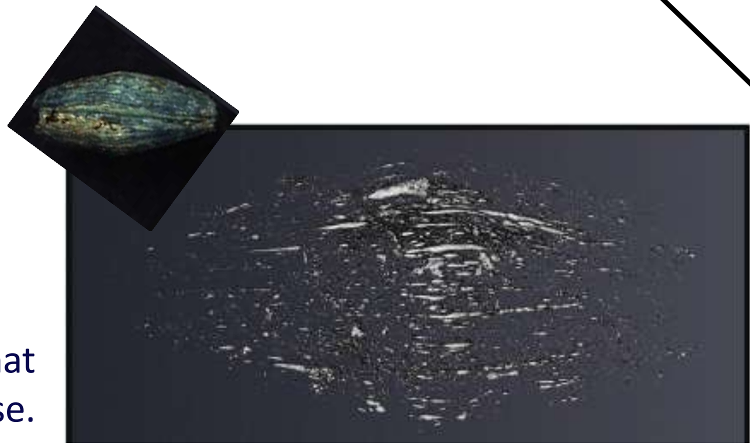

Elongated gas bubbles indicate that the bead was drawn lengthwise.

Over the rainbow? Micro-CT scanning to non-destructively study Roman and early medieval glass bead manufacture. Ngan-Tillard et al. 2018. Journal of Archaeological Science; 98:7–21.
https://doi.org/10.1016/j.jas.2018.07.007

- **Manufacturing tool**: shaft shape, radius and tapering angle
- Forming / **shaping method**: assembled, drawn, wound shaped..
- Polychrome **decorations** and technique
- Damage and **degradation** processes

(A) Pattern of fissures.
(B) Dissolution features: depressions at the surface and pores inside the glass indicate biologically promoted dissolution processes.

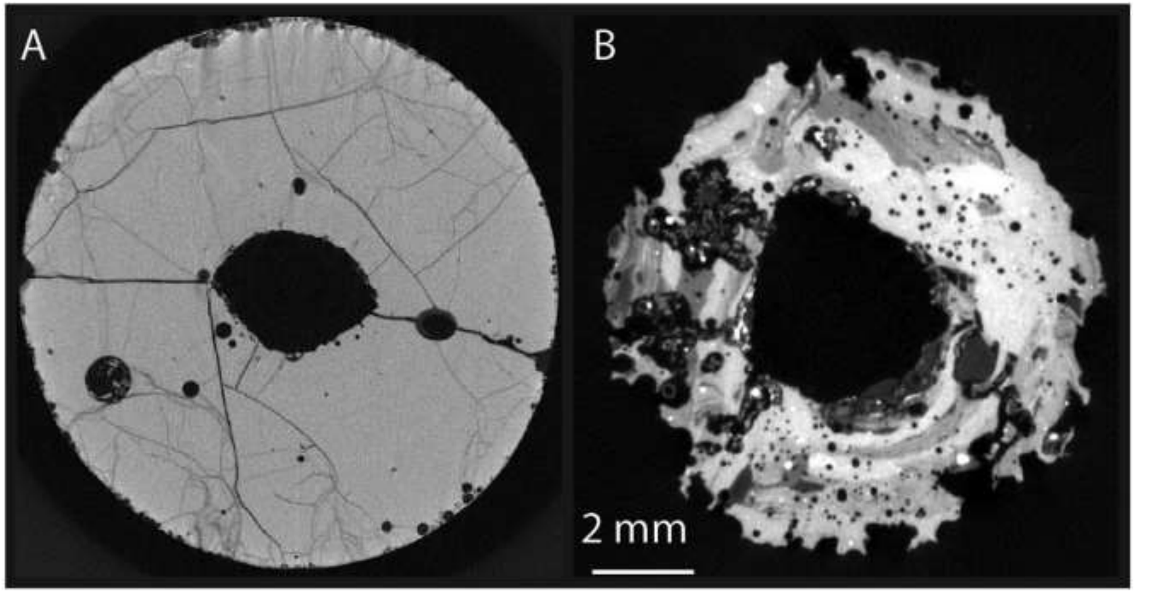

Scientific Opportunities at BEATS

BEATS

BEAmline for Tomography at SESAME

Health, Biology and Food:

- Musculoskeletal research
- Bone and dental implants
- Soft tissue imaging
- Animal and plant characterization
- Food science

Coleoptera fossil

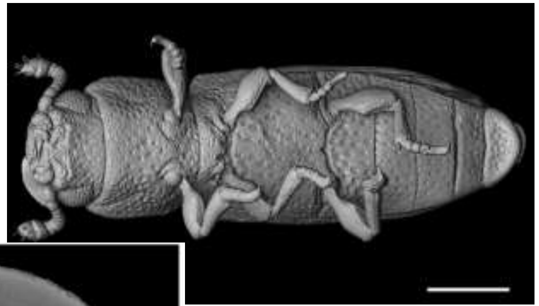

Green bean

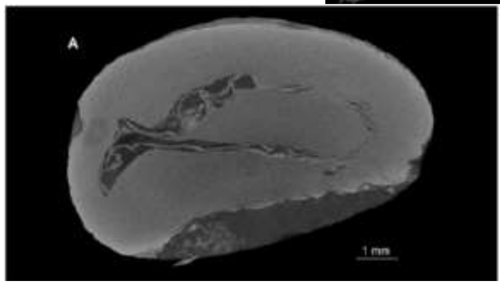

Mineralized algae (red sea)

Bone implant

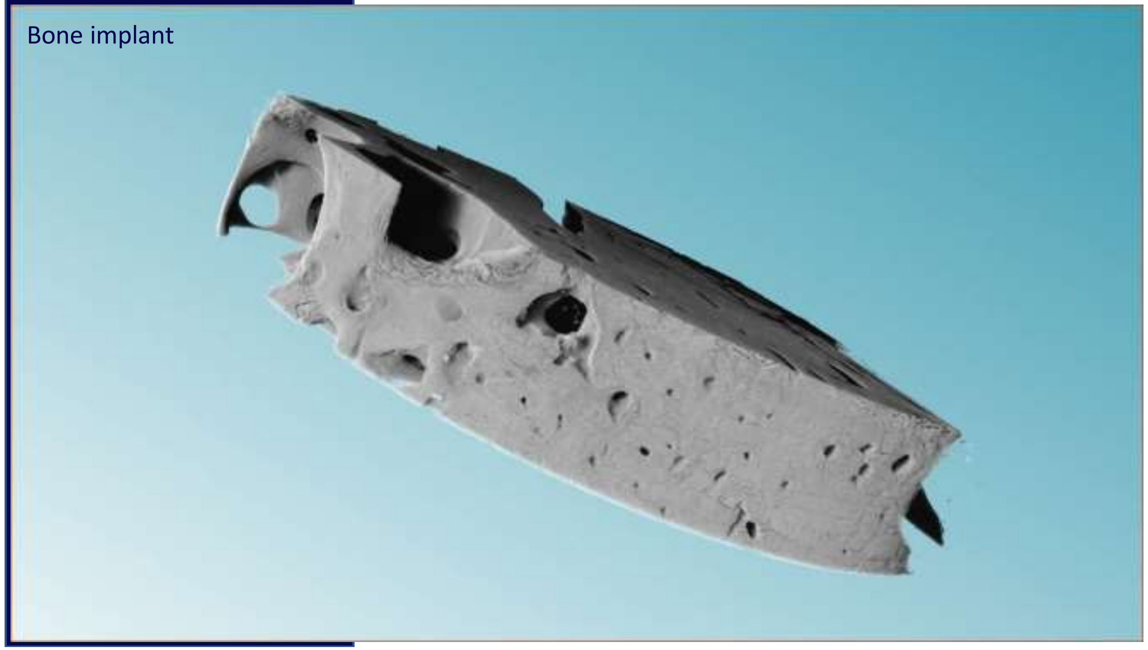

Dental implant

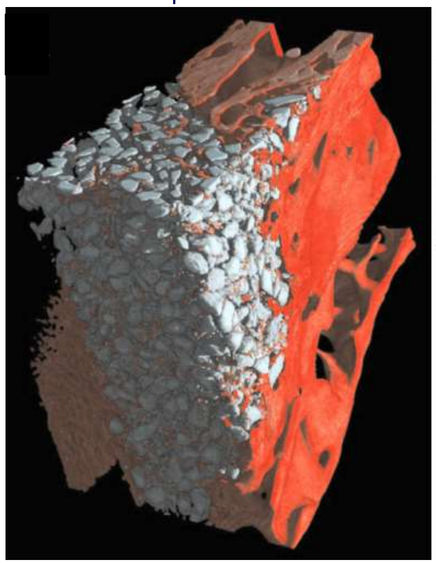

Caries

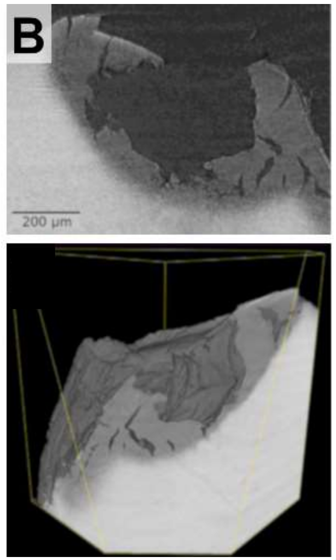

In Situ Characterization of Nanoscale Strains in Loaded Whole Joints via Synchrotron X-Ray Tomography.
Madi et al. 2020. Nature Biomedical Engineering 4 (3): 343–54.
https://doi.org/10.1038/s41551-019-0477-1

- Cartilage layers covering the ends of bones are the most efficiently lubricated surfaces in nature.
- Breakdown of the cartilage–subchondral bone interface can lead to osteoarthritis.
- Understanding load transfer and tissue strains throughout healthy and diseased joints could provide insights into the pathogenesis of osteoarthritis.
- **Tests under physiologically representative conditions are lacking!**

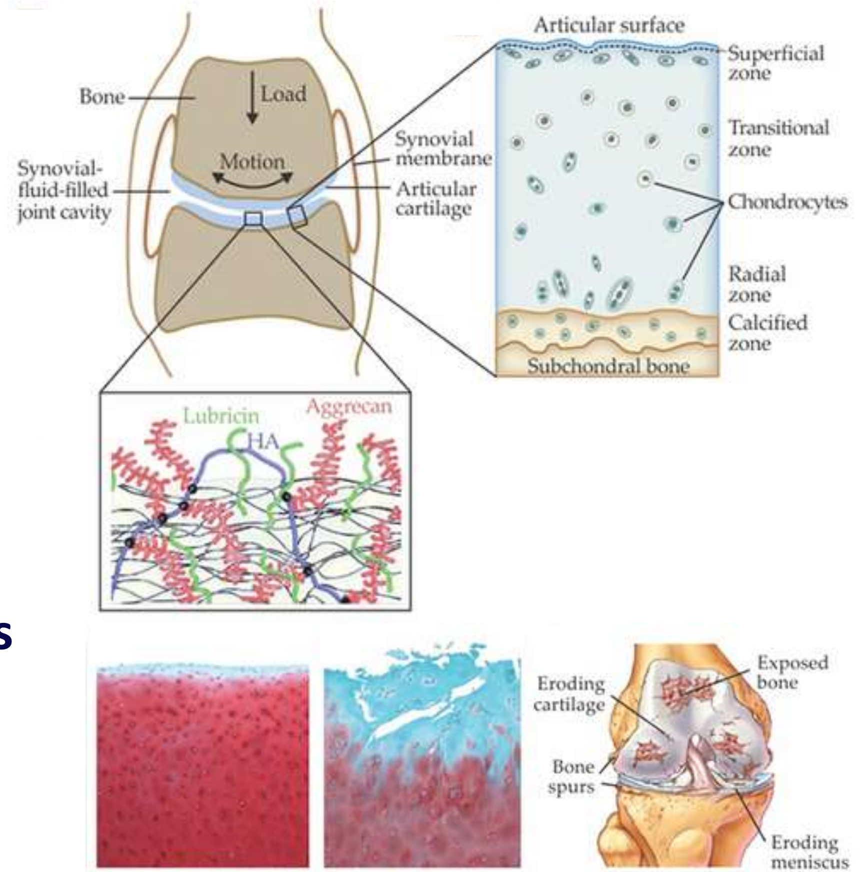

Jahn, Sabrina, and Jacob Klein. 2018. "Lubrication of Articular Cartilage." *Physics Today* 71 (4): 48–54. https://doi.org/10.1063/PT.3.3898.

In Situ Characterization of Nanoscale Strains in Loaded Whole Joints via Synchrotron X-Ray Tomography. Madi et al. 2020. Nature Biomedical Engineering 4 (3): 343–54.
https://doi.org/10.1038/s41551-019-0477-1

- **In situ mechanical testing** with nano-precision rig allows testing intact joints under realistic loading conditions
- Combination **with ultra-high-resolution, fast 4D SXCT**

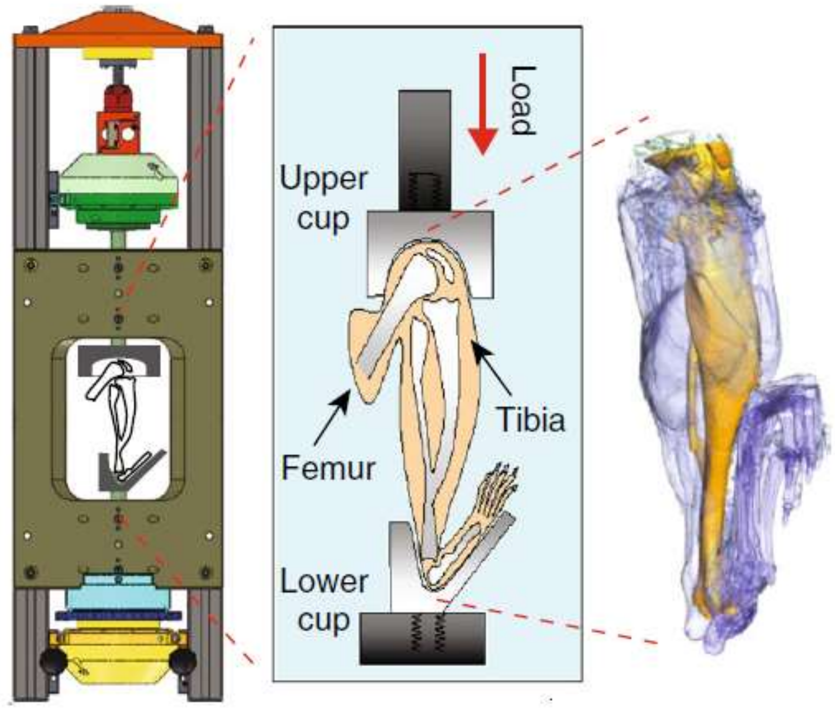

Hypertrophic chondrocyte lacunae

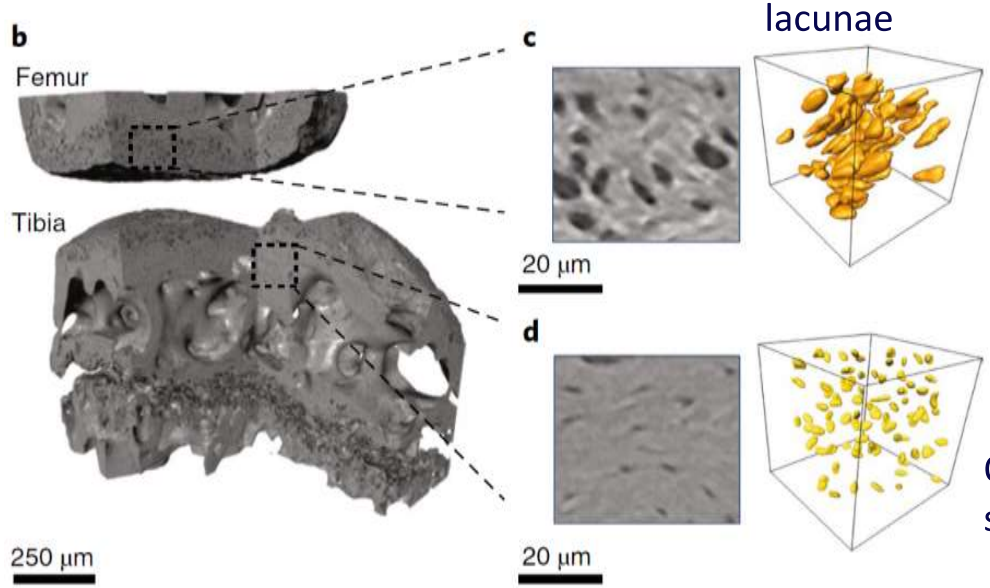

Osteocyte lacunae from the subchondral bone

In Situ Characterization of Nanoscale Strains in Loaded Whole Joints via Synchrotron X-Ray Tomography.
Madi et al. 2020. Nature Biomedical Engineering 4 (3): 343–54.
https://doi.org/10.1038/s41551-019-0477-1

Healthy

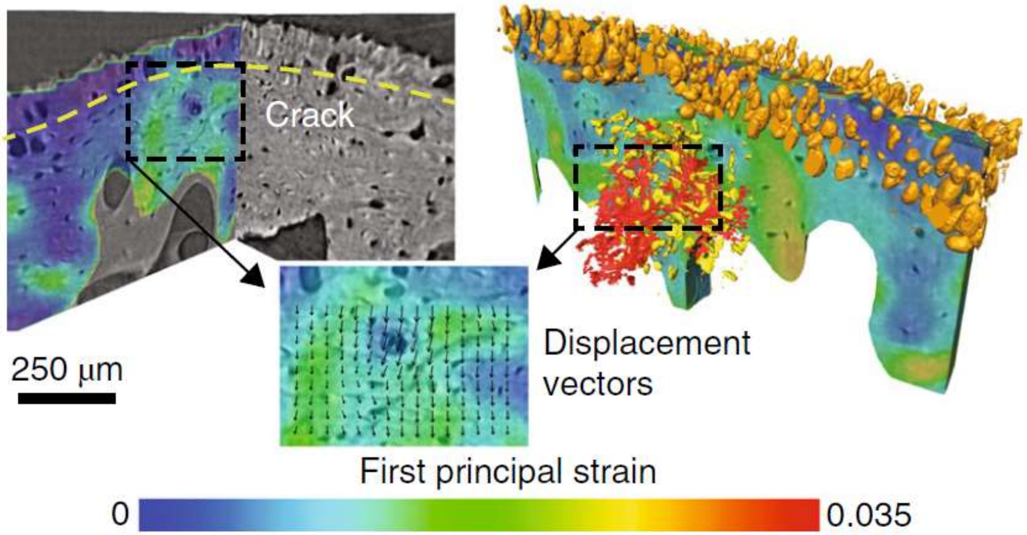

In healthy murine tissue, load-induced fracture was localized within the subchondral bone.

Osteoarthritic

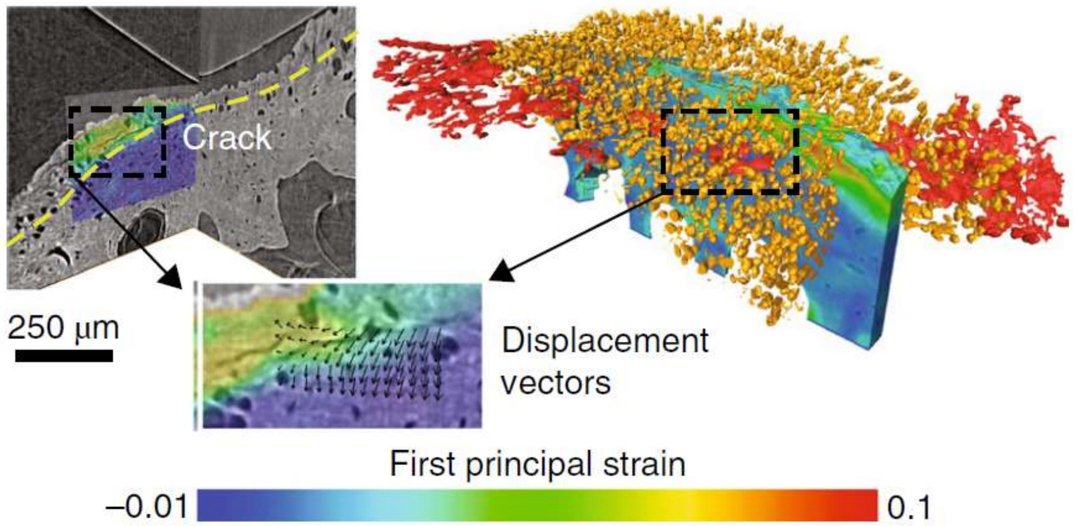

In osteoarthritic joints of older mice, the damage occurred in a calcified cartilage layer near the articulating cartilage.
In younger mice with osteoarthritis, the fractures occurred throughout the calcified cartilage.

BEAmline for Tomography at SESAME

Funded by the EU's H2020 framework programme under grant agreement n°822535

Scientific Opportunities at BEATS

Agriculture and Environment
- Simulation of rock properties
- Soil characterization
- Sustainable agriculture

Sandstone core

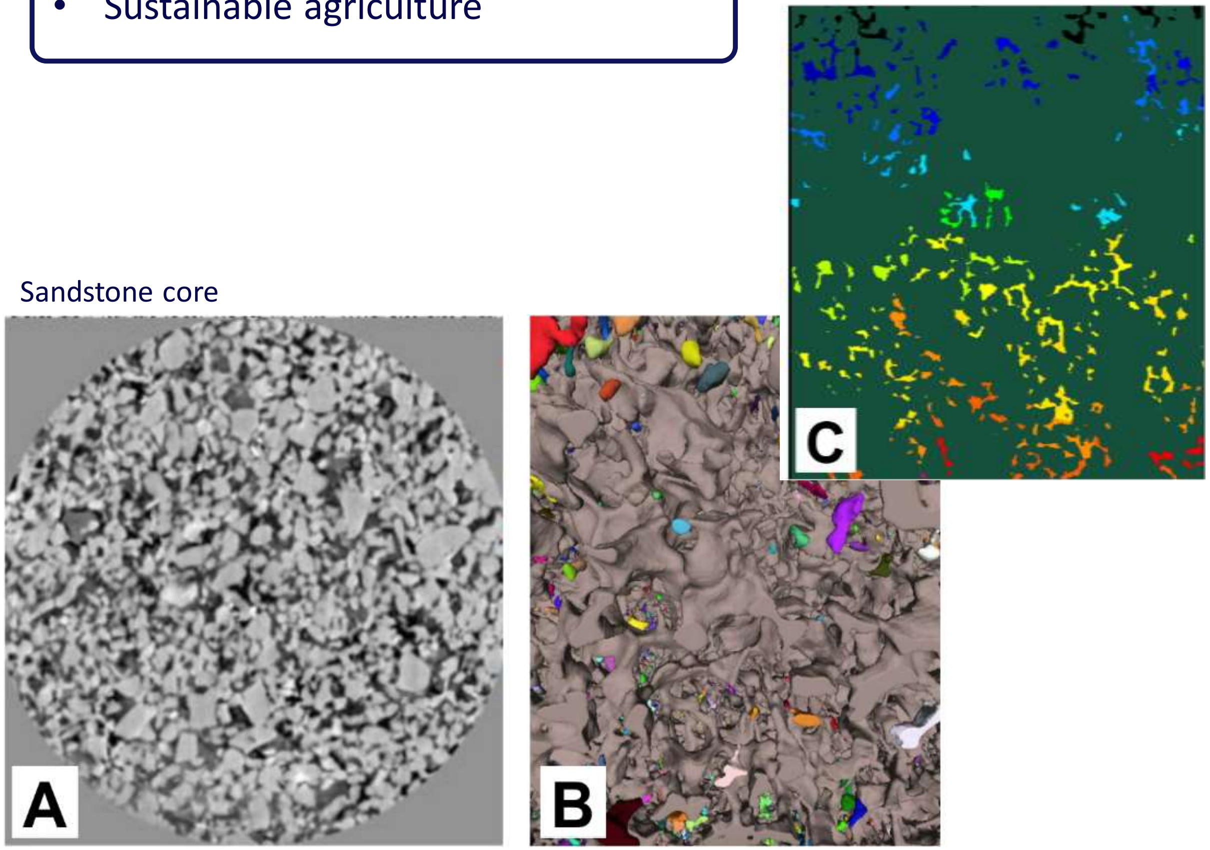

Kakouie, A. et al. In preparation. Courtesy Shiva Shirani.

Quantification of heterogeneous soils

Inorganics, pores + organics

Pores + organics

Pores

Organics

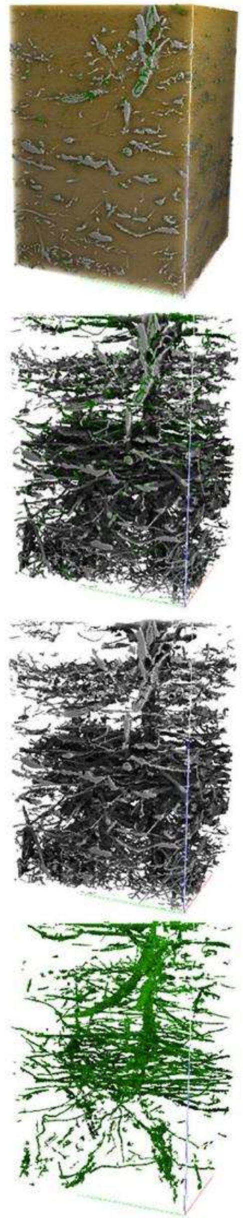

ENVIRONMENTAL RESEARCH
LETTERS

LETTER • OPEN ACCESS

To till or not to till in a temperate ecosystem? Implications for climate change mitigation

H V Cooper[2,1], S Sjögersten[1], R M Lark[1] and S J Mooney[1]

Published 27 April 2021 • © 2021 The Author(s). Published by IOP Publishing Ltd
Environmental Research Letters, Volume 16, Number 5
Citation H V Cooper *et al* 2021 *Environ. Res. Lett.* **16** 054022
doi: 10.1088/1748-9326/abe74e

Excessive soil tillage is associated with soil degradation processes such as compaction, a decrease in soil stability and structure, increased soil erosion.

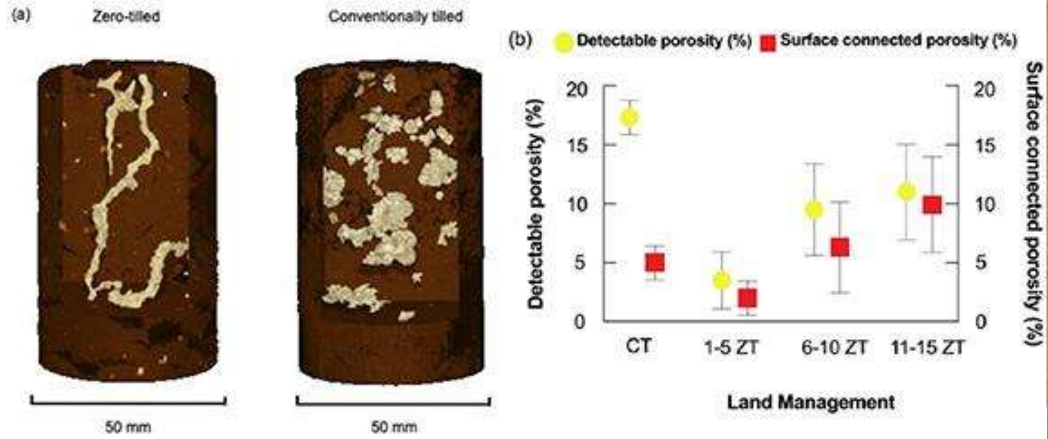

Why the fate of our planet's environment depends on the state of its soil

- Soil microstructural changes gradually protect soil organic matter
- It has been proposed that zero-till systems could increase soil organic matter sequestration
- Quantification of soil porous architecture with (High-energy) lab XCT (resolution 50 μm)
- Determination of organic matter functional chemistry with FTIR spectroscopy

Scientific Opportunities at BEATS

Material science and Engineering:

- Energy materials research
- Light materials and alloys
- Materials under mechanical stress
- From CT images to FE simulations

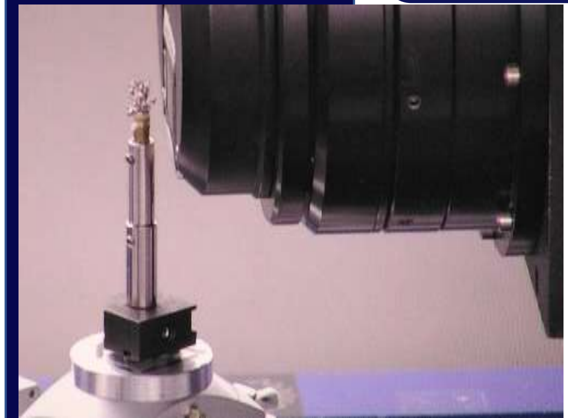

Markötter, H. et al. Journal of Power Sources (2019).

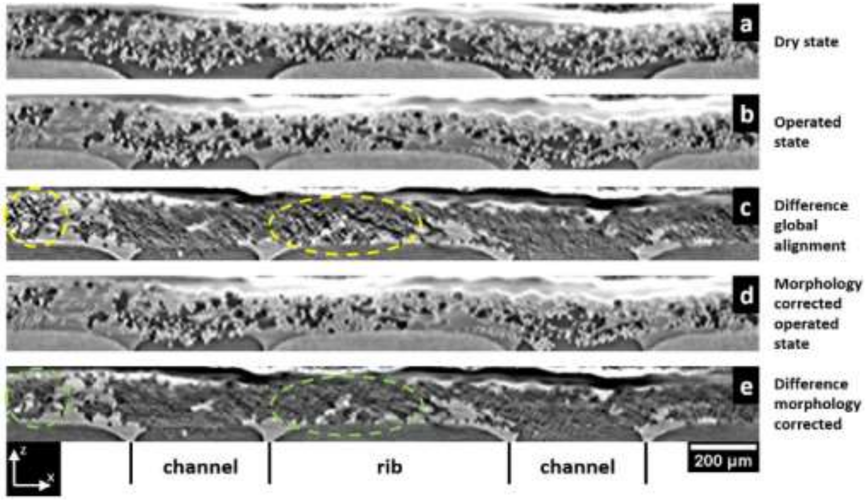

Operando studies of the gas diffusion layer in Polymer electrolyte fuel cells

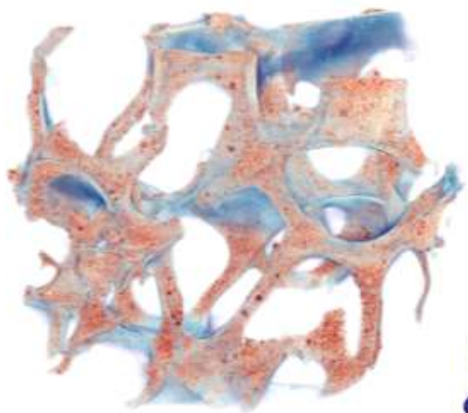

Light engineering materials (steel foam)

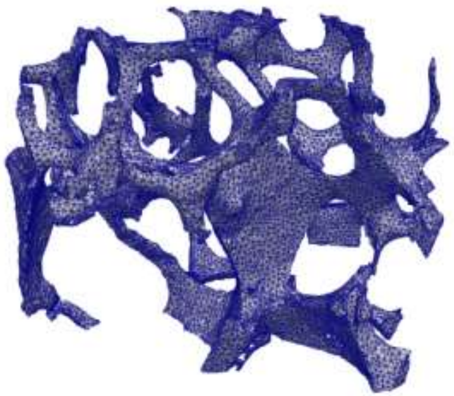

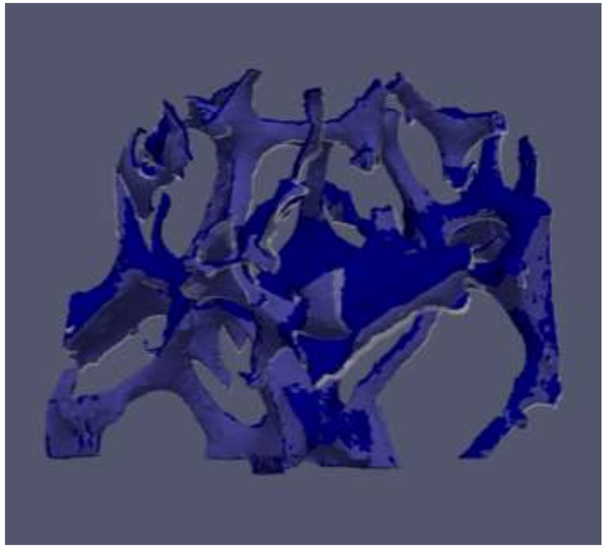

Advanced Engineering Materials 21, 1900080 (2019).
Kaya, A. et. Al. Foams of Gray Cast Iron as Efficient Energy Absorption Structures: A Feasibility Study.

Funded by the EU's H2020 framework programme under grant agreement n°822535

Tomography 3D rendering of a non-uniform hollow strut and overlay of the observed embedded micro/macropores in green

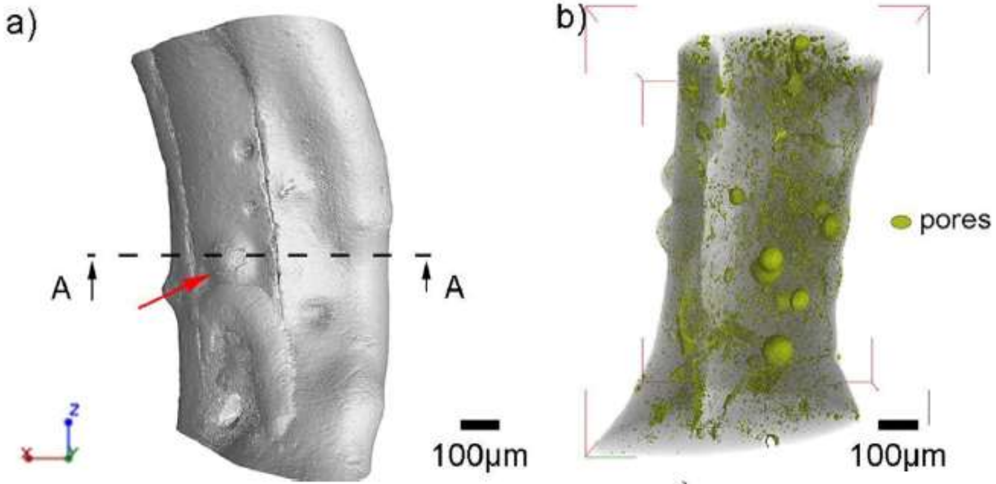

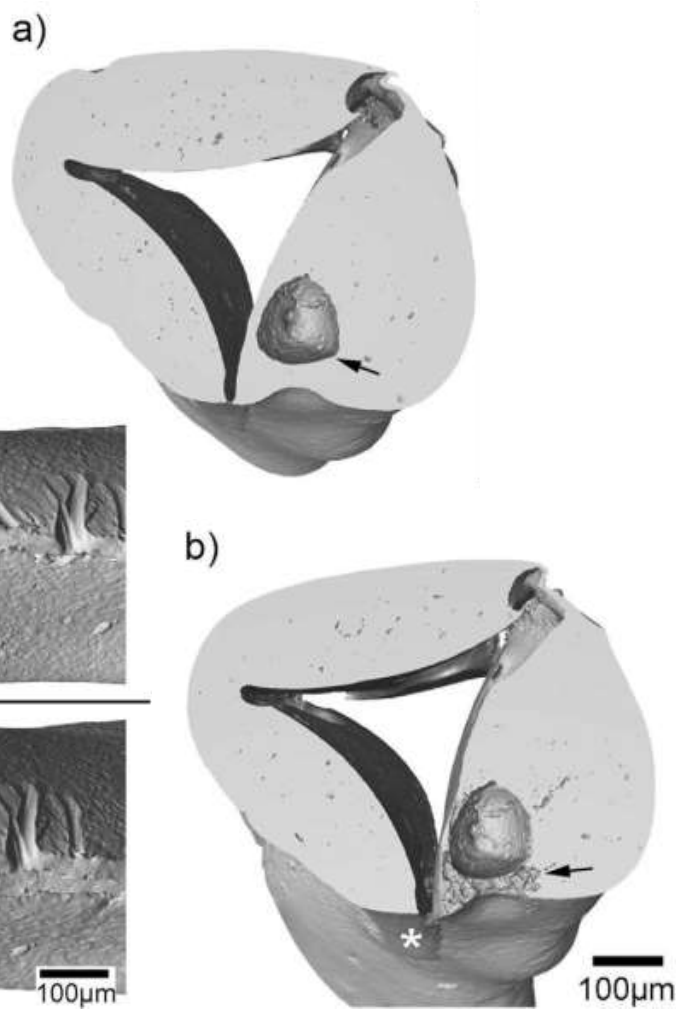

BEFORE loading

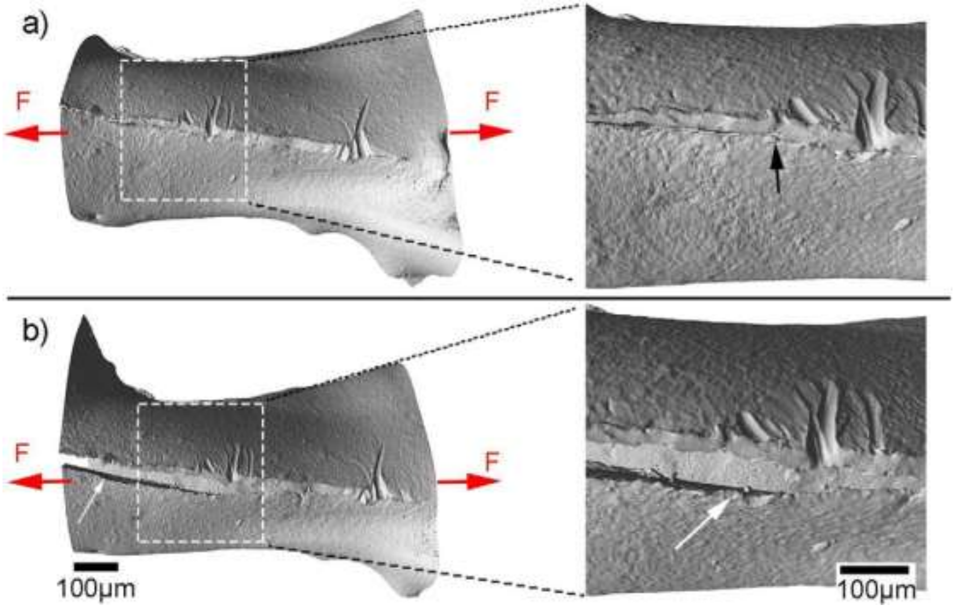

AFTER loading

Advanced Engineering Materials 21, 1900080 (2019).
Kaya, A. et. Al. Foams of Gray Cast Iron as Efficient Energy Absorption Structures: A Feasibility Study.

From synchrotron tomography data to FE models

Tomography scan

↓

Segmentation

↓

Meshing

↓

Material mapping and Boundary Conditions

↓

FE solution

↓

FE post-processing

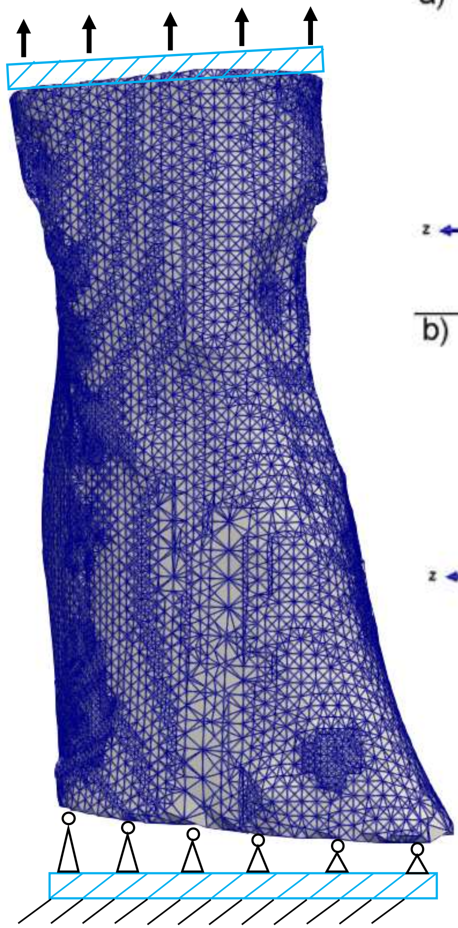

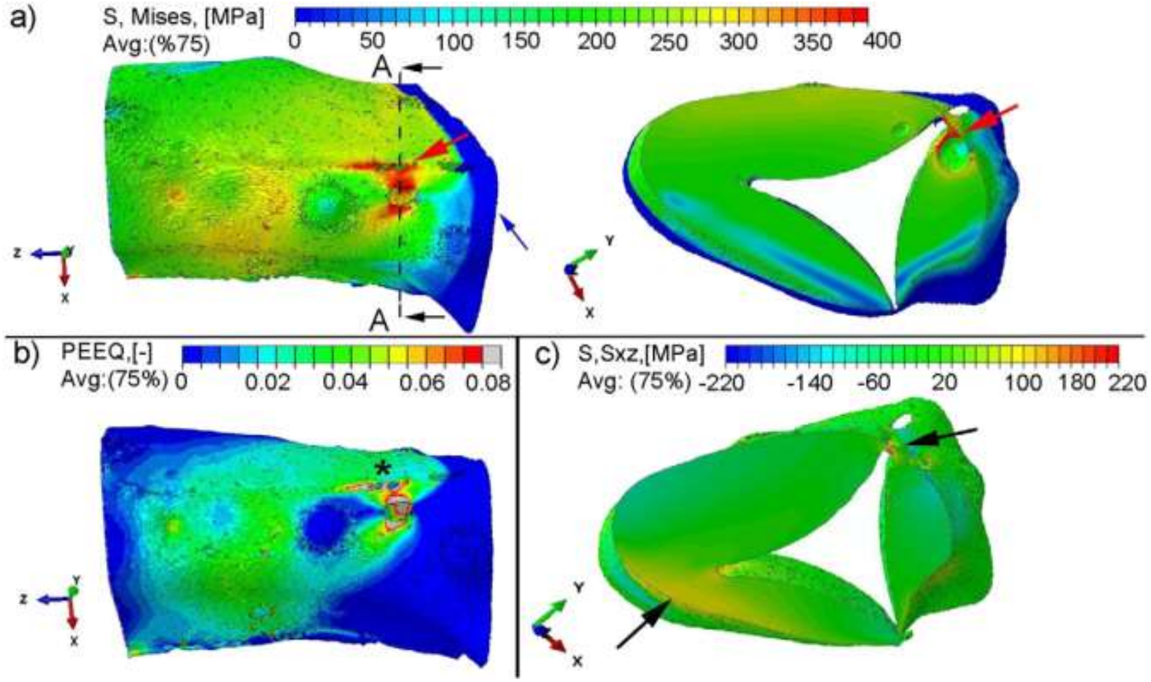

Advanced Engineering Materials 21, 1900080 (2019).
Kaya, A. et. Al. Foams of Gray Cast Iron as Efficient Energy Absorption Structures: A Feasibility Study.

From synchrotron CT data to FE models

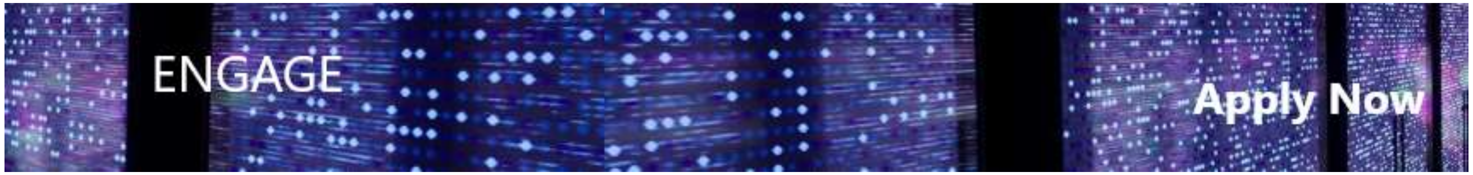

20 Marie Sklodowska-Curie PhD positions are now open

For more information click here

Marie Sklodowska-Curie PhD fellowships in Computational Physics and Engineering

https://engage.cyi.ac.cy/

- Soil percolation
- Oxygen transport in lung tissue
- Composite materials under mechanical stress
- Microfluidics
- Biomechanics of hard and soft tissue

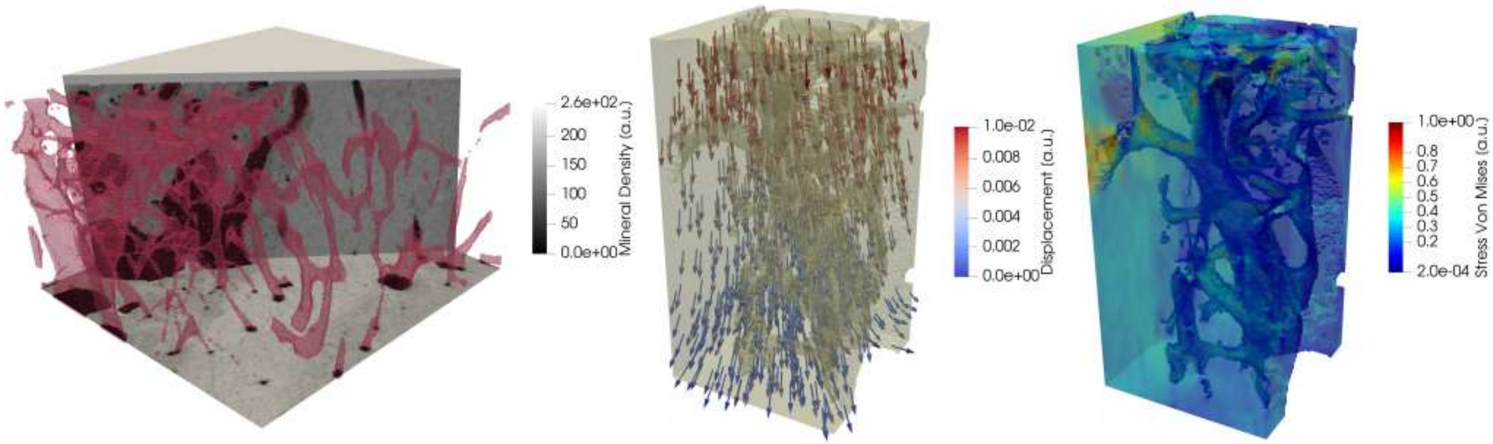

- AI-assisted pipelines for image-driven numerical simulations of biological tissues

Bibliography:

1. Willmot P. An Introduction to Synchrotron Radiation: Techniques and Applications. John Wiley & Sons; 2019. 501 p.
2. A. Rack et al., Comparative study of multilayers used in monochromators for synchrotron-based coherent hard X-ray imaging, J Synchrotron Rad, vol. 17, no. 4, pp. 496–510, Jul. 2010.
3. A. Pogany, D. Gao, and S. W. Wilkins, “Contrast and resolution in imaging with a microfocus x-ray source,” Review of Scientific Instruments, vol. 68, no. 7, pp. 2774–2782, Jul. 1997.
4. Cloetens P. Phase Contrast Imaging - Coherent Beams [Internet]. School on X-ray Imaging Techniques at the ESRF; 2007 Feb 5 [cited 2020 Apr 21]; ESRF, Grenoble, France. link
5. C. Muñoz Pequeño, J. M. Clement, P. Thevenau, and P. Van Vaerenbergh, “Development of a Linear Fast Shutter for BM05 at ESRF and BEATS at SESAME,” presented at the MEDSI’20, Chicago, USA, Jul. 2021.
6. F. Mokoena, M. Bhamjee, P. Van Vaerenbergh, G. Iori, A. Kaprolat, and S. Connell, “An FEA Investigation of the Vibration Response of the BEATS Detector Stage,” presented at the MEDSI’20, Chicago, USA, Jul. 2021.
7. A. Mittone, I. Manakov, L. Broche, C. Jarnias, P. Coan, and A. Bravin, “Characterization of a sCMOS-based high-resolution imaging system,” Journal of Synchrotron Radiation, vol. 24, no. 6, pp. 1226–1236, 2017.
8. M. Rivers and F. De Carlo, “TomoScan 0.1” https://tomoscan.readthedocs.io/en/latest/about.html.
9. F. Bernardini et al., “Beeswax as Dental Filling on a Neolithic Human Tooth,” PLoS One, vol. 7, no. 9, Sep. 2012.
10. D. J. M. Ngan-Tillard, D. J. Huisman, F. Corbella, and A. Van Nass, “Over the rainbow? Micro-CT scanning to non-destructively study Roman and early medieval glass bead manufacture,” Journal of Archaeological Science, vol. 98, pp. 7–21, Oct. 2018.
11. S. Jahn and J. Klein, “Lubrication of articular cartilage,” Physics Today, vol. 71, no. 4, pp. 48–54, Apr. 2018.
12. Kersh ME. Resolving nanoscale strains in whole joints. Nat Biomed Eng. 2020 Mar;4(3):257–8.
13. Madi K, Staines KA, Bay BK, Javaheri B, Geng H, Bodey AJ, et al. In situ characterization of nanoscale strains in loaded whole joints via synchrotron X-ray tomography. Nat Biomed Eng. 2020 Mar;4(3):343–54.
14. “Why the fate of our planet’s environment depends on the state of its soil.”, 2021, https://theconversation.com/.
15. H. V. Cooper, S. Sjogersten, R. M. Lark, and S. J. Mooney, “To till or not to till in a temperate ecosystem? Implications for climate change mitigation,” Environ. Res. Lett., Feb. 2021.
16. A. C. Kaya, P. Zaslansky, A. Rack, S. F. Fischer, and C. Fleck, “Foams of Gray Cast Iron as Efficient Energy Absorption Structures: A Feasibility Study,” Advanced Engineering Materials, vol. 21, no. 6, p. 1900080, 2019.